OULU 2014
D 1255

ACTA
UNIVERSITATIS OULUENSIS

Tuomo Starck

DIMENSIONALITY, NOISE SEPARATION AND FULL FREQUENCY BAND PERSPECTIVES OF ICA IN RESTING STATE FMRI

INVESTIGATIONS INTO ICA IN RESTING STATE FMRI

UNIVERSITY OF OULU GRADUATE SCHOOL;
UNIVERSITY OF OULU,
FACULTY OF MEDICINE,
INSTITUTE OF DIAGNOSTICS,
DEPARTMENT OF DIAGNOSTIC RADIOLOGY;
OULU UNIVERSITY HOSPITAL

ACTA UNIVERSITATIS OULUENSIS
D Medica 1255

TUOMO STARCK

DIMENSIONALITY, NOISE SEPARATION AND FULL FREQUENCY BAND PERSPECTIVES OF ICA IN RESTING STATE FMRI

Investigations into ICA in resting state FMRI

Academic dissertation to be presented with the assent of the Doctoral Training Committee of Health and Biosciences of the University of Oulu for public defence in Auditorium 7 of Oulu University Hospital, on 29 August 2014, at 12 noon

UNIVERSITY OF OULU, OULU 2014

Acta Univ. Oul. D 1255, 2014

Supervised by
Docent Vesa Kiviniemi
Professor Osmo Tervonen

Reviewed by
Docent Iiro Jääskeläinen
Docent Ricardo Vigário

Opponent
Docent Peter Fransson

ISBN 978-952-62-0517-5 (Paperback)
ISBN 978-952-62-0518-2 (PDF)

ISSN 0355-3221 (Printed)
ISSN 1796-2234 (Online)

Cover Design
Raimo Ahonen

JUVENES PRINT
TAMPERE 2014

Starck, Tuomo, Dimensionality, noise separation and full frequency band perspectives of ICA in resting state fMRI. Investigations into ICA in resting state fMRI

University of Oulu Graduate School; University of Oulu, Faculty of Medicine, Institute of Diagnostics, Department of Diagnostic Radiology; Oulu University Hospital

Acta Univ. Oul. D 1255, 2014

University of Oulu, P.O. Box 8000, FI-90014 University of Oulu, Finland

Abstract

The concept of resting state functional magnetic resonance imaging (fMRI) is built onto an original finding in 1995 that brain hemispheres present synchronous signal fluctuations with distinct patterns. fMRI measurements rely on blood oxygenation changes that indirectly mirror neural activity. Therefore, the origin of certain functional connectivity patterns, resting state networks (RSNs), has been a widely debated research question and numerous contributing factors have been identified. According to current understanding the fluctuations reflect maintenance of the system integrity in addition to spontaneous thought and action processes in the resting state. A popular method to study the functional connectivity in resting state fMRI is spatial independent component analysis (ICA) that decomposes signal sources into statistically independent components.

The dichotomy of functional specialization versus functional integration has a correspondence in fMRI studies where RSNs play the integrative viewpoint of brain function. Although canonical large-scale RSNs are broadly distributed they also express modularity that can be accomplished by ICA with a high number of estimated components. The characteristics of high ICA dimensionality are broadly investigated in the thesis. An enduring issue in resting state research has been the confounding noise sources like motion and cardiorespiratory processes which may hamper the analysis. In this thesis the ability of ICA to separate these noise sources from the default mode network, a major RSN, is studied. Additionally, the suitability of ICA for full frequency spectrum analysis, a relatively rare setting in biosignal analysis, is investigated.

The results of the thesis support the viewpoint of ICA as a robust analysis method for functional connectivity analysis. Cardiorespiratory and motion induced noise did not confound the functional connectivity analyses with ICA. High dimensional ICA provided better signal source separation, revealed the modular structure of the RSNs and pinpointed the specific aberrations in the autism spectrum disorder population. ICA was also found applicable for fully explorative analysis in both the spatial and temporal domains and indicated functional connectivity changes induced by transcranial bright light stimulation.

Keywords: BOLD, brain, fMRI, full frequency band, functional connectivity, ICA, model order, modularity, motion, physiological noise, resting state network

Starck, Tuomo, Dimensionalisuus, kohinaerottelu ja täyden taajuuskaistan näkökulmat itsenäisten komponenttien analyysiin lepotilan fMRI:ssä. ICA-tutkimuksia lepotilan fMRI:ssä
Oulun yliopiston tutkijakoulu; Oulun yliopisto, Lääketieteellinen tiedekunta, Diagnostiikan laitos, Radiologia; Oulun yliopistollinen sairaala
Acta Univ. Oul. D 1255, 2014
Oulun yliopisto, PL 8000, 90014 Oulun yliopisto

Tiivistelmä

Konsepti lepotilan tutkimisesta toiminnallisella magneettikuvauksella (engl. functional magnetic resonance imaging, fMRI) on rakentunut vuonna 1995 tehdylle löydökselle aivopuoliskojen välillä synkronisesta signaalivaihtelusta. Mittaukset perustuvat veren hapetuksen muutoksiin, jotka epäsuorasti heijastelevat hermostollista toimintaa. Tämän takia tietyt toiminnallisen kytkennällisyyden muodot, lepotilaverkostot, ovat olleet laajasti väitelty tutkimusaihe ja monia verkostoihin vaikuttavia tekijöitä onkin tunnistettu. Nykykäsityksen mukaan signaalivaihtelut lepotilassa heijastelevat järjestelmän yhtenäisyyden ylläpitoa spontaanin ajattelun ja toiminnan lisäksi. Suosittu menetelmä toiminnallisen kytkennällisyyden tutkimiseen lepotilan fMRI:ssä on spatiaalinen itsenäisten komponenttien analyysi (engl. independent component analysis, ICA), joka hajottaa signaalilähteet tilastollisesti itsenäisiin komponentteihin.

Aivotoiminnan mallintamisessa kahtiajaolla toiminnalliseen erikoistumiseen ja toiminnalliseen integraatioon on vastaavuus fMRI-tutkimukseen, jossa lepotilaverkostot vastaavat toiminnallisen integraation näkökulmasta. Vaikka kanoniset lepotilaverkostot ovat laaja-alaisia, ne ovat toisaalta modulaarisia, jota voidaan tutkia tutkimalla korkean komponenttimäärän ICA-hajotelmaa. Korkea- dimensioisen ICA-hajotelman ominaisuuksia tutkitaan laajasti tässä väitöskirjassa. Kestoaihe lepotilatutkimuksessa on ollut analyysiä hankaloittavien kohinalähteiden kuten liikkeen ja kardiorespiratoristen prosessien vaikutus. Väitöskirjassa tutkitaan ICA:n kykyä erotella kohinalähteitä ’default mode’ -verkostosta, joka on merkittävin lepotilaverkosto. Lisäksi tutkitaan ICA:n soveltuvuutta täyden taajuuskaistan analysointiin, joka on verrattain harvinaista biosignaalien analyysissä.

Väitöskirjan tulokset tukevat näkemystä ICA:n suorituskyvystä toiminnallisen kytkennällisyyden analyysissä. Kardiorespiratorinen ja liikkeestä lähtöisin oleva kohina ei häirinnyt merkittävästi ICA-tuloksia. Korkeadimensioinen ICA tarjosi paremman erottelun signaalilähteille, paljasti lepotilaverkostojen modulaarisen rakenteen ja määritti erityisen poikkeaman autismin kirjon oireyhtymän populaatiossa. ICA:n havaittiin olevan soveltuva täyseksploratiiviselle analyysille ajassa ja avaruudessa; tulos viittaa toiminnallisen kytkennällisyyden muutoksiin kallon läpäisevän kirkasvalostimulaation aikaansaamana.

Asiasanat: aivot, BOLD, fMRI, fysiologinen kohina, ICA, lepotila, liikeartefakta, mallin asteluku, modulaarisuus, toiminnallinen kytkennällisyys, täysi taajuuskaista

”Totuus paljastuu”
– vanha oululainen insinööriviisaus

Heidille sekä Tuoville ja Airalle

Acknowledgements

This thesis was made in the fMRI research group in Oulu University Hospital beginning in the end of 2005, while working in a medical physicist training program. Part of the time I was also working as a doctoral student at the Department of Diagnostic Radiology of Oulu University.

I want to express my greatest appreciation to the thesis supervisors MD PhD, Docent Vesa Kiviniemi and MD PhD, Professor Osmo Tervonen. It was their trust in me that opened the unexpected road to the world of brain research in hospital realm after my non-military service year in Oulu University Hospital in 2004-2005. In the beginning of my doctoral studies, the research field of so-called resting state fMRI was still relatively controversial, although ten years anniversary from the introduction in 1995 had already taken place. Docent Kiviniemi pioneered in this field already on the late 90's and due to his strong intuition and bold attitude, and Professor Tervonen's right questions and wise leadership, succesful research has carried on for so many years with such an impact on many people's lives. I have been priviledged to see the rise of the resting state fMRI research to its full extent.

I want to thank my chief in hospital work, Professor Miika Nieminen, for enduring support under the medical physics training program for the thesis process that at times appeared to be a moving goal.

I want to warmly thank my research fellows who have given great support during the long thesis project and been there for valuable discussions, about off-topic matters too. Especially I would like to thank PhD Jukka Remes, the master in ICA mathematics, for his pieces of advice keeping my analyses on the right track. PhD Ahmed Abou Elseoud I want to thank for fruitful co-operation in search of the essence for resting state networks. Docent Juha Nikkinen I wish to thank for all the research help during the long road. PhD Marianne Haapea I want to thank for guiding me in the jungle of statistical methodology, and at certain statistical issues I would have benefited by asking sooner.

Important impact for the resting state fMRI research has been contributed by the North Finland Birth Cohorts 1966 and 1986, from where well characterized study populations has been scanned using MRI. Two fMRI related psychiatric study projects, under the two birth cohorts 1966 and 1986, have been managed by Professor Matti Isohanni and Professor Juha Veijola, respectively. With their support we have been able to scan impressive amount of resting state datasets, and investigate timely issues of resting state fMRI.

People behind the special study of the thesis, light stimulation of the brain via ear canal, deserve a special acknowledgement. Valkee founders MSc Juuso Nissilä and MSc Antti Aunio, you certainly made the scientific life more interesting. In the same vein I would like to acknowledge PhD Timo Takala and Professor Markku Timonen for their efforts related to the project.

For the fMRI study on autism spectrum disorders, great effort has been devoted by many researchers of child psychiatry and psychology. Professor Irma Moilanen merits special acknowledgement in this regard, as well as co-authors MD Jukka Rahko, Docent Tuula Hurtig, PhD Helena Haapsamo, MSc Katja Jussila, PhD Sanna Kuusikko-Gauffin, PhD Marja-Leena Mattila, Docent Eira Jansson-Verkasalo, Professor David L. Pauls and Professor Hanna Ebeling.

I would like to thank the reviewers of the thesis manuscript, Docent Iiro Jääskeläinen and Docent Ricardo Vigário, for thorough work and excellent suggestions that improved the thesis. PhD Nick Hayward is thanked for language correction.

During the years, the research corridor in the former MRI unit has been an important social environment to meet colleagueas and research fellows. I want to thank you all the previous and present corridor inhabitants for the good working atmosphere in both science and medical physics. I wish to also thank the nice personnel of MRI unit, and all other röntgen units too, for the many common years. I want to express warm thanks to the hospitable personnel of the clinical neurophysiology department, who have given me space and time to finish my doctoral duties. Thanks to several secretaries, especially Leila Salo, for their help in so many issues that can come across.

From the era before doctoral studies, I wish to acknowledge the supervisors of my master's thesis. Professor Juha Röning and Professor Veikko Seppänen from the Department of Electrical Engineering of Oulu University steered my MSc thesis professionally and positively influenced the coming doctoral studies. I wish to also thank personnel from Ericsson, Microcell and Flextronics for their support during my MSc studies.

Besides Oulu University Hospital and Oulu University financing the present thesis, I would like to acknowledge the Finnish Radiological Society for their financial support for my PhD thesis.

My warmest thanks are addressed to my parents, Sinikka and Lasse, who have supported me and us during all these 30 years of studying. We will come to visit you more often, with children Tuovi and Aira, during the postdoc era.

Finally, my deepest love and gratitude is devoted to my beloved wife Heidi, who has had to carry a great share of my family duties while I was giving birth to the thesis. Afterall, I did this for all of us.

June 2014 Tuomo Starck

Abbreviations

ANS	autonomic nervous system
ASD	autism spectum disorder
ATP	adenosine triphosphate
B_0	main magnetic field
BOLD	blood oxygen level dependent
BSS	blind source separation
CBF	cerebral blood flow
CBV	cerebral blood volume
$CMRO_2$	cerebral metabolism rate of oxygen
CO_2	carbon dioxide
CSF	cerebrospinal fluid
DMN	default mode network
EEG	electroencephalography
e.g.	exempli gratia
EPI	echo-planar imaging
FA	flip angle
FC	functional connectivity
FNC	functional network connectivity
fMRI	functional magnetic resonance imaging
FSPGR	fast spoiled gradient echo
GABA	gamma-amino butyric acid
GICA	group independent component analysis
GLM	general linear model
GM	grey matter
HRV	heart rate variability
HRF	hemodynamic response function
ICA	independent component analysis
i.e.	id est
i.i.d.	independent and identically distributed
IPL	inferior parietal lobule
LFP	local field potential
LFF	low frequency fluctuation
MEG	magnetoelectrography
mPFC	medial prefrontal cortex
MR	magnetic resonance

MUA	motor unit activity
PCA	principal component analysis
PCC	posterior cingulate cortex
PCUN	precuneus
PDF	probability density function
PET-CO_2	end-tidal partial pressure of carbon dioxide
PICA	probabilistic independent component analysis
PI	parallel imaging
RETROICOR	retrospective image-domain correction
RF	radio-frequency
RRF	respiration response function
RSN	resting state network
RV	respiration variability
RVHRCOR	respiration variation heart rate correction
RVT	respiration volume per time
SCA	seed correlation analysis
SCP	slow cortical potential
SRS	social responsiviness scale
T1	spin-lattice magnetization relaxation time
T2	spin-spin magnetization relaxation time
*T2**	*T2* star
TE	time to echo i.e. echo time
TFCE	threshold free cluster enhancement
TPN	task positive network
TR	time to repetition i.e. repetition time
VIS	visual cortex network
WM	white matter

List of original publications

This thesis is based on the following publications, which are referred throughout the text by their Roman numerals:

I Starck T, Remes J, Nikkinen J, Tervonen O & Kiviniemi V (2010) Correction of low-frequency physiological noise from the resting state BOLD fMRI-Effect on ICA default mode analysis at 1.5T. J Neurosci Methods 186(2): 179–185.

II Abou Elseoud A, Starck T, Remes J, Veijola J, Nikkinen J, Tervonen O & Kiviniemi V (2010) The effect of model order selection in group PICA. Hum Brain Mapp 31(8): 1207–1216.

III Starck T, Nikkinen J, Rahko J, Remes J, Hurtig T, Haapsamo H, Jussila K, Kuusikko-Gauffin S, Mattila M-L, Jansson-Verkasalo E, Ebeling H, Moilanen I, Tervonen O & Kiviniemi V (2013) Resting state fMRI reveals a default mode dissociation between retrosplenial and medial prefrontal subnetworks in ASD despite motion scrubbing. Front Hum Neurosci 7: 802.

IV Starck T, Nissilä J, Aunio A, Abou-Elseoud A, Remes J, Nikkinen J, Timonen M, Takala T, Tervonen O & Kiviniemi V (2012) Stimulating brain tissue with bright light alters functional connectivity in brain at the resting state. World J of Neurosci 2(2): 81–90.

Table of contents

Abstract
Tiivistelmä
Acknowledgements **9**
Abbreviations **13**
List of original publications **15**
Table of contents **17**
1 Introduction **19**
2 Review of the literature **21**
2.1 Imaging physics for functional magnetic resonance imaging 21
2.1.1 Principles 21
2.1.2 Scanner related artefacts in fMRI 23
2.2 Blood oxygen level dependent fMRI in resting state 24
2.2.1 BOLD signal and contrast 24
2.2.2 BOLD signal fluctuations 29
2.3 Functional connectivity patterns 32
2.3.1 Stable and dynamic properties 34
2.3.2 Structural and functional connectivity 37
2.3.3 Resting state vs. stimulus-induced activity 38
2.3.4 Electrophysiological correlates 39
2.3.5 Rapid dynamics of the functional connectivity 41
2.4 Independent component analysis for BOLD fMRI 42
2.4.1 Spatial ICA principles 43
2.4.2 ICA approaches for fMRI data 46
2.4.3 ICA performance 48
2.5 Correcting for structured noise 52
2.5.1 Cardiorespiratory signal sources and removal 52
2.5.2 Motion related signal changes and removal 55
2.5.3 General methods for noise correction 59
2.5.4 Imaging based methods 60
2.5.5 Data-driven methods for de-noising 62
3 Aims of the study **63**
4 Participants and methods **65**
4.1 Participants 65
4.2 Imaging 66
4.3 Data pre-processing 68

4.4 Data analysis 70
5 Results **75**
5.1 Physiological noise correction of the ICA default mode network 75
5.2 Effect of ICA dimensionality on the resting state networks 76
5.3 Multi-dimensional ICA view on DMN hypoconnectivity in autism spectrum disorders and the effect of rigorous motion correction 79
5.4 Full frequency band ICA-approach for transcranial bright light stimulation 81
6 Discussion **83**
6.1 Separation of spurious signal sources with ICA (I-IV) 83
6.2 Effect of ICA dimensionality on RSN modularity (I-III) 85
6.3 Other considerations on ICA methods 87
6.4 Considerations on resting-state measurements 88
6.5 Future directions 89
7 Conclusions **91**
References **93**
Original publications **113**

1 Introduction

Functional connectivity (FC) is defined as statistical dependencies among remote neurophysiological events (Friston 1994) and can be used to characterize spatiotemporal dynamics of various neurophysiological time-series. For a long time mainstream functional magnetic resonance imaging (fMRI) dealt with controlled stimulations or tasks that were paced with resting state periods for purposes of generating signal contrast. Resting state was considered a low-level baseline characterized by unorganized background activity (Binder2012). However, distant signal dependencies in resting state blood oxygen level dependent (BOLD) fMRI were introduced in 1995 in a seminal study (Biswal *et al.* 1995) showing temporally correlated slow signal fluctuations between bilateral motor cortices. Following the introduction of the resting state concept, more inter-hemispheric correlations were detected (Lowe *et al.* 1998) and later several canonical resting state networks (RSNs) have been revealed (Beckmann *et al.* 2005). In retrospect, the old viewpoint of the brain as a mainly reflexive system seems overly mechanistic.

Resting state FC remained controversial for over 10 years (Birn 2012) as it was suspected to present scanner instabilities or aliased cardiorespiratory fluctuations due to low sampling rates. The extent of scanner related fluctuations in BOLD fMRI signal varies between scanners and at worst they could be mistaken as resting state brain activity (Smith *et al.* 1999). On the other hand, especially the cardiac fluctuations occur on higher frequencies than what can be unambiguously resolved by typical fMRI and the cardiac signal alias across the whole frequency band of the observed time-series (Lund *et al.* 2006). Additionally, the low frequency fluctuations in cardiorespiratory rhythms can be mistaken for distributed synchronous activity (Birn *et al.* 2006). Another more recent concern for the validity of resting state fMRI is motion that induces spurious FC measures. Relatively small head movements can cause hypo- or hyperconnectivity between distant brain regions (Power *et al.* 2012).

A popular exploratory analysis technique in fMRI is data-driven independent component analysis (ICA) that is inherently suitable with the exploratory and uncontrolled nature of resting state experiments. Spatial ICA decomposes the image time-series into components by maximizing the statistical independence between the components. Resulting three dimensional (3D) maps and their corresponding time-courses form a linear combination of the original data. Already early in fMRI research ICA was used to reveal task-related activity

(McKeown *et al.* 1998) and later it was applied for resting state studies in anesthetized children (Kiviniemi *et al.* 2003) and awake adults (Greicius *et al.* 2004). Even though ICA results are always accompanied with separate motion artefact and physiological noise components, these have not been an evidence for the non-artifactual nature of the detected RSNs. Another important aspect is ICA dimensionality that is the number of resolved independent components, which is a user-defined free parameter if automatic estimation is not used. Especially in group ICA, this has a prominent effect on RSN division, and use of high dimensionality and the ensuing fine-grained functional parcellation of the RSNs (Kiviniemi *et al.* 2009) are further explored in this thesis. Apart from noise separation and dimensionality viewpoints, the applicability of ICA for studying full frequency band data is studied in the thesis.

2 Review of the literature

2.1 Imaging physics for functional magnetic resonance imaging

2.1.1 Principles

Magnetic resonance imaging (MRI) (Lauterbur 1973) rests upon nuclear manipulation by electromagnetic waves. A nucleus of interest is the proton of hydrogen that is abundant in living tissue. The proton has a positive charge and is in constant rotational movement that induces a magnetic field, or magnetic moment, thus giving an elementary magnet known as spin. In the presence of an external magnetic field the protons tend to align according to the field direction with two possible quantum states (parallel and opposite) with different energies. However, the magnetic moment vector is always tilted from the external field direction and precesses around this axis with a nuclei specific Larmor frequency (63 MHz at 1.5 T) according to the Larmor equation

$$f = \gamma B_o \tag{1}$$

where γ denotes the nuclei specific gyromagnetic ratio and B_0 is the magnetic field strength. The spin state can be altered by absorption or emission of electromagnetic radiation on the Larmor frequency. The distribution between states obeys the Boltzmann distribution that yields only 10 parts per million excess occupation in the parallel state at 1.5 T but enough to produce net magnetization aligned with external magnetic field B_0. By operating on this net magnetization the principles of classical mechanics can be utilized and the magnetization can be manipulated on the Larmor frequency to tilt the precession to the transversal direction creating an alternating magnetic field which can be received by the RF-coil where a corresponding alternating electric current is induced.

The oscillating precession signal from the excited net magnetization fades away exponentially based on two main relaxation mechanisms. Relaxation process *T1* corresponds to recovery of initial thermal equilibrium state of longitudinal net magnetization by emission of the absorbed RF-energy to the environment. The other relaxation *T2* is due to accumulating phase incoherence of the net magnetization in the transversal direction. Spin de-phasing occurs due to differences in experienced magnetic field between spins leading to different

precession frequencies and increasing phase differences. Differences in the experienced magnetic fields can arise from interactions with neighbouring spins (spin-spin relaxation) or from static field inhomogeneities, which together form *T2** relaxation. MRI acquisition parameters dictate the contribution of different relaxation mechanisms and as tissues present different relaxation properties images with the required brightness and tissue contrast can be obtained. The main contrasts are *T1*, *T2* and proton density. In BOLD fMRI the *T2** weighting of the image is of interest, which can be obtained with a gradient-recalled-echo sequence.

MRI with gradient-echo pulse sequences begins with transmit coil generated RF excitation of the net magnetization to the transversal plane (90 degrees) or to another desired flip angle (FA). The imaging plane is of desired slice thickness defined by RF pulse bandwidth and amplitude of the slice-selection magnetic field gradient. Then the 2D MR images can be created by modulating spin precession phase and frequency in a controlled fashion with magnetic gradient coils. The dimensions are manipulated sequentially; first the spin phases across the phase encoding (PE) direction are modified by modulating the spin frequency for a short time with a field gradient. Simultaneously, orthogonal frequency encoding (FE) gradient is turned on and reversed in direction after the PE is turned off. Reversing the FE gradient direction results in gradient echo formation when the spins realign. The signal echo is collected while the FE gradient is still turned on. In single-shot echo-planar imaging (EPI) (Mansfield 1977) fMRI this cycle is repeated for a range of PE gradient moments without additional RF excitations before the net magnetization vanishes due to *T2* relaxation. In-plane matrix size and field of view (FOV) define the in plane resolution for the volume element (voxel). This procedure is carried out for a defined number of imaging slices in order to cover whole brain volume and after acquisition of all slices the imaging continues again from the first slice at a set repetition time (TR).

Pulse sequences are designed to collect RF signal on all applicable spatial frequencies yielding signal “k-space”. The acquired signal shares contribution from the whole excited volume and represents frequency domain information. Furthermore, k-space data is complex-valued consisting of frequency and phase and is in the form applicable for inverse Fourier transformation. Image formation by means of Fourier transformation yields spatial domain representation of the image with magnitude and phase parts although usually only the magnitude images are taken into consideration.

Relevant for modern fMRI, acquisition acceleration is achieved by means of parallel imaging, which deploys a number of receiver coils for simultaneous signal detection with spatial weighting according to coil position. This allows for a reduced number of sampled PE steps even though this leads to spatial signal aliasing. In the image domain reconstruction methods used in this thesis the aliasing is corrected by taking into account the sensitivity maps acquired before the fMRI scan.

2.1.2 Scanner related artefacts in fMRI

Fast imaging comes with a price of deteriorating image quality. In EPI there is a multitude of artefacts that can originate from suboptimal acquisition parameters or from failed scanner hardware or software, not to forget about the many complex ways the human subject can interact with the magnetic field that is always inhomogeneous to some extent. Only a couple of the most prominent MRI artefacts related to EPI fMRI are mention in the following. The major problems for image quality are distortion and dropout. Local distortions occur in the brain regions near air filled sinuses producing high magnetic susceptibility gradients that alter the expected resonant frequency. Distortions occur in the PE direction where acquisition bandwidth is low i.e. sampling is slow during one RF excitation of the slice. Parallel imaging (PI) can be deployed to speed up the signal acquisition, which at same time reduces distortions in the PE direction. One other major artefact is the signal dropout that is also caused by the same magnetic susceptibility gradients in the same brain regions. Gradient echo sequences are sensitive to the inhomogeneity of the B_0 field that causes rapid dephasing of the spins within a voxel and therefore loss of MR signal. Signal dropout could be alleviated with shorter TE but then the BOLD signal of interest would be lower on the other parts of the brain. If the scanner facilitates automatic shimming, this will markedly diminish the magnetic field inhomogeneities and alleviate the described image artefacts.

Instrumental instability is a common problem in measurement systems and in EPI fMRI it is largely related to the heat-intensive operation of imaging gradients that typically requires water cooling. Much heat is generated through mechanical vibrations of the gradient coils due to Lorentz forces resulting from electrical current through a magnetic field (Foerster *et al.* 2005), as well as from electrical resistance contributing to heating (El-Sharkawy *et al.* 2006). Importantly, if passive iron shims are used for inhomogeneity correction of the magnetic field,

eddy currents are induced by altering magnetic fields during imaging. Temperature affects the magnetic susceptibility of iron and the thermal expansion coefficient is large, thus the fact that these shims are not actively cooled makes the B_0 field slightly unstable. Heating and cooling processes together make it difficult to achieve steady state operating conditions during EPI fMRI (Foerster *et al.* 2005). It has been shown that resulting magnetic field drifts are not only linear but possess a quadratic term, both spatially and temporally (El-Sharkawy *et al.* 2006). The effect is most pronounced in the z-direction, which is the direction of the bore. Such degradation processes of the field homogeneity result in frequency shifts and apparent movement and distortion of the object during imaging. The signal drifts are especially apparent in regions with large gradients of image intensity (Bandettini *et al.* 1993). Even fat saturation pulses that are used to remove chemical shift artifact signal from fat have been found to induce signal fluctuations within EPI fMRI time-series in the presence of B_0 drift (Shimada *et al.* 2010).

2.2 Blood oxygen level dependent fMRI in resting state

Fluctuations of resting state BOLD fMRI signal started to gain wide interest after they were shown to present functional connectivity across hemispheres (Biswal *et al.* 1995). In the following, the nature of BOLD signal is presented before going into patterns of functional connectivity in the next section.

2.2.1 BOLD signal and contrast

BOLD contrast arises from the magnetic properties of haemoglobin in particular; it is the paramagnetic deoxyhaemoglobin that has positive magnetic susceptibility that enhances the local magnetic field and shortens the *T2** relaxation time of the MR signal in the capillary and venous blood. At first glance, this could be expected to lead to a decreased signal, as more oxygen is metabolized after an increased neural activity requiring higher energy supply. In reality, there is an oversupply of fresh oxygenated blood (functional hyperemia) delivered to the activation site which increases the cerebral blood volume (CBV) and decreases the proportion of deoxyhemoglobin in downstream venules (Fox and Raichle, 1986). This increased local cerebral perfusion of oxygenated blood flow (CBF) exceeding the increased oxygen metabolic rate ($CMRO_2$) increases the effective *T2** and gives rise to MR signal known as BOLD response (Ogawa *et al.* 1990).

Because over two thirds of the brain blood is located within the capillaries and venules of the microvasculature, the measured *T2** signal is thought to reflect the regional deoxygenation state of the venous system. The main determinant of the decrease in deoxyhemoglobin is the increase in blood velocity and thus an outwash effect, no recruitment of capillary reserves have been found to contribute to BOLD effect (Villringer, 2012). The venules are the most important signal source for BOLD signal (Frahm *et al.* 1994). Haemoglobin volume in the brain is only a few percent, but because the range of magnetic susceptibility is greater the *T2** induced image intensity increase can reach 10% for a task activation.

Given a task or stimulus, a typical BOLD response is characterized by a peak around 4–6 seconds after the neural response. Also, it is further accompanied with an initial negative dip preceding the peak and an undershoot following the peak. Early descriptions regarded the BOLD response largely as a unitary phenomenon acting as a hemodynamic filter for often vaguely defined neural activity (Buxton, 2012). The physiological basis under the hemodynamic BOLD response, the neurovascular coupling, is still a subject of research. The debate concerns especially the types of neuronal activity that lead to BOLD signal changes and which transmitters and messengers mediate the neurovascular coupling. Traditionally the energy consumption related to neuronal activity has been considered as a principal agent in inducing increased CBF, but current understanding points to other complex multi-factorial explanations (Fox 2012) where the excitatory neurotransmitter glutamate has a central role (Attwell *et al.* 2010). In order to model CBF, $CMRO_2$ and CBV in a unitary manner a so called balloon model has been proposed (Buxton, 2012). The assumption in the model is that the CBF and $CMRO_2$ responses can be modelled as tightly coupled, but based on recent research this has not been proven possible. Instead, a parallelism of hemodynamic and metabolic response is now favoured that is possibly driven by different aspects of neural activity. This complicates the interpretation of the BOLD signal and an additional specific MR measurement sensitive to blood flow may be required in some studies. Further, additional CBF measure does not suffice in case of the altering volume fraction of CBF, since concomitant CBV changes also modulate the BOLD signal. Moreover, one must keep in mind that BOLD contrast is a relative measure and does not provide useful information about a physiological baseline. Regional and inter-individual variations of the BOLD response also pose challenges for interpretation.

Neurogenic origin of the BOLD signal

Based on measurements of the sensory cortex, evidence supports a connection between BOLD and local field potentials (LFP) with tight coupling between gamma band power of LFP signals and BOLD signal response to a sensory stimulus (Logothetis *et al.* 2001, Niessing *et al.* 2005, Shmuel *et al.* 2006). LFPs are measured directly from the brain tissue with microelectrodes and reflect both excitatory and inhibitory post-synaptic activity, estimated to account for 74% of the brain energy budget (Attwell and Iadecola, 2002). Negative BOLD response has also been found to correlate with decreases in LFPs (Shmuel *et al.* 2006), supporting the view that the sustained negative BOLD response is the counterpart of reduced neural activity (Moraschi *et al.* 2012). In addition to post-synaptic activity, LFPs also measure dendritic afterhyperpolarization and intrinsic membrane oscillations (Logothetis 2003). LFP as a combination of above activities can be described to reflect peri-synaptic activity (Ekstrom, 2010) whereas multi-unit activity (MUA) reflects neuronal spiking activity and action potentials. The spiking activity has been found to occasionally correlate with LFP (Heeger *et al.* 2000), but most often action potentials and spiking activity present dissociation from regional CBF and BOLD (Lauritzen *et al.* 2003). LFP can be thought of as a measure of synaptic input into a region, whereas spiking activity can be thought of as the output of a region (Logothetis 2003). Indeed, the BOLD signal seems to present the input to neuronal population as well as the intrinsic processing of the population (Lauritzen *et al.* 2005). In typical measurements the BOLD signal cannot be assumed to reflect spiking activity although this has frequently been assumed as an explanation for the detected BOLD responses in diverse fMRI studies (Logothetis 2008). Although there are numerous studies reporting dissociations between BOLD, electrophysiological measurements and metabolic measurements the BOLD-LFP model is firmly established in the neocortex (Ekstrom, 2010). Recent evidence suggests the neural inhibitory activity to be a primary driver for the dissociation of spiking activity from LFP and metabolic measurements (Li and Freeman, 2013). The additional models explaining the dissociations relate mostly to local differences in neural circuitry and in vascular properties.

From systemic a perspective, the neurogenic origin of the BOLD signal is primarily affected by changes in the excitation-inhibition balance (Logothetis 2008). The effect of the excitation-inhibition balance has been shown in the visual cortex where inhibitory neurotransmitter GABA concentration diminished the

BOLD response (Muthukumaraswamy *et al.* 2009). This balance is determined within excitation-inhibition networks (Logothetis 2008), or canonical microcircuits, that by the event of activation set in a sequence of excitation and inhibition in every neuron of the module. Thus the microcircuits form complex feedback loops, which is in contrast to the simple idea of sequential activation of separate neurons. Then again, the excitation-inhibition balance is largely determined by neuromodulative processes which act electrophysiologically via a volume transmission mechanism i.e. the extracellular fluid acts as a communication media. This is clearly a more diffuse and broader way of communication compared to neurotransmission, where neurotransmitters bind directly to receptors coupled to ion channels (Logothetis, 2008). Overall, there is plenty of evidence that BOLD signal does not differentiate between function-specific processing and neuromodulation, or either between bottom-up and top-down signalling in the functional hierarchy. Moreover, excitation and inhibition are likely to get mixed in the BOLD signal since inhibitory neural activity may decrease BOLD signal depending on the microcircuit configuration. Although the BOLD signal has been stated neurogenic at all times despite of all ambiguities (Logothetis, 2008) there are recent discoveries of study conditions under which the hemodynamic BOLD response component cannot be explained by traditional evoked response characteristics (Cardoso *et al.* 2012). It seems the top-down control of the brain hierarchy is able to drive the hemodynamic BOLD response to an event that is not delivered but is anticipated by the subject.

Neurovascular coupling and energy consumption

The majority of the energy use in the brain goes towards the reversal of the ion fluxes underlying synaptic potentials and action potentials (Attwell and Laughlin, 2001). The cellular chemical energy transporter ATP (adenosine triphosphate) in the brain is almost entirely produced by oxidative glucose metabolism where glycolysis is followed by oxidative phosphorylation. It has been recently found that at the onset of increasing neural activity oxidative phosphorylation powers the initial information processing (Hall *et al.* 2012) in contrast to an established view that glycolytic ATP production would be responsible for the initial energy supply (Hyder *et al.* 2006). During the course of continuing increased local neural activity the non-oxidative metabolism increases markedly but oxidative metabolism still corresponds to a dominant share of the energy supply (Lin *et al.* 2010). As there are no oxygen or glucose reserves in the brain the varying

physiological demands have to be maintained by sophisticated CBF control that reallocates the resources.

Neurovascular coupling in the microvasculature is the key process to control regional CBF by increasing the vessel diameter (vasodilation) in response to metabolic demands and synaptic transmission (Cauli and Hamel, 2010). Synaptically released glutamate is the major CBF regulator that signals for both neurons and astrocytes and gives rise to a signalling cascade leading to vasodilation by relaxation of the vascular smooth muscle cells (Attwell *et al.* 2010). Numerous processes are involved in the CBF control regarding the astrocytes: reciprocal signalling between neurons and astrocytes, concentration changes of metabolites and electrolytes, and change in vascular tone (Kowianski *et al.* 2013). Moreover, these processes are not independent of each other and it seems that the role of astrocytes in CBF regulation is currently still underestimated. Overall, the main factors of neurovascular coupling can be devided into vasoactive metabolites (e.g. lactate, oxygen), vasoactive ions (e.g. Ca^{2+}), neurotransmitters and –modulators (e.g. glutamate, gamma-aminobutyric acid (GABA)) and gliotransmitters (e.g. adenosine) (Kowianski *et al.* 2013). On the other hand, the neurovascular coupling model varies between stimulation conditions. In short, transient stimulation by vasoactive mediators produced by pyramidal neurons and interneurons are responsible for the CBF changes. However, with sustained stimulation the response is also considerably mediated by astrocyte-derived messengers (Cauli and Hammel, 2010). In resting state fMRI there are indications that the peak timing of the BOLD response following slow oscillations in neuronal activity is similar in both resting state and task-fMRI (Hyder and Rothman, 2010). Nevertheless, the contribution of different mediators of CBF control in resting state activity remains to be further studied.

Imaging parameters characterize BOLD signal

Some MRI acquisition parameters play a considerable role in defining the relative contributions of various signal sources. There has been a brain vs. vein – debate regarding the issue of GRE-EPI BOLD signal originating mainly from draining veins at 1.5 T magnetic field strength. The signal arises mainly from intravascular macroscopic susceptibility effects, instead from capillaries, in lower magnetic field strengths (Ogawa *et al.* 1993), which limits the spatial point spread function to around 3 mm in 1.5 T (Engel *et al.* 1997). The draining vein effect can produce additional BOLD activation in downstream veins (Gati *et al.* 1997) that may not

be a faithful representation of the primary activity site in brain parenchyma. However, this may not be a dramatic issue in typical 1.5 T studies where the imaging voxel size is larger than the point spread function. In order to improve the spatial specificity of the BOLD signal a higher magnetic field and longer echo time are advantageous, and also spin echo sequences that are not sensitive to intravascular effects may be used if the signal-to-noise ratio permits (Menon, 2012). Magnetic field strength and imaging parameters also affect the relative contribution of the physiological noise in the BOLD signal, the BOLD-like noise signal increases with higher field strength and decreases with voxel size (Triantafyllou *et al.* 2005). Voxel size dependency is related to changes in blood volume fraction in the imaging pixel due to vasodilation and vasoconstriction.

2.2.2 BOLD signal fluctuations

Assessment of the brain energy balance is illustrative for appreciating the significance of the fluctuations in ongoing brain activity, thought to be reflected in BOLD signal fluctuations. It is known that the brain's relative energy demand is ten times more than its portion of the weight (Clark and Sokoloff, 1999). However, regional blood flow induced by high demand tasks does not increase more than 5–10%. This is further alleviated by a very low increase (~1%) in local energy demand associated with low glucose utilization and even lower oxygen consumption (Raichle and Mintun, 2006). Furthermore, by magnetic resonance spectroscopy, 80% of the brain energy metabolism has been shown to relate to glutamate cycling (Sibson *et al.* 1997) and thus to neural signaling processes. This cost-based analysis points towards intrinsic neuronal activity of the brain operating on its own and interacting with any possible stimulation (Raicle and Mintun, 2006).

Fluctuation of the main BOLD factors

Already early physiological studies found spontaneous fluctuations in different parameters like in oxygen availability and CBF (Cooper *et al.* 1966). Nowadays the physiology underlying the task- or stimulus-evoked BOLD signal is regarded as rather well known but how the physiology differs in spontaneous BOLD fluctuations is an open issue. The numerous haemodynamic and metabolic factors contributing to BOLD signal have been found to fluctuate too (Obrig *et al.* 2000; Fox and Raichle, 2007). This regards for instance blood volume, blood flow,

oxygen availability, neurotransmitter levels and cytochrome oxidase activity that reflects neural metabolism. However, spontaneous electrophysiological activities and their relations to BOLD fluctuations have been of great research interest. Local correspondence has been repeatedly demonstrated between BOLD fluctuations and slow fluctuations (<0.1 Hz) in the high frequency gamma band (above 30–40 Hz) power of LFPs (Leopold *et al.* 2003; Lachaux *et al.* 2007; Schölvink *et al.* 2010). Measured BOLD signal may reflect the coordination of neuronal firing mediated by gamma oscillations (Fries *et al.* 2005). Intriguingly the slow fluctuations in LFP power were found to not only present local correlations with BOLD signal but they also exhibited similar correlation with almost the entire cortical surface (Schölvink *et al.* 2010). This links together the baseline neuronal activity and the global BOLD signal that has often been removed in fMRI analysis (Hyder and Rothman, 2010). The results also suggest that neurovascular coupling of spontaneous and stimulus-evoked BOLD signal is similar since hemodynamic delay to modulations in high gamma band power is in agreement with stimulus-related delays (Schölwinck *et al.* 2010). Additionally, the slow cortical potentials (SCPs) between 0.01 and 0.4 Hz, which seem to modulate the power of higher frequency activity, also present close correspondence to BOLD fluctuations (He and Raichle, 2009).

Neurotransmitter levels also contribute to the BOLD oscillations and to the interplay between distant brain regions as has been depicted in a recent study (Kapogiannis *et al.* 2013) mapping glutamate and GABA concentrations in the posteromedial cortex. It was shown that both neurotransmitters present significant positive correlation with the power of the BOLD oscillation.

Fluctuation of the non-BOLD signal sources

Besides functionally relevant sources for BOLD signal there is also a multitude of potential confounders. Periodic cardiac noise in BOLD signal has been thought to arise from several sources (Dagli *et al.* 1999): In-flow enhancement by fresh blood, dephasing of the phase coherence between spins due to flow, and pulsatory movement of vessels, brain tissue and CSF. Immediate respiratory-induced perturbations in the BOLD signal occur due to the moving chest wall and organs which modulate the static magnetic field with a dominant effect in global resonance frequency shift in the brain (Noll *et al.* 1994). There is also inferior-superior dependence in the field modulation caused by relative proximity to the chest (Durand *et al.* 2001). In single-shot EPI the resonance frequency changes

lead to positional shifts mostly in the PE direction (Raj *et al.* 2000). Respiration related true head motion is another source of BOLD signal fluctuation (Noll *et al.* 1994; Glover and Lee, 1995). An important factor for BOLD signal is carbon dioxide (CO_2), a by-product of glucose metabolism in the brain and a strong vasodilator leading to increased CBF. Arterial CO_2 levels are commonly found to oscillate due to respiratory feedback mechanisms like chemoreceptor regulation (Modarreszadeh and Bruce, 1994). Moreover, arterial blood pressure changes cause fluctuations in both respiratory and cardiac rates which again influence the BOLD fluctuations. Breathing alters the CBF also via intrathoracic pressure changes, which affects the heart rate (Berne and Levy 1993).

Another considerable factor in CBF oscillation is alteration of the vascular tone in response to blood pressure changes. The arterial and arterioral systems attempt to maintain a stable CBF by means of vasoconstriction and vasodilation processes but the delays in the autoregulation process cause CBF fluctuations. Arterial blood pressure and heart rate explain around one third of the fluctuation in oxyhemoglobin concentration (Katura *et al.* 2006) which also influences the BOLD signal fluctuations. Cerebral vascular tone is additionally related to vascular tone throughout the body, which exhibits low frequency fluctuations (LFF) called vasomotion (Aalkjaer *et al.* 2011), which would influence CBF. This fluctuation sometimes presents characteristic 0.1 Hz oscillation (Mayhew *et al.* 1996). However, the origin of vasomotion is not well known, although myogenic origin is suspected, and it is not certain if it is independent of fluctuations in cardiac, respiratory, blood pressure and arterial CO_2 concentration (Murphy *et al.* 2013). Another source of fluctuation in CBF, also present around 0.1 Hz, is the systemic oscillation of blood pressure called Mayer waves that are related to sympathetic nervous activity (Julien 2006). Interestingly, the systemic LFFs of total haemoglobin concentration measured from a fingertip has been shown to significantly correlate with resting state BOLD signal in brain regions of sensory modality i.e. sensorimotor, auditory and visual cortices (Tong *et al.* 2013).

BOLD as a broad band phenomena

The BOLD signal fluctuations possess the highest signal power at frequencies below 0.1 Hz due to inherent low pass filtering by hemodynamics. Very slow BOLD signal drifts below around 0.008–0.01 Hz are typically removed prior to analysis. However, the drifts bear also signals of physiological origin as these signals in grey matter (GM) share similar TE dependent properties as task-evoked

BOLD signal (Yan *et al.* 2009). The signal intensity level has also been shown to be modifiable by a vasoconstrictive drug (Bruhn *et al.* 2001). On the other end of the fMRI frequency spectra the recent advances in PI techniques have enabled investigation of intrinsic BOLD fluctuations on high frequencies. Results show there is also signal of interest above the typical frequency band between 0.01–0.1 Hz (Lee *et al.* 2013), thus indicating that the intrinsic activity is a wide band phenomena.

2.3 Functional connectivity patterns

Most part of the brain areas that show relatively high regional cerebral blood flow at rest (Raichle *et al.* 2001) also present a deactivation pattern in task-fMRI studies. This RSN is the so-called default mode network (DMN) (Greicius *et al.* 2003) (Fig. 1) that is thought to support core mental processes such as self-awareness (Gusnard *et al.* 2001) and conscious self-representation (Lou *et al.* 2004). Especially frontal and parietal lobes maintain higher cognitive functions and host RSNs like the DMN and task-positive network (TPN) that constitutes networks associated with functions like attention, salience processing and executive control. Other large scale RSNs include networks of varying sensory modality, visual, auditory and sensorimotor networks. Similar RSNs have been revealed with fMRI sequences sensitive to CBF (De Luca *et al.* 2006) and CBV (Miao *et al.* 2014). The RSN organization has been shown to be relatively reproducible across individuals, over repeated scanning sessions and between very different datasets (Fornito and Bullmore, 2010). On the other hand, network specific individual variations in FC patterns have been found to relate to personality traits (Adelstein *et al.* 2011). Also, practically all known neurological and psychiatric disorders have been shown to be associated with altered FC properties (Zhang and Raichle, 2010) and a wide variety of pharmacological substances have been shown to modulate the networks (Fornito and Bullmore, 2010). Behavioural performance for example in executive tasks (Seeley *et al.* 2007) and working memory tasks (Hampton *et al.* 2006) has also been shown to correlate with the strength of certain RSNs. In clinical utilization resting state fMRI holds a great promise in advances of pre-surgical functional mapping (Kokkonen *et al.* 2009) and outcome prediction (Castellanos *et al.* 2013).

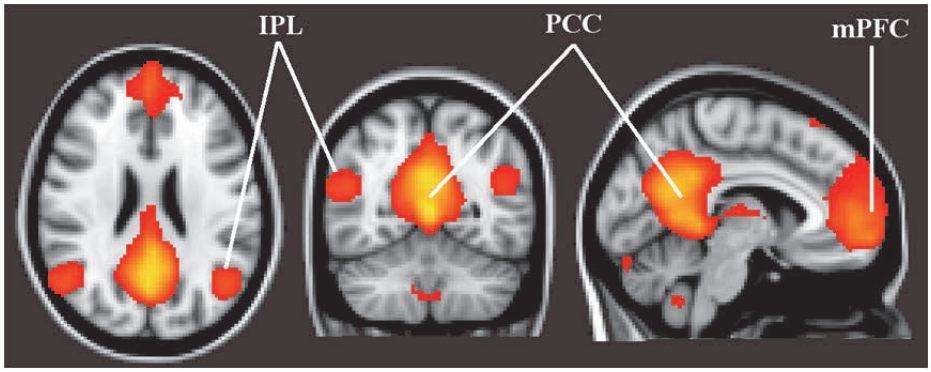

Fig. 1. The most prominent resting state network is the default mode network (DMN) that activates during the resting state. The core nodes of the DMN are posterior cingulate cortex (PCC), medial prefrontal cortex (mPFC) and bilateral inferior parietal lobule (IPL).

The functional brain imaging science has operated on the dichotomical axis of functional segregation and integration. Functional segregation, or specialization, is established as a fundament of the brain organization (Friston, 2009). In fMRI this is being mapped by means of stimulus induced responses. The functional connectivity studies on the other hand address functional integration and distributed information processing. As a whole, both principles of segregation and integration are implemented by dynamically reshaping networks that share a varying but consistent degree of interaction (de Pasquale *et al.* 2012). Consequently the distinction into separate RSNs is a rather limited representation of the modular organization. In fact the brain organization is well characterized by a so called small-world topology (Stam 2004) that demonstrates efficient node clustering and path length between nodes. In the brain the high clustering (i.e. modularity) supports the segregated functions and short path length between any nodes is compatible with integrated information processing. Central nodes in this organizational architecture are thought to serve to balance the pressure to evolve segregated pathways by integrating local networks and thus minimizing the cost of wiring and metabolism (Bassett *et al.* 2006).

Modularity or clustering of the brain functional organization can be expressed by RSNs that have been mapped with widely varying methods demonstrating the modularity continuum. A common comprehension is that there is no clearly optimal division into a certain number of networks. On the coarse level of clustering there are the negatively correlated intrinsic task-negative DMN system

and the extrinsic task-positive TPN system. They indicate two partially competing processes, such as internally and externally oriented cognition (Fransson 2005, Fox *et al.* 2005). Both the DMN related system and the TPN system obtained from resting state data can be further divided into numerous sub-networks which vary depending on the clustering technique and its parameters. Different clustering studies suggest varying optimal modularity levels but with less than ten modules the representation has been found to be stable (Meunier *et al.* 2009; He *et al.* 2009). Nevertheless, there are relatively stable hierarchical levels also with a higher number of modules. For instance with ICA, the resting state data have been demonstrated to parcellate even to more than 40 RSNs (Kiviniemi *et al.* 2009). With increasing accuracy of the clustering it has become evident that many brain regions of higher level information processing (e.g. DMN) are functionally connected to different networks at a time, whereas low level sensory cortices are clearly isolated (Yeo *et al.* 2013).

Current ideas on the dynamics of the brain activity fluctuations are centered on the one hand around criticality, which can be described as a transitional zone between ordered and disordered dynamics. Simulations have shown that RSN dynamics can be best modelled when the networks function near instability (Deco *et al.* 2013), which provides efficiency and flexibility for resource utilization on task demands. On the more in depth view of the brain dynamics the function of the brain can be described as being a statistical inference machine that constantly predicts and tries to explain its sensations (von Helmholz, 1867). The brain serves to update the information about the internal and external circumstances and use that information for making decisions about required actions (Friston 2010). The fundamental principle describing these actions is called free-energy principle, meaning that the brain attempts to minimize surprise. The key mechanisms of this internal model are the generated top-down predictions for sensory input and in case of error in the prediction the bottom-up control issues an update for the model (Friston 2010). In the rest of this chapter the aspects of FC are discussed from several standpoints that cast light to its relevance for brain function.

2.3.1 Stable and dynamic properties

The FC measures are known to present both stable and dynamic properties (Fornito and Bullmore, 2010). The stable properties stand for maintenance of the functional integrity and reflect brain organization. The alterations in stable properties would reflect changes in the underlying brain physiology. Dynamic

properties on the other hand could mirror the fast information processing, neuromodular mechanisms (Friston 2009). Overall, the static versus dynamic properties can be contemplated for instance from a developmental perspective, in light of different stages of consciousness and by correlating intrinsic fluctuations in resting state to measures of thoughts and cognition. Also, functional plasticity is an important aspect for the dichotomy between stable and dynamic.

Investigation of the different age populations has revealed brain functional connectivity representations of development and aging. In the infancy the brain functional architecture is wired to support perception-action tasks as reflected by location of functional hubs in the homomodal brain regions like auditory, visual and sensorimotor cortex. However, in adulthood the hubs reside in heteromodal association cortex (Fransson *et al.* 2011). In varying ways RSNs shape up especially during the third trimester of gestation (Doria *et al.* 2010), indicating their emergence before cognitive abilities. During childhood the DMN FC gradually integrates into a cohesive network like it appears in adulthood (Fair *et al.* 2008). As a general observation, from childhood to young adulthood the FC evolves from local to a distributed organization (Fair *et al.* 2009), by mechanisms of decreasing short-range connections and increased long-range connections. In aging from adolescence to middle age the process is partially reversed, manifesting as declining FC in a broad set of RSNs on both heteromodal and homomodal cortices (Littow *et al.* 2010). In the aging brain, a decline in connectivity of the RSNs has been a repeated finding, especially for the DMN (Andrews-Hanna *et al.* 2007, Damoiseaux *et al.* 2008). A neural origin of the activity decline has been confirmed by a simultaneous EEG-fMRI study (Balsters *et al.* 2013) that indicated several of the frontal RSNs to be affected. Indeed, prediction of the individual maturity from the FC analysis has been shown to be feasible with reasonable explanatory power (Dosenbach *et al.* 2010) although from spectral properties of EEG measurement the maturation can be depicted more accurately (Wackermann and Matousˇek, 1998).

Intriguingly, the RSNs are largely sustained also in sleep and anaesthesia. A general finding in fMRI studies of light sleep has been the preservation of the FC patterns (Horovitz *et al.* 2008, Larson-Prior *et al.* 2009) with minor reduction in connectivity strength (Samann *et al.* 2011). Consistent with the interpretation that the DMN reflects self-awareness the decoupling of the antero-posterior DMN connectivity relates to deep sleep (Horovitz *et al.* 2009, Samann *et al.* 2011). On the other hand, sleep deprivation (Samann *et al.* 2010) and light anaesthesia (Greicius *et al.* 2008) suppress the DMN connectivity. Then again anesthetized

children present increased synchrony in sensory RSNs (Kiviniemi *et al.* 2005). The patterns of BOLD signal connectivity in animals have been found to present highly similar connectivity to that of humans in the homologous areas, in anesthetized monkeys (Vincent *et al.* 2007) and in awake rats (Liang *et al.* 2011). In contrast to the results of sleep and anaesthesia studies in humans, anaesthesia was not found to relate to a decrease in long-range connections but showed a clear reorganization of the whole brain connectivity (Liang *et al.* 2012).

Intimately related to the question of stable vs. dynamic properties of the FC is the extent to which measured RSNs represent unconstrained cognition, whether conscious or not. The resting state is thought to reflect a free thinking state and measured RSNs, especially the DMN, are probably significantly related to the content of these thoughts (Mason *et al.* 2007). Indeed, the spontaneous activity of the DMN has been shown to be modulated by mind wandering, related to past or future considerations (Andrews-Hanna *et al.* 2010). One example of classifying the prevalent inner experiences are division into permanent sensory monitoring, seeing inner images, certain kinds of thought described as inner speech, feelings and unsymbolized thinking (Heavey and Hurlburt, 2008). The distribution of these categories varies highly between individuals. Importantly, although the inner thoughts have been shown to alter the RSN activity and synchronization, only a small fraction of the fMRI signal variance can be explained by them (Doucet *et al.* 2012).

Functional connectivity studies of brain plasticity have been scarce although varying training-induced changes have been shown with volumetric and structural connectivity measures. In fact, already two hour training in a car racing game was shown sufficient to induce structural changes in the hippocampus (Sagi *et al.* 2012) as measured by diffusion tensor imaging. Nevertheless, recently also a resting state fMRI study was able to determine brain plasticity during a three month preparation for the law school admission test that induced strengthening of the fronto-parietal FC (Mackey *et al.* 2013). Another excellent example of neural plasticity has been shown in congenitally blind people who recruit the brain regions typically allocated for spatial processing of visual information for spatial processing of sounds (Collignon *et al.* 2013). Also bilateral FC in the visual cortex during auditory tasks was significantly higher in congenitally blind vs. late-onset blind participants. This crossmodal plasticity occurs only if vision is lost during an early sensitive period, plasticity in the late-onset blind people relies more on the feedback loops on the heteromodal associative cortex.

2.3.2 Structural and functional connectivity

The resting state networks reflect the patterns of anatomical connectivity as measured with FC and diffusion tensor imaging based tractography (Greicius *et al.* 2008, Hagmann *et al.* 2008). Also reflecting anatomical connectivity, distinct FC patterns have been found from structurally and functionally different nuclei of the amygdala (Roy *et al.* 2009). However, a lack of anatomical connection does not constrain the FC (Vincent *et al.* 2007). The relation of the functional to structural connectivity has been studied with patients with deficits in brain anatomy (Uddin *et al.* 2008, Johnston *et al.* 2008), but these case studies where single patient underwent a split-brain operation for intractable epilepsy are a slightly contradictory. However, a conclusive study (Tyszka *et al.* 2011) shows intact bilateral FC in participants with a complete callosal agenesis, a birth defect, which indicates that the structural connectivity is not a necessary prerequisite for FC. Instead the results suggest that functional networks emerge with the development of normal cognition. Current advanced model on the relation between structural and FC suggest that deterministic anatomy facilitates certain functional networks but instantaneous functional patterns reflect the exploration of all possible configurations around the anatomical skeleton (Deco *et al.* 2013). In this model the essential elements for spatiotemporal FC patterns are local dynamics, information transmission delay and noise, that serve the purpose of efficiency and speed of network mobilization for action or other demand.

The view on the relation between structural and functional connectivity has been that there is no reciprocity, i.e. structural connectivity is highly indicative of functional connectivity but not vice versa (Honey *et al.* 2009, Vincent *et al.* 2007). Recent whole brain study firstly found long-range intrahemispheric structural properties that support FC changes in attention and memory related task-fMRI (Hermundstad *et al.* 2013). However, the same study reliably identified long-range intrahemispheric structural properties that could be inferred from FC changes in attention and memory related task-fMRI compared to rest (Hermundstad *et al.* 2013). Moreover, in another study the power of the FC during a task was found to deviate more from structural connectivity than during rest (Baria *et al.* 2013).

2.3.3 Resting state vs. stimulus-induced activity

Functional connectivity and task activation MR signal changes appear to arise from the same BOLD-related origins (Peltier and Noll, 2002). This was shown with multi-echo data where both FC and BOLD activation modulated the transversal magnetization signal ($T2^*$) but not the spin density signal (S_0). Also, the task-fMRI responses have been found to possess a voxel-wise positive linear relationship with the resting state BOLD fluctuations, thus they are thought to share similar physiological origins (Hyde *et al.* 2001; Kannurpatti *et al.* 2012). It has been proposed that BOLD FC patterns may be partitioned into two conceptual layers (Fransson, 2006), one consisting of stimulus-induced activity as well as unconstrained cognition and conscious mentation, the other reflecting the spontaneous intrinsic activity more closely reflecting the underlying anatomy. Indeed, an emerging view, especially regarding neural activity, is that separation of the ongoing and evoked activity is not well grounded (Raichle 2011).

Analysis of task-fMRI, with a general linear model, is based on the assumption that activity in task and control conditions sums linearly, which implies that task and control condition do not influence each other, that is a concept known as pure insertion. The assumption has been shown not to hold (Friston *et al.* 1996) and the view is that the measured brain activity represents a dynamic system whose activity is influenced by the previous activity. With varying methods it has been shown how resting state activity and stimulus-induced activity influence one another (Northoff *et al.* 2010). An influential study (Fox *et al.* 2006) of the relationship between resting state and task-related activity investigated the contribution of spontaneous BOLD fluctuations to unilateral motor event-related responses by taking contralateral spontaneous BOLD signal into account. It was found that the contralateral activity, although not a fully independent measure (Sadaghiani *et al.* 2010), explained a considerable proportion of the response variability. Thus, the result indicated approximately linear superposition of task-evoked neuronal activity and spontaneous BOLD signal. However, the model of linear superposition has not been found to hold on all brain areas (Becker *et al.* 2011). The picture of the relationship has lately been complemented with evidence pointing to certain negative interaction between the baseline of spontaneous activity and following stimulus-induced activity (He, 2013): higher prestimulus baseline results in decreased activation (or increased deactivation). The result is that BOLD signal variability in the directly related brain region is diminished during task execution.

The behavioral significance of the varying prestimulus brain activity level for a task performance has been shown in a somatosensory detection task near the perceptual threshold (Boly *et al.* 2007). It was found that higher activity in brain areas encompassing the task-positive network predicted perception of the stimulus, whereas higher activity on the main nodes of the default mode network predicted missed stimulus detection. However, this principle does not generalize to other task circumstances, the way certain networks predict the behavioural outcome are very context specific (Sadaghiani *et al.* 2009).

2.3.4 Electrophysiological correlates

Electrical activity of the brain is most often measured on the scalp with electroencephalography (EEG) that is a summation of local field potentials (LFPs). Correspondence of spontaneous electrical activity to the RSNs revealed with fMRI has been a subject of challenging research which has shown that high temporal correlations between electrical and BOLD signals cannot be obtained (Leopold and Maier, 2012). However, very high spatial concordance between spontaneous electrical activity patterns and fMRI RSNs has been found with magnetoencephalography (MEG) that measures magnetic fields associated with electrophysiological brain activity (Brookes *et al.* 2011). The electrophysiological basis of BOLD FC patterns has been studied with patients undergoing pre-surgical fMRI monitoring and intracranial LFP recordings. Evidence from these local measurements has accumulated that interhemispheric synchronous gamma band oscillations are a significant neural basis for BOLD connectivity (Nir *et al.* 2008; He *et al.* 2008). The power of high frequency activity on the gamma band shows spatial correspondence to BOLD fMRI only during awake and rapid-eye-movement sleep (He *et al.* 2008). With whole brain MEG measurements, however, low and mid-range frequencies are found to form the FC patterns (Hipp *et al.* 2012; Ghuman *et al.* 2013). On the other hand, SCPs have been found to present spatial patterns of coherent activity comparable to BOLD fMRI networks across broadly different levels of consciousness including even anaesthesia (Breshears *et al.* 2010).

High frequency oscillations shown to be related to FC patterns in BOLD have the property that relative phase between distal regions of these synchronous oscillations is near zero (Roelfsema *et al.* 1997, Nikouline *et al.* 2001). This cannot be facilitated by typical neural communication mechanisms that have non-zero lag (Lord *et al.* 2013). It has been suggested that slow oscillations would be

coordinating activity across longer distances (von Stein and Sarnthein, 2000) which is consistent for instance with local synchronization in the high frequency band. However, current understanding of the spatial coordination is more complex and it is concluded that single frequency bands are not driving the BOLD signal (Whitman, 2013). Although, for instance, somatosensory and auditory cortices seem to have their own preferred frequency bands for synchrony, similar in intrinsic and task evoked activity (Ghuman *et al.* 2013), it is the full band frequency activity working in concert to connect the distant regions of networks (Whitman, 2013). Converging evidence points to phenomena called cross-frequency coupling that manifests as high-frequency activity modulated by slow oscillations (Wang *et al.* 2012). Slow oscillations (SCPs and their BOLD representation) are thought to be fluctuations of cortical excitability (Vanhatalo *et al.* 2004) that have marked effects on the measured spectrum of electrical activity (Lakatos *et al.* 2005). The mechanism works step-wise from SCP frequencies to the highest frequencies by phase-amplitude dependency between frequency bands. The amplitude of the higher frequencies is dependent on the phase of the lower frequency oscillations and this relationship between frequency bands forms the so-called nested oscillations (Monto *et al.* 2008). The cross-frequency phase-amplitude coupling is always present in the brain activity even though brain activity is always arrhythmic (or scale free) (Chialvo 2010). The scale free brain activity can be described by 1/f spectral property, where power is inversely proportional to frequency, which is a ubiquitous property in complex systems. Also, the BOLD signal of the brain exhibits scale-free spatiotemporal connectivity patterns (Equiluz *et al.* 2005). Altogether the scale-free activity might be a unifying concept for spontaneous brain activity and behavior (He *et al.* 2010, Palva *et al.* 2013). Parameters describing scale-free behavior of the long range temporal correlations, and those describing rapid cascades of neural activity called neuronal avalanches, are highly correlated with each other and with behavioral performance (Palva *et al.* 2013). The scale-free dynamic is tightly related to the question of whether the brain operates in a critical state (Bak, 1998). The latest comprehension however is that criticality may not fit to all wide-ranging findings, although the theory has a strong explanatory power (Boonstra *et al.* 2013).

2.3.5 Rapid dynamics of the functional connectivity

The variability and dynamic properties of the FC have only recently come up to the center of the research focus in the field. So far mostly the average properties of FC have been under investigation as analysis techniques implicitly assume stationarity of the time series. However, in practice the observed FC is clearly non-stationary (Chang and Glover, 2010). Moreover, the non-stationarity issue is fully spatiotemporal of nature as the FC patterns markedly evolve during time.

Investigating the dynamic features of the FC requires different analysis approaches, like sliding window based methods (Karvanen & Theis, 2004). Yet revealing population level characteristics of connectivity dynamics, under undirected resting state scanning, is challenging (Kiviniemi *et al.* 2011, Sakoglu *et al.* 2010). However, research on variability of RSNs has demonstrated a rich variety of connectivity configurations across the brain (Smith *et al.* 2012). Furthemore, an impressive collection of FC configurations can be detected from single time frames which mix and merge parts of conventional RSNs (Liu & Duyn 2013). The EEG correlates of the varying BOLD connectivity have been found especially on the alpha band around 10 Hz, thus supporting the neural basis (Chang *et al.* 2013). Furthermore, the non-stationary FC has been found to relate to state of the autonomic nervous system (ANS) by investigating heart rate variability (HRV) (Chang & Metzger *et al.* 2012). Synchronization of brain regions mediating vigilance effects and the brainstem was associated with the high frequency component of the HRV. Furthermore, on the whole brain level the momentary connectivity formation between all RSNs has been shown to present certain global connectivity states that in part strongly diverge from traditional RSN patterns (Allen *et al.* 2014). The global connectivity states can fluctuate quickly but there are typically relatively stable states that can sustain for over a minute. Also, the average occurrence rate in certain connectivity states presents a linear or curvilinear trend during a typical resting state of 5–10 minutes. These states are thought to reflect alterations in arousal and vigilance.

Transient modulations of FC patterns have been studied in pharmacological studies that can potentially shed light on fundamental properties of the brain function. For instance, nodes of the DMN have been shown to present varying connectivity dynamics after different emotional arousals (Eryilmaz *et al.* 2011). By measuring fractal properties of the endogenous brain dynamics a cognitive effort has been shown to induce a deviant state of the dynamics that takes several minutes to recover back to baseline value of the fractal estimate (Barnes *et al.*

2009). Also, transient effects of various substances on FC have been investigated. For example, caffeine has been found to increase the non-stationarity of the motor cortex BOLD fluctuations by inducing varying phase differences between left and right cortices (Rack-Gomer *et al.* 2012), which supports the MEG study showing widespread decrease in neural connectivity following caffeine administration (Tal *et al.* 2013). Another common substance, cholinergic nicotine, is known to modulate cognitive performance, and the mechanism has been demonstrated in a resting state fMRI study, where the decrease in DMN suggested a shift to external information processing and the increase in lateral visual RSN corresponded to increase in visual attention (Tababe *et al.* 2011). Also alcohol has been found to affect specifically the visual RSN by inducing a slow increase in the synchronous BOLD fluctuations likely mediated by GABA (Esposito *et al.* 2010). Using psilocybin to induce a psychotic state, it has been found that decreased connectivity between the anterior and posterior DMN nodes, decreased negative temporal correlation between the DMN and the TPN, and an increased thalamocortical connectivity are hallmarks of psychosis (Carhart-Harris *et al.* 2013). These results emphasize the importance of the DMN integrity for normal cognition.

2.4 Independent component analysis for BOLD fMRI

Independent component analysis (ICA) is a data-driven method for performing blind source separation (BSS) (Jutten and Herault, 1991), from a set of measurements by maximizing statistical independence between the source estimates. In the ICA context the measured dataset is assumed to be a linear mixture of the estimated independent sources, which corresponds to the generative model used in conventional hypothesis based task-fMRI analysis. In practice each independent component (IC) presents a spatial map and a corresponding time-course indicating coherent temporal dynamics among voxels of the map. The maps are thought to depict FC between brain regions (Friston 1994) or signal sources like motion artefact and physiological noise. The key criterion in source estimation is non-Gaussianity that can be used for finding non-linearly decorrelated components. In the estimation process the mutual information between the components is minimized, which yields to maximization of the statistical independence between components. ICA was developed for solving the so-called “cocktail party” problem where a number of individual voices have to be separated based on multiple parallel microphone recordings

(Bell and Sejnowski, 1995). Similar problems exist in numerous application domains, in particular, ICA was found to be widely useful in biomedical imaging research.

Due to spatiotemporal dimensions of typical fMRI data (good spatial resolution, poor temporal resolution), ICA is usually operated in the spatial domain i.e. time-points act as channels/variables and voxels represent measurements. Maximization of mutual independence is then carried out for spatial maps, which conforms to the localization paradigm of classical neuroscience. Temporal ICA would yield to an underdetermined condition, since there are typically at least hundred times more brain voxels (20000–30000) than time-points (~200–300). In order to carry out temporal ICA in fMRI, the analysis can be restricted to a region of interest for instance by selecting the region based on one spatial IC (Seifritz *et al.* 2002). Due to the recent advent of faster fMRI sequences enabling sub-second temporal resolution and more time-points it has become possible to carry out full brain temporal ICA without drastic data dimensionality reduction in the spatial dimension (Smith *et al.* 2012, Boubela *et al.* 2013). In this thesis, the acronym ICA will be used to denote spatial ICA unless stated otherwise.

2.4.1 Spatial ICA principles

The typical generative model used in the ICA is the linear mixture of random variables defined as X = AS. Observed data are X and the task is to decompose X into appropriate rows and columns of so-called mixing matrix A and a matrix of samples from statistically independent random variables S. Generally in the ICA estimation the unmixing matrix W is first computed so that source estimates S have properties maximixing the statistical independence. This is followed by computing the mixing matrix A as an inverse of unmixing matrix W. In spatial ICA the final independent components (ICs) are spatial maps that are orthogonal to each other and maximally independent statistically. However, the strength of ICA is that the IC time-courses are not required to be orthogonal unlike in principal component analysis (PCA). Formally the assumption of the statistical independence means that the joint probability density function (PDF) of the variables can be factorized into marginal PDFs of individual sources. In effect ICA searches for non-linearly uncorrelated source estimates which allow the separation of signal sources that cannot be separated by requiring only uncorrelatedness (Hyvärinen *et al.* 2001). During recent years there has been

controversy about spatial sparseness of the sources (Daubechies *et al.* 2009) as the driver for the decomposition, but current understanding is that ICA indeed seeks for statistical independence rather than sparseness (Calhoun *et al.* 2013).

Typically the data is assumed to be conditioned before ICA estimation by centering (i.e. de-meaning) and whitening using PCA that results in linearly uncorrelated principal components with unit variance. The uncorrelatedness simplifies the problem of blind source separation by reducing the number of free parameters. PCA is also used as a data reduction step before ICA to define the signal space of interest by finding projection directions of maximal variance. In the basic form of the ICA equation, the noise is not included but can be included as in the probabilistic ICA (PICA) framework (Beckmann & Smith 2004) that is mostly used in this thesis. In the PICA model the data is additionally normalized voxel-wise by a standard deviation of a PCA derived noise estimate to comply with the assumption of isotropic noise (Beckmann & Smith 2004).

The principles of different ICA estimation methods can be understood on the basis of mutual information that is a natural information–theoretic measure for dependence of the random variables (Hyvärinen & Oja 2000). Mutual information is defined using entropy that measures the amount of information contained in the random variable. From mutual information definitions it can be further defined that minimizing the mutual information is equivalent to maximizing the sum of nongaussianities of the estimates under the assumption of uncorrelated estimates. Indeed, in fMRI research a common ICA approach is the use of nongaussianity in the decomposition, as is done in the FastICA method (Hyvärinen 1999), the ICA algorithm used in this thesis. Nongaussianity is the key for ICA estimation and this can be reasoned also using a central limit theorem that states the sum of independent and identically distributed (i.i.d.) random variables to present more gaussian distribution than the original variables. This property justifies the maximization of the non-normality of the marginal PDFs i.e. the algorithm seeks for nongaussian PDFs. Other common ICA method in fMRI is Infomax (Bell and Sejnowski, 1995) that seeks to maximize information transfer from the input networks (observations) to output networks mapped through a nonlinear function to be optimized. Later the Infomax ICA was further developed to be able to also detect sub-Gaussian sources in extended Infomax (Lee *et al.* 1999). There are over one hundred published ICA methods and recent advances indicate that FastICA and Infomax may not be optimal ICA methods for fMRI. For instance, abandonment of i.i.d. random variables assumption by modelling sample

correlation, yielded certain ICs with correct sign of the time-course compared to given task (Calhoun *et al.* 2012).

At the heart of the ICA algorithms is then the contrast function that is to be optimized and which allows for an approximation of the statistical independence. In theory, the nongaussianity in ICA estimation could be measured using negentropy, which in information theory describes the randomness of the variable. An important result from the theory is that a gaussian variable has the largest entropy, and thus the smallest negentropy with a value equalling zero. However, exact estimation of the negentropy is difficult and in current FastICA implementations it is approximated using varying contrast functions that the user can choose from. Typical contrast functions for finding nongaussian marginal PDFs are based on higher order moments. The first and second order moments, mean and variance, are set to zero and one respectively during the data pre-processing stages. The third and fourth order moments are called skewness and kurtosis, and are well suited for detecting nongaussian signal sources. Other types of contrast functions are based on hyperbolic cosine or exponential function (Hyvärinen *et al.* 2001).

In the FastICA-algorithm (Hyvärinen 1999) computation of the unmixing matrix is performed with a fixed-point optimization scheme based on Newton's iteration method. The starting point of the iterative FastICA-algorithm is random which leads to many possible convergence paths to global minima along the optimization landscape if the estimation error is defined as a 3D space (Ylipaavalniemi & Vigário 2008). In the case of noisy data or overlapping signal sources it is also possible for the algorithm to get stuck on the local minima in the optimization landscape. The iterations are repeated as long as the predefined stopping criterion, or convergence threshold, for the algorithm has been achieved. Factorization of the joint PDF into marginal PDFs takes place via orthogonal transformations for the whitened data matrix. After each iteration of the factorization, the matrix has to be re-orthogonalized as statistical independence implies uncorrelatedness corresponding to orthogonality (Hyvärinen *et al.* 2001). Within iterations the orthonormalization can be performed in two ways, symmetrically for the whole matrix or one column at a time so that later estimated columns are orthogonalized with respect to earlier estimated columns.

After the above described ICA estimation, the final presentation of the ICs still requires more processing. Firstly, there is an inherent sign ambiguity in ICA estimation that can be solved on the presentation phase by selecting the sign based on maximum voxel or skewness of the PDF. The raw-valued IC maps are

generally presented in statistically meaningful Z-scored values and the thresholding of the maps is desired for better inference and visualization. In the framework of PICA implemented in FSL Melodic (Beckmann & Smith 2004), z-scoring of the map voxel values is achieved by dividing the raw values by the standard deviation of the voxel-specific noise estimate. Once the voxel values are Z-scored, the statistical thresholding can take place. However, simple thresholding based on e.g. Z-score > 2.0 will yield an arbitrary and uncontrolled false-positive rate. This is due to fact that non-gaussian spatial histogram of the ICs do not relate to the null-distribution that would be needed for correct calculation of the mean and variance (Beckmann & Smith 2004). Instead a method called mixture modelling of the probability density (Everitt & Bullmore 1999) is applied for Z-transformation. In PICA the specific method used is Gaussian mixture modelling in which the noise in the main lobe of the histogram around zero is modelled as one Gaussian distribution, and two gamma distributions model the positive and negative BOLD effects. The signal of interest is assumed to be present only in gamma shaped sidelobes of the histogram implying the fact that a rather small set of voxels contribute to the non-Gaussianity of the ICs. After fitting the Gaussian and gamma models to the distribution of all intensity values the voxels presenting significant effect can now be defined using posterior probability, controlling for the balance between false positive and false negative findings (Hartvig & Jensen 2000).

2.4.2 ICA approaches for fMRI data

In neuroscience it is essential to be able to perform group-level statistical analyses. This has been addressed in many different ways in ICA (Calhoun & Adali 2012), given the prerequisite that fMRI data from different subjects have been spatially normalized to a common space. First it was common to perform subject level ICA and combine matching IC maps between subjects which have the advantage to allow spatiotemporally unique ICs for different subjects. On the other hand, this approach suffers from high variability across subjects especially on ICs representing highly inter-connected associative cortices. This variability makes the comparison difficult. Self-organizing group ICA (Esposito *et al.* 2005) has been proposed for performing group-level analyses from single subject ICA decompositions based on hierarchical clustering. However, by concatenating data of all subjects it is possible to perform the ICA estimation on the group level. Spatial ICA that has been found suitable for fMRI can be implemented on a group

level by temporally concatenating the subject data. In that model the subjects are assumed to have common spatial ICs while time-courses are allowed to be unique. A reverse principle of spatial concatenation has not been found to be widely useful, probably due to much higher temporal than spatial variation in the fMRI data (Calhoun & Adali 2012). In this thesis, group ICA will refer to temporal concatenation type of group ICA unless otherwise stated.

The first implementation of the temporal concatenation group ICA was available in the GIFT-tool (Calhoun *et al.* 2001). Large volumes of data in group ICA require data reduction that is firstly performed by a subject-level PCA followed by a group-level second PCA step before ICA estimation. In order to obtain subject-level spatial map and time-course representations for each estimated group ICs, the PCA-reduced data is back-projected through inverse PCA projections. A recent modified version (GICA3) of the back-projection reconstruction in group ICA (Erhardt *et al.* 2011), implemented in GIFT, has the desirable property that the sum of individual IC maps equals the corresponding group IC map. Later the so-called dual-regression, or spatiotemporal regression (Calhoun *et al.* 2004), based on least squares solutions has become a common method for solving the individual spatial and temporal manifestations corresponding to group-level IC maps. The dual-regression procedure involves taking group IC maps first to the spatial regression against full pre-processed fMRI time-series of each individual. This first regression step produces spatial parameter estimates for every time-point, and for each IC and subject. The formed time-series are secondly used in the temporal regression again against the full pre-processed fMRI time-series. This produces parameters estimate values for every voxel and thus forms a spatial map for that IC and subject. A comparison study of the above described GICA3 and dual-regression (used in this thesis) methods suggests that GICA3 combined with subject-level PCA and a noise-free ICA model yields the more accurate subject-level estimates (Erhardt *et al.* 2011).

A known issue with ICA is the varying outcome on each run of the algorithm, although Infomax ICA has been found to produce more stable decompositions than FastICA (Correa *et al.* 2007). Result variability is related to the random initiation matrix of the iterative algorithm and noisy data, which lead to different convergence paths along the optimization landscape where the algorithm may be trapped into the local minimum instead of the global minimum (Hyvärinen 2000). A user selectable option in ICA is the convergence threshold which when under a stringent mode can reduce algorithmic variability. On the other hand the random starting conditions allow the algorithm to find more optimal convergence that

may not be approached from other directions. Therefore, by random initialization, the variability in the data can be exploited to find estimates that are difficult to find otherwise (Ylipaavalniemi & Vigário 2008). To analyse the consistency of the results and find reliable estimates certain repeatability measures have been introduced. The first such framework is ICASSO (Himberg *et al.* 2004) which uses hierarchical clustering for spatial correlation values between IC maps to reveal the cluster centre estimate "centrotype" among the repeated results. The resulting centrotype decomposition does not represent an orthogonal base in the whitened data base and if orthogonality is desired then the individual ICA run closest to centrotypes can also be chosen (Ma *et al.* 2011).

Spatial ICA analyses have been the workhorse in fMRI research but the accompanying time-courses have not been exploited widely. The concept of functional network connectivity (FNC) among RSNs incorporates temporal correlation and lag information into analysis (Jafri *et al.* 2008). In FNC, the maximum lagged correlation between RSNs is sought within a −5 to +5 s window. Recently FNC has been successfully applied for patient-control classification with very high accuracy (Arbabshirani *et al.* 2013). A simpler version of the FNC can be performed with full correlation without accounting for lag and has been termed simply between network connectivity (Joel *et al.* 2011). Full correlation reflects both direct and indirect connections. To obtain a direct measure of the functional connections, partial correlation, accounting for variance shared with other RSNs, can be calculated (Marrelec 2006). Direct connections revealed by partial correlation can be considered to present effective connectivity instead of functional connectivity that features apparent connectivity (Friston 1994). The above temporal correlation analyses do not take into account amplitude information. Yet, also temporal analyses have been carried out with amplitude markers such as the standard deviation of the time-course (Tian *et al.* 2013).

2.4.3 ICA performance

The univariate hypothesis based analysis method general linear model (GLM) can be viewed as the golden reference analysis method in fMRI. However, that method can be criticized from a multivariate data-driven ICA point of view that does not require a priori hypothesis. The hypothesis-based analysis may leave artifactual signal unmodelled, which will bias the parameter estimates in the case of structured noise temporally orthogonal to the assumed regression model. Also,

with orthogonal noise the residual error is inflated and statistical significance is reduced (Beckmann & Smith 2004). Furthermore, typically the univariate GLM analyses discard the richness of spatial relationships between multiple data points. Allowed non-orthogonality of the time-courses is one key factor for ICA to be able to separate networks with spatially overlapping activity whereas seed correlation analysis (SCA) shows only the average of the overlapping processes (Xu *et al.* 2013). The relationship between seed correlation analysis and ICA has been studied and was found to conceptually show correspondence so that the sum of ICs and connectivity between ICs is equal to one SCA result map (Joel *et al.* 2011). In fact, it may be desirable in some cases to combine ICA and SCA by letting ICA define the strongest connectivity regions and use these as optimal seed regions in SCA (Marrelec & Fransson 2011).

Incomplete separation of spatially overlapping signal sources has been shown with ICA whereas a temporal dependence between sources did not lead to deterioration in separation quality (Calhoun 2001). Physiological noise poses a challenge for ICA decomposition especially in posterior DMN areas that overlap with prominent signal changes related to slow fluctuations in respiration variations (Birn *et al.* 2006). This issue is complicated by the fact that the midline brain regions of the DMN are involved in physiological regulation (Khalili-Mahani *et al.* 2013), and therefore neural and cerebrovascular sources cannot be separated from the BOLD fMRI signal alone. Mixing of the physiological noise and DMN IC has been detected, in varying extent between subjects and repeated sessions, by measuring correlation between RVT and DMN time courses (Birn *et al.* 2008). In another study, cardiac signals were found to correlate especially with the auditory RSN time course and physiological correction clearly diminished correlations between physiological signals and all studied RSN time courses (Beall and Lowe 2010). Aliased physiological noise due to a low sampling rate has been claimed to not pose a problem for ICA due to relying on spatiotemporal patterns instead of temporal information alone (Brooks *et al.* 2008). Group ICA followed by a dual regression approach was found robust against basic physiological noise models, but cardiac and respiratory noise convolved with corresponding hemodynamic response functions were less accurately eliminated (Khalili-Mahani *et al.* 2013). Also, inclusion of subject-wise measures of average cardiac and respiratory frequencies onto second stage regression had a prominent impact on statistical test results between different physiological noise conditions induced by alcohol and morphine.

Motion is the greatest source of spurious signal changes and the complex dynamics of the motion artefacts violate the assumption spatial stationarity in the ICA components (McKeown *et al.* 1998). Therefore ICA cannot model all the motion artefacts, which makes ICA variant to data quality. Even subtle motion related signal changes can falsely enhance, attenuate or distort the results of seed correlation analysis (Power *et al.* 2012). However, in ICA dual regression analysis, motion induced artifactual connectivity has been less clear as two large sample size studies report non-overlapping results. Motion contribution to increased connectivity was found in all examined RSNs and the motion effect in DMN is detected on all nodes of the network (Mowinckel *et al.* 2012). A further study (Satterthwaite *et al.* 2012) showed increased FC in parietal and temporal areas in particular but no definite effects in the DMN core areas. Nevertheless, in 7 T high field fMRI with neurological patients ICA was found clearly superior to GLM analysis in revealing the task responses and provided robust estimates even in the presence of motion (Robinson *et al.* 2013).

An inherent problem for ICA decomposition of resting state data is that selection of the ICs by visual inspection is subjective and laborious and interpretation of the ICs can be difficult. However, visual inspection principles have been formulated more in detail in a study in which good 96% inter-rater agreement was found (Kelly *et al.* 2010), which speaks for the validity of the visual inspection process. Many researchers have utilized RSN templates, defined in earlier studies (Beckmann *et al.* 2005) or based on brain atlases, for selecting RSNs from their ICA results based on spatial correspondence but this approach has been shown notably error prone (Zuo *et al.* 2010). It is challenging to create reliable metrics for ordering or classifying the ICs according to their type. In principle the ICs end up in a random order but they can be sorted, for example, with a decreasing amount of explained variance (McKeown *et al.* 1998). Comprehensive IC classification methods are able to categorize all types of RSN and noise components have been proposed with a varying extent of spatial, temporal and spectral features (Di Martino *et al.* 2007, Tohka *et al.* 2008). The latest development in classification scheme adopted nearly 200 features which form the basis for an automatic multi-classifier (Salimi-Khorshidi *et al.* 2013). However, before automatic use the classifier needs to be manually trained for particular data characteristics. Another recent classification tool relying on only four measures (spatial smoothness, activity near edges, CSF activity and temporal high-frequency noise) offers a fully automatic operation without training

requirements (Bhaganagarapu *et al.* 2013), but the performance may be compromised.

The algorithmic variability is known to increase with increasing ICA dimensionality while being very stable at around a typical model order 20–30. At higher dimensionalities in single subject ICA with task data, the ICASSO stability index (derived from spatial correlation) is above 0.8 only for about 15 ICs out of 90 estimated ICs (Li *et al.* 2007). However, in group ICA with resting state data the situation seems more stable with more than 50 ICs having the quality index over 0.8 in model order 70 decomposition (Kiviniemi *et al.* 2009). Another aspect of variability arising from data properties has been investigated by scanning the same subject repeatedly. Test-retest reliability of the RSNs in dual-regression analysis has been found moderate to high both on the group and subject level (Zuo *et al.* 2010). However, in another study not using dual-regression, but comparing single subject ICA vs. group ICA, the subject level reproducibility was clearly lower than for group analysis (Franco *et al.* 2013). Decreased performance in single subject ICA is likely due to lower SNR of individual datasets compared to concatenated group data (Allen *et al.* 2012). A greater number of subjects in group ICA indeed enables the estimation of weaker, noisier and rarer RSNs.

Lastly, determination of the appropriate decomposition dimensionality i.e. model order has been a difficult issue and a prominent source of variability in ICA fMRI studies. In principle, under- or over-fitting the model compared to data may yield to distorted results, therefore optimal dimensionality is desirable (Beckmann & Smith 2004). Dimensionality estimation approaches based on information theoretic criteria have been applied successfully for simulated data (Li *et al.* 2007) but for real data the role of dimensionality estimation is debatable. Group ICA has been shown to represent varying functional segmentation with varying dimensionality (Kiviniemi *et al.* 2009, Smith *et al.* 2009) and a rich set of varying RSN configurations can be explored (Abou Elseoud *et al.* 2011). Higher dimensionality in group ICA involves splitting the networks into sub-networks, considered as possible artifactual fragmentation i.e. over-fitting (McKeown *et al.* 1998) and yielding to less generalizable RSNs across subjects (Pendse *et al.* 2012). More specifically, over-fitting manifests as sources with a single smooth peak and zero elsewhere (Särelä & Vigário 2003) that optimizes non-gaussianity but bears little interesting information in the functional connectivity sense. With other kind of over-fitting with simulated data, it has been shown how subject-wise anatomical variability, and hence the inadequacy of the typical spatial normalization methods, together with functional variability assigned to

anatomical loci can lead to forced splitting of the RSNs on high model orders without functional reason (Allen *et al.* 2014).

2.5 Correcting for structured noise

BOLD fMRI measurements have low SNR due to a multitude of noise sources, various physiological and motion related sources that form structured noise. Random thermal noise with no structure is present too but typical fMRI is not operating under the random noise regime. Correction for structured noise improves the validity of the statistical inference as the error term is assumed i.i.d. in GLM (Lund *et al.* 2006). In GLM analysis the noise processes are commonly regressed out in the same time as the regressors of interest are modelled. Typical nuisance regressors are motion estimates plus regressors representing nonspecific noise signal of a non-neural origin, such as average white matter signal and average CSF signal from ventricles.

2.5.1 Cardiorespiratory signal sources and removal

In conventional EPI BOLD fMRI the acquisition times for whole brain imaging are typically on the order of 2–3 seconds, which is too slow to measure the cardiorespiratory processes unambiguously without aliasing. The cardiorespiratory signal fluctuations, at about 1 Hz for cardiac and 0.3 Hz for respiratory, distribute to the whole measured bandwidth due to aliasing (Lund *et al.* 2006). This makes attempts to frequency filter the cardiac pulsations almost worthless. Cardiac and respiratory-induced fluctuations also present a problem for conventional task-fMRI and thus correction techniques were developed relatively early. Retrospective correction schemes which used heartbeat and respiration recordings for regressing out physiological noise fluctuations have been introduced (Hu *et al.* 1995, Glover *et al.* 2000).

In fMRI the RETROICOR (Glover *et al.* 2000) method has become almost golden standard for performing the physiological corrections. RETROICOR is able to remove signals that are time-locked to particular physiological cycle and operates in the MR image domain. In RETROICOR phases of the physiological signal cycles in each imaging slice are estimated from measured cardiac and respiratory signals, obtained typically with photoplethysmography or a thoracic belt, respectively. Cardiac and respiratory signals are assumed quasi-periodic, which allows for their modelling with Fourier series, i.e. a function of sine and

cosine signals. Respiration is additionally estimated with a histogram based normalization method to account for amplitude variations in respiration. Fourier series coefficients are obtained by Fourier summation and the resulting Fourier series are fit to each voxel's time series prior to removal. In an original publication with 1.5 T data (Glover *et al.* 2000), second order Fourier series were shown to suffice for adequate performance. More recently, it has been noted that in 3 T data higher order modelling would improve the fitting of the noise model (Harvey *et al.* 2008). In order to avoid over-fitting i.e. not to lose also signal of interest with an increasing amount of noise regressors, a compact set of effective regressors have been determined (Beall 2010). Determined impulse response functions with differing temporal shapes were shown to be consistent between subjects and the proposed set of regressors included four cardiac and two respiratory response functions that produced higher sensitivity in FC analysis.

Accounting for variability in an impulse shape and amplitude are not fully accounted for in the above presented correction methods. However, a recently developed method of physiological correction termed DRIFTER is also able to dynamically take into account the amplitude and shape variations, as well as variations in cardiorespiratory frequencies (Särkkä *et al.* 2012). The method is based on estimating momentary frequency trajectories of the given cardiac and respiratory signals.

Respiration related low frequency fluctuations (LFF) of fMRI signal, occurring on the lower frequencies than the direct respiration frequency, were first identified by measuring end-tidal partial pressure of carbon dioxide (PET-CO_2) fluctuations in resting state fMRI (Wise *et al.* 2004). The measured PET-CO_2 signal has most power on frequencies around 0.01–0.05 Hz and it presents pronounced correlations with BOLD fMRI signal on the regions overlapping especially with the DMN and medial visual network. Moreover, in directed respiration conditions with constant rate and depth, the DMN map is markedly less noisy than in normal free breathing (Birn *et al.* 2006). Identified slow CO_2 fluctuations were hypothesized to relate to respiration rate and depth variations. Subsequently, a low frequency respiration correction method, regression of respiration volume per time (RVT) estimate, was introduced (Birn *et al.* 2006). The RVT estimate is calculated by dividing the height of the each respiration wave with its duration, thereby reflecting both respiration depth and rate. Another proposed measure is respiration volume (RV) computed as standard deviation over a 6 second sliding window of respiration waveform providing better robustness against artefacts in the respiration belt signal (Chang & Glover 2009b).

Nevertheless, the RVT estimate was found to oscillate at approximately 0.03 Hz during the resting state and it showed increased fMRI "response" at an average latency of 5 s after decreases in respiration depth. In addition to this negative correlation there was a positive correlation with −1 s lag, possibly reflecting feedback of CO_2 levels in blood modulating the respirations at a later time. In order to more accurately correct for respiration related signal changes, the BOLD signal response function of respiration was created (Birn *et al.* 2009). It was found that the respiration response function (RRF) presents an early overshoot, preceding the peak of canonical HRF, and is followed by a later undershoot peaking at around 16 seconds. The RRF convolved RV variation was then compared to PET-CO_2 measurements in resting state FC analysis (Chang & Glover 2009a), and were found to possess a highly linear relationship. This supports the validity of the respiration belt measurements as a surrogate for end-tidal gas monitoring. Relevant to physiological noise in resting state studies, the way the resting state scanning is conducted seems to have a broad effect on physiological noise contribution. The RVT estimate was clearly less correlated with the GM BOLD signal in eyes-open condition compared to eyes-closed (Yuan *et al.* 2013).

Cardiac LFFs also affect the BOLD signal and correction methods that share similarities with respiratory corrections have been proposed. Since BOLD fMRI is a measure of hemodynamic changes is inherently strongly linked to heart rate fluctuations. HRV is affected by e.g. sympathetic and parasympathetic nervous activity, respiration and arterial pressure fluctuations and many interacting physiological factors (Cohen and Taylor, 2002). The first study on correcting for cardiac LFF (Shmueli *et al.* 2007) investigated the relation of cardiac LFFs to the resting state BOLD fluctuations using a broad set of lagged regressors. They found a marked negative response in GM BOLD signal around 6–12 s and positive signal correlations at around 30–42 s. Another study on the contribution of varying cardiac rate to resting state BOLD signal found a negative BOLD signal change after 3–6 s in response to altered heart beat interval (de Munck *et al.* 2008). Subsequently, the cardiac response function was introduced (Chang *et al.* 2009) and a detailed temporal response shape was designed where the positive peak occurs at a 4 s lag and the negative dip at a 12 s lag. Further progress into cardiac noise correction has been subsequently proposed (van Houdt *et al.* 2010) as variation in pulse height as measured through photoplethysmography was shown to explain a significant amount of variability. The GM contributions of

pulse height variation were found to occur with marked variability between subjects that is typical for fMRI studies in general too.

The combination of the above described correction methods, RETROICOR and respiration and cardiac response functions, is referred as RVHRCOR (Chang & Glover 2009a). Cardiac and respiration response functions were found to explain mostly spatially disjointed variability in GM. The amount of explained variance by physiological correction methods has been found to be rather modest, RETROICOR for instance modelled only about 5% of the average variance over GM (Bianciardi *et al.* 2009, Jo *et al.* 2010). The correction methods for physiological LFF, RVT for respiratory and HR for cardiac, can each explain around 8% of resting state BOLD variance (Chang & Glover 2009b). Recent refinement to the combined RVHRCOR method introduced individualized responses to cardiorespiratory changes (Falahpour *et al.* 2013). The individual response functions were derived from a global brain signal by deconvolution and results show improved fit over those of standard response functions.

Neural underpinnings of the physiological processes pose a difficult dilemma for physiological noise correction since the assumption of noise as non-neural process does not hold. Many brain regions and networks participate in driving or monitoring of the autonomic nervous system (ANS) (Iacovella & Hasson 2011) which relates cardiorespiratory fluctuations. Using HRV as a proxy for the ANS state, the brain regions known to mediate the effects of vigilance and arousal were found to express increased FC with a broad set of other brain regions during elevated HRV (Chang & Metzger *et al.* 2013). ANS activity measured with skin conductance has also been related to FC strength of the DMN and task-positive network (Fan *et al.* 2012) which speaks for holistic consideration of mind, brain and body in future studies.

2.5.2 Motion related signal changes and removal

Motion is the greatest source of signal variance in the MR signal with contributions ranging typically from 30% to 90% (Friston *et al.* 1996). The primary motion artefact relates to movement of the object within the scanner reference frame, which disrupts the establishment of spatial encoding with magnetic gradients. Considering typical voxel dimensions on the order of 3–4 mm, already a 1 mm transition will replace around 30% of the spins within the voxel which is easily capable of overriding the BOLD effect strength (~2–5%) particularly at tissue interfaces. Motion induced effects depend on a multitude of

factors that are affected by the moment the motion occurs in relation to phase of the scanning sequence. Motion during the short data collection period is considered negligible (Muresan *et al.* 2002). Also, pulse sequence type and parameters, as well as the type of motion, naturally affect the artifactual signal changes. In fact, any factor affecting the resonance frequency change will alter the interpretation of the signal location. Scanner instabilities, particularly the ones related to heating, create drifts to the magnetic field and alter the resonance frequency (Foerster *et al.* 2005). This is reflected mainly in the slow PE direction of the image by creating apparent motion (Durand *et al.* 2001), which can be corrected using self-navigated echo. Prominent linear and non-linear spatiotemporal inhomogeneities prevail in the slice-encoding direction too (El-Sharkawy *et al.* 2006). In a well-operating scanner the instability noise is generally ~2% of the physiological noise in the brain cortex and less than 10% in WM (Greve *et al.* 2011).

The time series realignment based on voxel signal intensities is estimated with a rigid body model on the whole head (Friston *et al.* 1995). The assumption that motion would occur between the successive volumes is obviously a simplification with respect to true motion, and as a result the amount of motion will be underestimated. The time series motion is often calculated with an ordinary least squares method, but that has been found to be prone to brain activation induced signal intensity changes (Freire and Mangin, 2001). Increased tissue contrast has been demonstrated to enhance the motion correction performance (Gonzalez-Castillo *et al.* 2011). Image contrast can be improved by several image acquisition parameters including TE, FA, suppression of fat signal, and in post-processing by bias field correction (i.e. removal of RF field heterogeneity). However, ultimately the rigid-body estimation is bound to be of limited accuracy due to complicated signal changes. Slice-wise registration of the motion (Kim *et al.* 1999) has been introduced rather early in fMRI history but it has not been adopted into major fMRI analysis tool packages.

In addition to motion correction under the rigid-body assumption there are non-linear effects arising from interactions between magnetic field distortions and motion (Jezzard and Clare, 1999). EPI is sensitive to variation in B_0 due to low bandwidth in the PE direction and thus geometric distortions appear along that direction (Jezzard and Balaban, 1995). The shim field generated by shim coils is used to counteract the low order inhomogeneity in the magnetic field. However, the susceptibility artefacts around tissue borders with markedly different magnetic susceptibility values remain. When the head moves in a slightly non-linear

magnetic field, this also changes the artefacts in a non-linear fashion which is why the effect is called a susceptibility-by-motion artefact. The strongest susceptibility effects lie near air-filled sinuses adjacent to the temporal and frontal lobes. In order to correct for these, a deformation map image needs to be acquired to map the frequency shifts caused by susceptibility effects. In fMRI this information can be applied to estimate the warping artefacts in the time-series with the help of estimated movement parameters (three translational and three rotational). By knowing the extra variance after realignment and movement parameters, the derivatives of the magnetic field with respect to movement can be estimated.

Motion also destroys the steady state magnetization of the object, which leads to the so-called spin history effect. The spin history effect alters the signal intensity by dependence on through-plane position history of the scanned object (Friston *et al.* 1996). Steady state magnetization of the tissue is disrupted by movements in the through-plane direction if recovery of the *T1* magnetization is incomplete at the time of subsequent RF excitation. The most typical head motion during scanning is nodding, that results in spin-history effects via through-plane motion. The spin-history effect influences the next few acquired volumes after the time of motion. Aligning the volumes is not sufficient for obtaining a fully faithful representation of the signal changes in the brain. In line with the original proposal, the Friston 24 model (Friston *et al.* 1996), approach for typical correction of the spin-history artefact included additional motion regressors into the GLM that are derived from translational and rotational movement estimates. Of each estimate, a differential time series is calculated and then a quadratic version of the time series is computed for all other estimates. All these are then regressed in GLM (Satterthwaite *et al.* 2013). The spin history correction has not been considered important until lately and now it receives increased interest as subtle motion effects have been found to affect FC analyses (Power *et al.* 2012). Indeed, the Friston 24 model was found to cope best with motion affected data (Yan *et al.* 2013), it was even superior to voxel-wise metrics of motion (Satterthwaite *et al.* 2013; Yan *et al.* 2013) suggesting more imaging physics principled considerations over the spin history effects may be needed. More accurate image realignment with slice-wise correction of motion has also showed improved performance in correction of the spin history effects (Bhagalia 2008). On the other hand, instead of correction, the spin-history can be minimized by aiming at more complete signal relaxation before collecting the adjacent image slices. This can be accomplished by using lower FA, longer TR and interleaved

slice-acquisition. An efficient way of minimizing spin-history modulations would be the use of prospective motion correction in image-space during scanning (Thesen *et al.* 2000), but this slows down the acquisition speed.

Recently, typical motion correction methods have been found to be deficient in fully correcting for motion artefact (Power *et al.* 2012), and these remaining subtle artefacts affect several FC measures. The remaining artefacts tend to increase lateral connectivity and decrease vertical or anteroposterior connectivity. The proposed remedy, termed "scrubbing", for the issue was removal of motion affected time points from the time series using either motion estimates or brain signal variance as the criterion. Along the detected time point with excess motion one preceding and two following time points are also removed in an attempt to completely eliminate the artefact (Power *et al.* 2012). Further investigation on the issue using resting state scans of 1000 young adults showed even subtle motion average differences between groups to result in spurious differences in DMN connectivity (van Dijk *et al.* 2012). Following these concerning findings a proposal for an improved analysis framework has been suggested (Satterthaite *et al.* 2013) in which full 36-parameter regression model plus motion spike removal by regression are suggested to be employed in a high motion study population. Despite efforts to correct for motion by modelling with a broad set of regressors and removal of time points with a strict threshold of 0.2 mm, the motion related residuals persist in the processed data (Yan *et al.* 2013). Therefore, it is recommended to covary motion effects at the group-level, which is a conventional procedure in fMRI.

Advanced imaging techniques also come with the price of new motion artefacts. Parallel imaging has increased sensitivity to head motion (Wald 2012) especially when image reconstruction relies on a single reference scan of coil sensitivities without repeated auto-calibration during imaging (Blaimer *et al.* 2004). If motion occurs during the reference scan it will degrade the image quality for the entire following scan and motion leads to residual aliasing in the fMRI time-series. Under-sampled PI data acquisition also has extra sensitivity to perturbations of the magnetic field by limb or chest movements. The type of artefacts depends on the PI image reconstruction that can be performed in k-space or image-space. Additionally, inhomogeneous sensitivity in the phased array coil used in PI introduces signal modulation when the object moves through the sensitivity gradient (Wald 2012), creating a receiving field contrast. Because receive field heterogeneity remains after the image reconstruction the phased array coil sensitivity imparts a spatially fixed contrast and motion correction

procedure will move this contrast relative to the object, which leads to complex signal modulations. With a higher number of receiving coils in the phased array coil there is greater RF field inhomogeneity and higher susceptibility for spurious signal modulation due to motion. Acquiring a measurement scan of the B1 field inhomogeneity before an fMRI scan diminishes this problem.

2.5.3 General methods for noise correction

Typical data pre-processing methods in fMRI do not directly deal with either motion or physiological processes, but to both, such as regression of ventricular, white matter and global average signals (Fox *et al.* 2005). The signal variations common to the whole brain have been considered nuisance effects that require elimination but they may confound the estimation of interesting effects (Friston *et al.* 1995). Indeed, global signal regression has caused long lasting controversy (Desjardins *et al.* 2001; Macey *et al.* 2004; Fox *et al.* 2005). Averaged global signal consist of physiological noise, motion related signal changes, instrumental drifts and unavoidably also of true BOLD effects. Global signal has been shown to correlate significantly with respiratory/cardiac LFF estimates in the majority of subjects studied (Chang & Glover 2009b), whereby the shared variance between RVHRCOR and global signal is around 30% (Marx *et al.* 2013). Also, BOLD fluctuations of neural origin are included in the global signal and their unintended removal cannot be avoided. Indeed, a link between global signal amplitude and vigilance state as measured by EEG was demonstrated recently (Wong *et al.* 2013). Another problem in global signal regression is that it introduces artificial negative correlations in the data (Murphy *et al.* 2009, Weissenbacher *et al.* 2009, Saad *et al.* 2012).

Global signal regression has certain advantages over retrospective motion correction methods in that it has been shown to effectively remove the relationship between motion and FC metrics (Yan *et al.* 2013). This effect is based on the standardization effect of global signal removal; motion increases connectivity across the brain (Satterthwaite *et al.* 2013) but global signal removal shifts the FC correlation distribution towards zero (Murphy *et al.* 2009). Intriguingly, similar decoupling of motion and varying FC results as achieved with global signal regression can be obtained by voxel-wise signal Z-standardization, which is mean centering and variance normalization (Yan *et al.* 2013). Z-standardization eliminates inter-individual differences in global brain signal features and allows more comparable resting state data analysis. After all,

global signal regression is often applied pre-processing routine in univariate analysis methodology, but is not typically included in multivariate methods like ICA that separates all the signal sources.

2.5.4 Imaging based methods

Noise sources in a gradient-echo EPI pulse sequence are always characterized by either apparent spin density fluctuations $S_0(t)$, transverse relaxation rate fluctuations $T2^*(t)$ or thermal noise $n(t)$ (Wu & Li, 2005). The separation of the noise sources by multi-echo EPI relies on echo time dependence of BOLD contrast (Bandettini *et al.* 1994). Secondly, the introduction of a spectroscopy sequence to characterize relaxation $T2^*$ and initial signal intensity of brain activity changes (Hennig *et al.* 1994) allowed further development of the multi-echo sequences. The signal across multiple echo times varies as a function of initial signal intensity S_0 and relaxation time $T2^*$ according to the equation

$$S = S_o e^{\left(-\frac{TE}{T_2^*}\right)} \tag{2}$$

The mean $T2^*$ and S_0 are estimated by fitting the measured signal values to the equation (2). After the fitting operation a combined time-course can be computed (Posse *et al.* 1999).

A simple version of the multi-echo technique is dual-echo acquisition that was proposed already in 1996 for separating the blood inflow effect from the BOLD effect (Glover *et al.* 1996). The method relies on the ability to differentiate changes in initial signal intensity S_0 and relaxation time $T2^*$ based on signal TE-dependency. The short time echo is collected right after excitation to prevent significant BOLD-weighting in the signal and the second echo is acquired at an echo time optimizing the BOLD contrast. By calculating a ratio between the two echo signals (Glover *et al.* 1996), the resulting time series presents a more faithful representation of the BOLD signal of interest. Alternatively, the short time echo signal time-series can be regressed out from the second echo signal, yielding a time-series corrected for a mixture of noise sources (Bright & Murphy, 2013). Optimally the first echo is obtained during the "dead time" prior to the usual BOLD-weighted echo, thus the method has no time penalty, only the advantage of additional signal.

The assumption in regression is that the short echo signal has no BOLD contribution but there is likely to be some cross-talk between short echo data (S_0)

and BOLD signal (*T2**) changes of interest even with an echo time as short as 3.3 ms with spiral-out EPI acquisition (Bright & Murphy 2013). Spiral-out EPI signal collection is advantageous for short echo imaging since it has minimal delay between the RF excitation and the k-space center signal acquisition. The cross-talk is related mainly to the blood volume changes during the early phase of the BOLD response, which would be ideal to remove from the BOLD signal. However, unavoidably the cross-talk is to some extent intrinsic due to BOLD signal contribution, which is undesirable in signal correction.

A short echo provides a more direct measure of the head motion compared to motion correction algorithms working on the whole brain (Bright & Murphy 2013). Motion occurring within volume can be more accurately captured with voxel-wise short echo signal. Also, the spin history effect that is independent of echo time has been corrected for by dual echo signal reconstruction with a superior result compared to regression of rigid body motion estimate derivatives (Ing & Scwarzbauer 2012). Indeed, the short echo data were found to be closely related to both subtle and extreme motion artifacts (Bright & Murphy 2013). The short echo method can be used instead of time point removal ("scrubbing") in correcting for motion. The positive consequences would be that the full time series is preserved and also very small movements not exceeding the scrubbing threshold can be accounted for.

Regarding the efficiency of physiological correction by short dual echo data, it seems that existing correction regressors based on PET-CO_2, RVT and cardiac rate are sufficient to capture physiological signal variations since approximately similar amounts of variance were explained with dual-echo correction (Bright & Murphy 2013). Only slight reductions in long-distance anteroposterior DMN correlations were observed, suggesting removal of additional noise compared to existing modelling techniques.

Interestingly, it has been recognized only recently that the basic imaging parameter FA can be tuned to obtain BOLD data with a markedly decreased contribution of physiological noise (Gonzalez-Castillo *et al.* 2011). The maximal SNR is obtained using so-called Ernst flip angle that is dictated by the desired TR and *T1* of the GM tissue. However, under the physiological noise dominated regime, the functional contrast measured by temporal SNR is nearly invariant to the FA even at less than 10 degrees. One of the advantages in using low FA is diminished contribution of CSF originated signal to the BOLD fMRI (Renvall *et al.* 2014). Other advantages include decreased inflow effect, reduced through-plane motion artefact, lower physiological noise and improved tissue contrast.

Lastly, low FA yields lowered RF energy deposit which is of great importance in the future ultra high field fMRI.

2.5.5 Data-driven methods for de-noising

Data-driven, or exploratory, methods are suitable for de-noising purposes as they are able to estimate expected and also unexpected noise processes. ICA classification tools described earlier provide means for running the data de-noising process in an automatic manner. Early on, PCA was used in fMRI noise correction such as in CompCor (Behzadi *et al.* 2007). CompCor noise estimation is based on noise related voxels with the highest temporal standard deviation from where typically six significant principal components are detected and used as nuisance regressors in GLM. Another study compared PCA and ICA in the ability to nominate components into signal, physiological structured noise and random noise based on spectral characteristics (Thomas *et al.* 2002). ICA was found to be more effective than PCA in isolating structured noise, whereas ICA is not well suited for random noise separation, which is expectable considering the principles of ICA and PCA respectively. Subsequently, an ICA based method called CORSICA has been proposed (Perlbarg *et al.* 2007). In their method, time-courses of the ICs were correlated with BOLD signal time-courses from the ventricles and brainstem, which are associated with motion and physiological noise. De-noising of the dataset after noise component detection is performed by reconstructing the corrected data set from spatial maps and corresponding time courses of the remaining ICs of interest.

Multi-echo imaging described in the previous section can also be used as a basis for data-driven component classification. In particular, a comprehensive signal determination can be achieved by collecting more than two echoes. The obtained parallel time-series can be utilized in a de-noising scheme with spatial ICA in a special data arrangement (Kundu *et al.* 2012). By concatenating the multi-echo data spatially the spatial ICA treats the multi-echo dimension as a fourth spatial variable in addition to three spatial dimensions. Thus the computed independent components share a common time series across spatial location and across multiple echoes. The produced IC maps are then subjected to statistical estimation that assesses the signal characteristics and assigns the component into BOLD-like or non-BOLD-like groups. The non-BOLD ICs can subsequently be regressed out in FC analysis.

3 Aims of the study

The purpose of this study was to investigate the use of ICA in resting state fMRI analysis. The particular aims were to study:

1. the effect of physiological noise on ICA estimation of the default mode network from the fMRI data;
2. the effect of ICA dimensionality on detecting resting state networks, especially the default mode network;
3. the disorder and motion related effects on default mode functional connectivity with respect to varying ICA dimensionality;
4. ICA approach in detecting spatiotemporally unknown stimulation effects from the full frequency band.

4 Participants and methods

All the studies were conducted in Oulu University Hospital, Finland.

4.1 Participants

The studies were approved by the Ethical Committee of Oulu University. Written informed consent was obtained from all participants. Volunteers were obtained from other studies.

Study I

Initially 32 subjects constituted the sample of which half were volunteering medical students and the other half belonged to a Northern Finland Birth Cohort (NFBC) of 1986. The final sample was diminished to 23 after quality control of the cardiorespiratory recordings parallel to fMRI scanning.

Study II

Three separate fMRI data projects including resting state scanning were used for collecting the data of 55 healthy participants for this study: NFBC 1966, NFBC 1986 and a resting state study of brain tumours. The mean age was 25 ± 5 years and gender distribution was 32 ♀ and 23 ♂.

Study III

In the original sample there were 30 high-functioning adolescents with autism spectrum disorder (ASD), including autism and Asperger's syndrome, gathered from a community based study and from a clinic based study. Diagnosis was based on the use of a broad set of structured interviews, questionnaire tools and medical records of Oulu University Hospital. In the community based study, school-day observations and teacher interviews were also used. Psychometric information with Social Responsiveness Scale (SRS) was collected four years prior to fMRI scanning that took place in 2007. Importantly for the present study, our subjects were un-medicated. Thirty age- and gender-matched typically developing control participants were recruited from mainstream schools.

The final sample population was reduced due to the following issues: One participant with ASD refused to undergo imaging and the dataset of one participant with ASD was lost. One control participant was excluded due to severe MR artifacts caused by teeth braces. Two control participants were discarded due to clinically significant ASD symptoms. After further exclusion of datasets due to excess motion (criteria described in the following section 4.3.3) the final sample consisted of 24 participants with ASDs (18 ♂, 6 ♀, age 14.9 ± 1.4, three left-handed) and 26 controls (19 ♂,7 ♀; age 14.8 ± 1.7; two left-handed). In the ASD group there were 17 participants diagnosed with Asperger's syndrome and 7 with autism.

Study IV

Alltogether 51 adult volunteers aged 29 ± 6 years were recruited for examining responses to continuously exposed bright light stimulus via the ear canal in order to study hypothesised inherent photosensitivity of the brain outside the retina. First, 10 subjects were scanned in December, then 27 subjects in February and finally 14 subjects in May. All light stimulation imaging sessions took place during the dark season of the year, in December and February; sham control sessions were imaged during February and May. After exclusion of one subject with failed light stimulation timing, 24 light stimulus subjects and 26 sham control subjects were available for analysis. Additionally, separate 9 volunteers were scanned in March to test for immediate responses to light stimulus.

4.2 Imaging

Magnetic resonance imaging of the all studies was performed with GE 1.5T Signa LX upgraded in 2006 to Signa HDx (GE Healthcare) and equipped with an 8-channel head coil provided by the scanner manufacturer. In studies I, II and IV a respiration belt measuring air flow changes and a photoplethysmograph placed on a fingertip to measure attenuation differences of light were used when collecting data regarding respiration and heart rates respectively.

In the beginning of every MRI session, an anatomical brain scan with image quality similar to that of clinical practise was collected. The imaging parameters of the T_1-weighted 3D fast spoiled gradient echo (FSPGR) sequence were as follows: FOV 24 cm with 256 × 256 matrix, slice thickness 1 mm, TR 12.1 ms, TE 5.2 ms, and FA 20 degrees. The following functional resting state scans were

carried out with eyes open and with the instruction for the participant to lie still and rest watching a white cross in the middle of the projected dark screen visible via a mirror attached to the head coil. Within the MRI session in study III, the resting state was scanned before any task-fMRI scans.

In fMRI, parallel imaging based on image domain image reconstruction, provided by the scanner manufacturer, was used with an acceleration factor of 2. Functional scans were always preceded by a short calibration scan required by PI. BOLD fMRI scanning of 7.5 min consisted of 253 whole brain volumes of which the first three were discarded due to T_1 non-equilibrium state. Parameters of the gradient echo single-shot EPI were TR 1.8 s, TE 40 ms, FA 90 degrees, FOV 256 mm, 64×64 in-plane matrix, 4×4×4 mm voxel size, 28 oblique axial slices with a 0.4 mm gap and interleaved acquisition order.

Study IV

There were special arrangements in study IV to deliver bright light stimulus via the ear canal during resting state scanning, while sight of the light stimulus was prevented. Light was produced by two 3 W LEDs (main light spectrum peak at blue light 465 nm and a secondary peak at 550 nm) and delivered via 5 meter long polycarbonate colourless fibre optic light guides connected to ear-plugs in the subject's ears while laying inside the scanner. The produced output luminous flux (circa 7–8 lumens) in the ear canal was of an order of magnitude comparable with sunlight intensity in the ear canal under bright sunny day conditions when directed towards the sun, according to our measurements.

Scanning sessions with constant stimulus consisted of two consecutive resting-state scans with eyes properly covered. The first scan was always without light stimulus, and it was used to achieve better scanner stability before the actual scan of interest. During echo-planar imaging with the used scanner, the gradient coils warm up and cause marked signal drifts typically during the first five minutes of the scanning. Thus, a valid comparison between the first and the second scans on the full frequency band was not possible. The first scan also worked as a control condition for between group comparisons. The second scan was light on for the light group and no light for controls.

The scanning parameters of the block-design setup for separate participants were otherwise similar but the duration was 15 minutes, TR was 2 s and 31 slices were recorded without an inter-slice gap. Resting-state data were collected while

alternating light on and off every 30 seconds. Light switching was operated manually, while checking the timing from a stopwatch.

4.3 Data pre-processing

Data pre-processing is required to condition the data to be better suited for the analysis. Firstly, the typical pre-processing steps are presented in the following, and the order of the steps approximates their order of use in practice although not all described steps were performed in any of the individual studies I-IV. Then the special pre-processing routines used in studies I & III are described.

- To correct the data for scanner artefacts, appearing as broadly distorted signal within individual image slices, the de-spiking procedure was carried out with the AFNI 3dDespike tool (Study III). De-spiking involves smoothing the time-series voxel-wise in time-points exceeding the specified threshold for deviating signal intensity that cannot originate from normal physiological processes.
- Motion correction, applied in a similar manner in all studies, consists of first estimating the motion with respect to the middle volume of the time-series, and then re-aligning the time-series based on those estimates. In study I, motion correction was performed with AFNI while in studies II-IV the MCFLIRT tool (Jenkinson *et al.* 2002) of the FSL software package was used.
- Brain extraction was performed using BET to remove non-brain tissue from the image. This is carried out to be compatible with the reference brain images for spatial normalization in FSL, which are also brain-only.
- 2D image acquisition was carried out in an interleaved order which yields about TR/2 temporal difference between adjacent slices. These timing differences were corrected for by interpolating the time-series slice-wise in studies III-IV.
- Smoothing via spatial Gaussian filtering was performed to increase SNR. Full width at half maximum (FWHM) defines the filter, and the following widths were used: 5 mm (study III), 6 mm (study I, IV), 7 mm (study II). The exception was in study IV where no additional spatial smoothing was applied for the full frequency band data since smoothing may increase the relative prevalence of low frequency noise (Wang *et al.* 2005). However, the filter width was 6 mm in block-design stimulus part of the study IV.

- Temporal filtering of the data was carried out to remove very low frequency drifts. High-pass filtering cut-off frequencies were 0.008 Hz (study II) and 0.01 Hz (study III). Low-pass filtering was applied to estimate RSN maps of interest in study III with a cut-off frequency of 0.1 Hz. The exception was study IV, where no temporal filtering was applied, to investigate responses on the full spectrum. However, to create spatial template maps from the same datasets a cut-off frequency of 0.0067 Hz was used. In the block-design stimulus part of study IV the cut-off frequency used was 0.017 Hz.
- Intensity normalization (grand mean scaling) of the volumes so that all datasets have the same mean intensity. This conditions the individual datasets to be better comparable for group ICA and it was used in studies II–IV.
- Spatial normalization to the common *T1*-weighted template provided by FSL was performed using FLIRT in all studies. Multi-resolution affine co-registration (Jenkinson and Smith, 2001) with 6 degrees-of-freedom was used to co-register fMRI volumes to structural scans of corresponding subjects, and structural images were co-registered, with 12 degrees-of-freedom, to the MNI standard structural space template.

Study I

In study I the pre-processing operations included also a broad set of physiological correction routines:

- Physiological correction with RETROICOR of the AFNI 3dretroicor tool was used to remove cardiac and respiratory oscillations and their first harmonic signals. After first converting the input respiratory and cardiac signals to phase signals relative to the image timing, 2nd order Fourier series of the phase signals were fitted to the data and regressed out.
- Physiological correction with respiration volume per time (RVT) was applied using eight lagged RVT regressors. An RVT regressor is calculated from the respiration belt measurement by dividing the difference between maximum and minimum of the wave period amplitude by the time between successive peaks in the waveform. Firstly, respiration waveform was smoothed with a Gaussian kernel and then waveform peaks were detected by using varying criterion for signal deviation from the mean. After this automatic signal envelope detection, high frequency fluctuations were removed from the envelope estimate. The quality of the detected envelope signal was checked

by manually. Finally, the waveform was resampled into every TR similar to the BOLD data and seven additional lagged RVT regressors spaced every 3 TR from −6 TR to +15 TR were created. The time span for lagged regressors ranged from −11 s to +27 s. Generated estimates were regressed out using an ordinary least squares method.

- HR LFF correction for cardiac rate low-frequency fluctuation was applied according to the original study by Shmueli *et al.* (2007) using five lagged regressors. Cardiac rate was computed from heart pulse trigger data provided by the scanner. The pulse interval was first calculated from successive pulses, and then inverting the cardiac rate at that point in time. Spurious pulses were removed using a threshold of 1.7 times the standard deviation of the cardiac rate. As a result, eleven subjects from the original study population were discarded since percentage of spurious cardiac pulses was over 5%. Then the cardiac rate time course was smoothed and interpolated to every TR corresponding to the BOLD data, and four additional lagged cardiac rate LFF regressors spaced every 3 TR from 0 TR to +15 TR were created. The time span for lagged regressors ranged from 0 to about 27 seconds. Generated estimates were regressed out using an ordinary least squares method.

Study III

In study III the motion related signal elimination was performed rigorously to investigate the efficacy of conventional motion correction methods. A so-called scrubbing procedure considered 0.2 mm motion as an exclusion criterion and the subsequent time-point was always removed. The actual removal of time-points was carried out for fully pre-processed time-series that were not low-pass filtered so that motion effects would not smear to adjacent time-points. High-motion subjects (4 ASD participants and 1 control participant) with less than 4 min of data remaining after scrubbing were excluded from the analysis. For the remaining sample the percentage of average scrubbed time-points was 13.5% for the ASD and 11.4% for the TD group.

4.4 Data analysis

The main tool in the present study, ICA, was used in every sub-study either on a subject level (Study I), or on a group level via temporal concatenation group ICA (Studies II-IV). A FastICA-algorithm implementation in FSL MELODIC that

comprises a probabilistic ICA (PICA) framework was carried out using skewness as a contrast function. The same contrast function was used in repeatability analyses with ICASSO as well. ICA dimensionality estimation methods were not used in any of the studies.

Study I

Posterior weighted DMN centrotype ICs from ICASSO of each subject were subject to a comparison between physiologically corrected and non-corrected data. The comparison was carried out on three dimensionalities, or model orders: 20, 30 and 40. Statistical testing was carried out with paired t-tests in AFNI, and no correction for multiple comparisons was performed to remain sensitive to subtle changes. Determined statistical significance threshold was uncorrected $p>0.05$ with a spatial extent of at least 20 voxels. DMN maps produced with different pre-processing schemes were spatially correlated and the changes in correlation coefficients were assessed as a function of model order using a paired t-test.

Study II

Evolving spatial characteristics of the default mode, visual, sensorimotor and striatal RSNs along increasing ICA dimensionality from 10 to 200 were investigated. Parcellation of the large-scale RSNs on the low model orders into sub-networks on the high model orders was visually determined. RSNs were obtained as centrotypes from repeating 100 runs of ICA, using ICASSO. Analysis emphasis was on the one hand put into identification of the RSN detection points meaning the model order where the RSN first appeared. On the other hand, branching points depicting the model orders where the RSN in question split into sub-networks, was also of interest. RSN characteristics were further investigated by measuring their volume and z-score, and ICASSO produced reliability metric Iq, as a function of model order. Also spatial coverage of RSNs against the Juelich histological atlas regions was calculated.

Study III

Analysis aimed at exploring the effect of ICA model order and motion scrubbing on DMN connectivity in ASD. DMN RSNs were selected from group ICA of low

to high dimensionality (20, 30 and 100), with special attention in identifying the DMN sub-networks on high dimensionality. The manual DMN selection was assisted with a "canonical" reference DMN, produced with very low model order ICA (8 ICs). ICASSO analysis indicated that DMNs from a single ICA run with 100 ICs were from moderately to highly reproducible, when using a stringent convergence threshold (0.0000001) for single ICA runs. Spatial FC in DMN sub-networks was then compared between ASD and control participants using an ICA dual-regression tool that incorporates the non-parametric permutation test tool FSL Randomise (Nichols & Holmes 2002). The number of permutations was 5000 and threshold-free cluster enhancement (TFCE) (Smith & Nichols 2009) was used to control for the multiple comparisons. The significance level was determined as $p<0.05$ on each tested DMN sub-network separately.

Temporal full correlation between time-courses of the same RSNs was carried out to assess the FC between DMN sub-networks (i.e. between network connectivity) which was hypothesized to be decreased in the ASD group. Testing was carried out with FSL Randomise with 10000 permutations and multiple comparison correction, with a significance threshold of $p = 0.05$ determined over DM-SN pairs within each dimensionality. In other words the statistical testing was carried out separately on each ICA dimensionality.

All above tests were carried out for both motion scrubbed and full datasets. Tests included average subject-level absolute and relative motion estimates as nuisance regressors to control for linear motion effects. The amount of motion, as measured by average values of absolute and relative motion estimates by MCFLIRT tool from pre-processing phase, was compared between groups. Finally, the effect of age and psychometric measurements was studied on the investigated group differences in DMN connectivity by setting age and psychometric data as covariates in nonparametric tests using FSL Randomise.

Study IV

Group ICA with model order 30 was used for spatial FC analysis with dual-regression between bright light stimulus and sham control groups. In both regression stages of the dual-regression data and design were demeaned. Before the 2nd regression the time-courses were variance normalized. Therefore the emphasis is on the temporal shape of the time-series instead of its amplitude. Statistical testing and multiple comparison correction was performed similarly to study III with nonparametric permutation testing.

Regarding further temporal analysis of RSNs that showed significant differences in spatial FC analysis the time-courses and their spectra were investigated using Matlab. A second degree polynomial was fitted for individual time-courses and the polynomial coefficients describing the trend were statistically tested with two-sample t-tests (assuming unequal variance). In order to illustrate spectral differences, time-courses were also converted into the frequency domain usin standard discrete Fourier transformation (FFT-function, no zero-padding). Group mean single-sided amplitude spectra between ~0.002 - 0.1 Hz were plotted.

The scans analysed were the second resting scans of the MRI session. Yet, the first scans were also compared between groups in order to assure that the baseline was similar between the light stimulus group and the control group. Longitudinal comparison on the full band could not be performed due to prominent scanner drifts prevalent in the first scan. Another control measure was to compare group-wise the amount of motion, as measured by average values of absolute and relative motion estimates by MCFLIRT tool from pre-processing phase. Absolute estimate is computed in reference to the middle time-point and relative estimate is computed differentially between adjacent time-points.

Additional analysis of block-design bright light stimulus was performed in FSL, where the data was first pre-whitened before GLM analysis, taking into account hemodynamic response function with regards to stimulus timing. Estimated motion parameters were included as nuisance regressors. The statistical group-level testing was done in FSL Randomise in a similar manner to the main analysis.

5 Results

5.1 Physiological noise correction of the ICA default mode network

The DMN revealed by ICA was found to be effectively similar in group level analysis with and without specific physiological correction, physCorr and noCorr respectively. On this group level comparison of the individual ICA DMNs, the precuneus near the sagittal sinus was shown to present subtle decreased connectivity in physCorr datasets, suggesting a putative site of improved estimation. However, subject-level examination (Fig. 2) showed plausible differences only in a few datasets of the 21 studied subjects. In some subjects the differences clearly reflected dissimilar RSN splitting, rather than a direct effect of physiological noise correction.

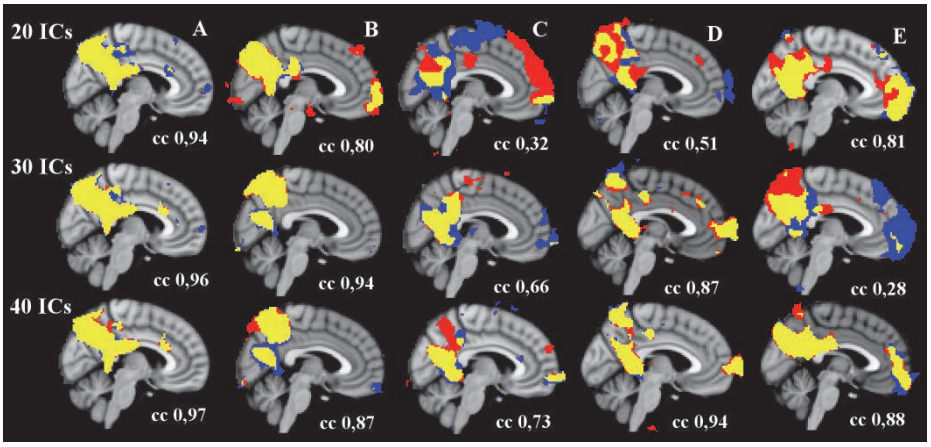

Fig. 2. Individual subjects illustrating the differences in DMN maps between noCorr (red) and physCorr (blue) are shown on the left, map intersection shown in yellow. Typically the major differences do not present improvement in the DMN estimation but different RSN splitting. Example subjects present one with high noCorr–physCorr correlation coefficient (A), one with possible enhancements in DMN appearance (B), one with low cc at all model orders and major inconsistency at 20 components (C), one with divergence at 20 components (D) and a subject with marked inconsistency at 30 components (E). (Study I, published with permission from Elsevier.)

Several ICA dimensionalities were analysed in an attempt to map the ability of ICA to separate cardiac and respiratory noise sources from the DMN. Individual ICA runs with decomposition into 20, 30 and 40 components showed higher

dimensionality to yield more similar DMNs between physCorr and noCorr data. The average physCorr - noCorr correlation was 0.87 in model order 40 while there were marked outliers in lower dimensionalities, decreasing the mean correlation to around 0.80. While results indicate better physiological noise separation at higher model order, the difference may be even smaller than it seems. This is due the worst outliers, especially on low model orders, cannot be considered as true effects of improved DMN estimation due to physiological correction (Fig. 2). It would be reasonable to expect the true improvement to show as decreased FC in regions with prominent physiological noise. However, several of the substantial differences between physCorr and noCorr DMNs are present in regions considered part of the DMN. This suggests that some of the observed differences arise due to altered splitting of the DMN into sub-networks after changes in the ICA optimization landscape, or even removal of DMN signal of interest, by broad physiological noise regression.

5.2 Effect of ICA dimensionality on the resting state networks

RSN expression was highly dependent on model order with the largest changes on low dimensionality and minor changes at very high dimensionality (range 100–200). ICs covering DMN and visual network (VIS) related areas were found to present a very dynamic manifestation as a function of ICA dimensionality. Typically the large-scale networks tended to branch into sub-networks around model order 20–40 after they were detected between model orders 10–30. On the other hand, model order 30 was not enough to reveal all RSNs as for instance the striatum RSN emerged only at dim = 40. On very high model orders lateralization of the initially bilateral RSNs occurred frequently.

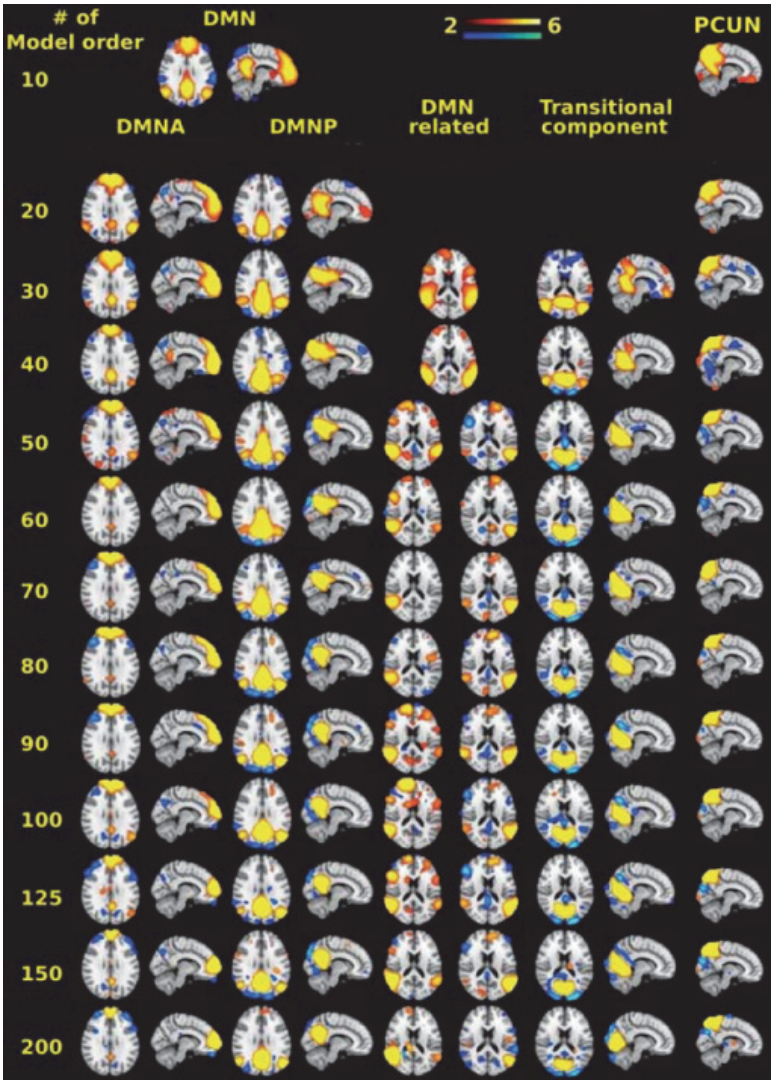

Fig. 3. The effect of increasing ICA model order on the estimated resting state DMN related components. At model order 10, the main DMN and precuneus centered PCUN can be detected, while at model order 20 the DMN branches into DMN-A and DMN-P. Then at model order 30, the DMN-related bilateral and the transitional component emerge. At model order 50, the DMN-related branched into two sub-components. Model orders 30–40 presented a transitional zone where most spatial overlap and transition of connected brain regions took place. (Study II, figure is combined from two figures published in Study II, published with permission from Wiley.)

At the lowest dimensionality of 10, the default mode areas were not covered with one component. The DMN's posterior and anterior nodes were well present at dim = 10, but there was also the precuneus (PCUN) centred RSN extending into core default mode areas. Then at dim = 20 the main DMN was split into distinct anterior and posterior RSNs in addition to the PCUN. At dim = 30 the picture of DMN connectivity turns more versatile as the posterior DMN is effectively split into dorsal and ventral sub-networks (Fig. 3). At further higher dimensionalities the DMN appearance stays rather stable with regards to anterior and posterior RSNs although spatial extent diminishes gradually as the components get more confined. The PCUN RSN evolves into a more distinct dorsal component that is not part of the core DMN areas as found from model order 40 onwards. The ventral posterior part of the DMN (transitional component in Fig. 3) is partially fused with medial visual areas at dim = 40 but these are separated into their own sub-networks from dim = 50 onwards. Ventral DMN is not shown in the original figure after dim = 40. The lateral posterior parts are present in all DMN sub-networks on low model orders while with higher dimensionality they reside on dorsal and ventral DMNs (DMNP and 'Transitional component' in Fig. 3., respectively) and in separate lateralized RSNs called "DMN related" in Fig. 3.

VIS RSNs presented quite hierarchical splitting behaviour starting from a unitary visual signal source at dim = 10 covering the whole visual cortex including visuo-associative areas. At dim = 20, the splitting occurs into medial and lateral visual networks that are further parcellated in higher model order decompositions. The medial VIS RSNs were more stable in their spatial coverage compared to lateral VISs that varied considerably from model order 70 onwards. Regarding sensorimotor RSNs the motor and somatosensory cortices are fused to one RSN at dim = 20. The essential splitting into more fine-grained functional compartments of separate motor and somatosensory networks occurs around dimensionalities 30–40. Very high dimensionalities after around 100 model order do not alter the decomposition significantly.

Measures of volume and z-score indicated marked changes in RSN characteristics on average up to model order range 60–100, after which no significant improvements or changes could be observed. The stability measure of the ICA decomposition decreased with increasing dimensionality but not in a linear fashion. On low model orders (20–30) the ICASSO repeatability index (Iq) showed high average and low variability on the studied RSN. Increased variability and decreased mean repeatability was detected between model orders

40–100, however, the mean value was still high between 0.85 and 0.90. Beginning after dim = 100 the decomposition stability measured by mean Iq gradually decreased below 0.80. Individual RSNs expressed varied repeatability across ICA dimensionality, but between dim = 80–100 the Iq's were stable around 0.90 without clear outliers. Anterior DMN was highly variable in the dimensionality range 40–50. A possible indication of over-fitting the ICA model order compared to data dimensionality was the presence of white matter centred smooth blobs with no connectivity to the rest of the brain. However, these ICs had correspondence in individual datasets.

5.3 Multi-dimensional ICA view on DMN hypoconnectivity in autism spectrum disorders and the effect of rigorous motion correction

Investigation on low and high ICA model orders revealed anteroposterior DMN hypoconnectivity in ASD compared to typically developing controls. Firstly, on low model order the clear division into two DMN compartments confirmed earlier indications of anteroposterior hypoconnectivity. Further on model order 30 the parcellation of the DMN into two posterior sub-networks (dorsal and ventral) showed decreased connectivity between anterior and posterior sub-networks but without clear difference between anterior-dorsal or anterior-ventral hypoconnectivity in ASD. Finally on high model order 100, with clearly more confined spatial coverage in DMN sub-networks, the picture of the hypoconnectivity was found highly specific with strongest hypoconnectivity between anterior and ventral DMN sub-networks. In contrast to the typical findings in the literature, no spatial within sub-network FC differences were detected between ASD and control groups.

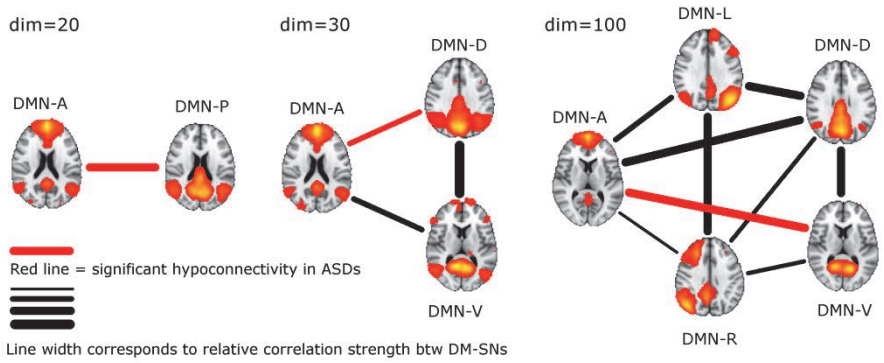

Fig. 4. The lines between DMN sub-networks illustrate the tested connections on varying ICA dimensionalities between the participants with ASDs and typically developing controls. The red line denotes statistically significant hypoconnectivity in ASD between the nodes, and black denotes non-significant hypoconnectivity. The line width denotes the connection strength. (Study III, published with permission from Frontiers.)

Although the scientific community has recently been widely concerned about subtle motion effects that have been suspected to be the cause for earlier observations of anteroposterior hypoconnectivity in ASD, motion was not found to explain that finding in our analysis. Repetition of the FC analyses with fMRI time-series where motion related time-points were eliminated led to effectively the same results; the alterations in statistical scores were minor and could be attributed to increased sampling error due to eliminated time-points by scrubbing.

In additional statistical tests the relationship between connectivity and age was found positive but clearly insignificant (p-value almost 1). Similarly, no significant covariance between the anteroposterior FC measures with the SRS total score or any of the SRS sub-scale scores was found. The relationship with the SRS total was slightly negative but the p-value again was nearly one. Gross motion estimates were not found to reach statistical significance in covariance with DMN correlations on any ICA dimensionality, with or without the motion scrubbing procedure.

5.4 Full frequency band ICA-approach for transcranial bright light stimulation

The ICA dual-regression approach on full band time-series showed an fMRI response to bright light stimulation via the ear canal that suggests the presence of the hypothesized photosensitive opsins acting in the brain. The RSNs that presented strongest FC findings were the visuoassociative network on the lateral visual cortices (Fig. 5A) and the sensorimotor network. Lateral VIS spatially conforms to combined ventral and dorsal visual stream and it presented almost 200 voxels in distributed locations with significantly higher FC in the light stimulus group. However, the group difference did not survive for more stringent multiple comparison correction with $p<0.01$, which indicates the finding not to be statistically very robust. Yet, VIS also presented a temporally slowly increasing group mean activity during the resting state scan as observed from the group mean activity plot (Fig. 5B). In spectra the lowest resolvable frequency bin of about 0.002 Hz and frequencies around 0.015 Hz were more prominently involved (Fig. 5C). The first and second order polynomial fit coefficients of the lateral VIS time-course were found elevated in the light stimulation group, $p = 0.12$ and $p = 0.08$ respectively, although not statistically significant. The sensorimotor RSN also presented significant spatial difference in one locus of 21 voxels on the sensory cortex but the temporal course during the measurement was rather similar between groups. No significant findings were detected from the light stimulus delivered in conventional block-design fashion.

The results were from the second scan of the MRI session. As a control the first scans with prevalent scanner drift were also compared group-wise between the same subjects. However, no baseline differences in lateral VIS or sensorimotor RSNs could be detected that could explain the results during bright light stimulation. Estimated subject-wise mean motion parameters were not found to significantly differ between groups, although the light stimulation group had elevated absolute motion in the 1st scan ($p = 0.19$) and slightly in the 2nd scans ($p = 0.42$).

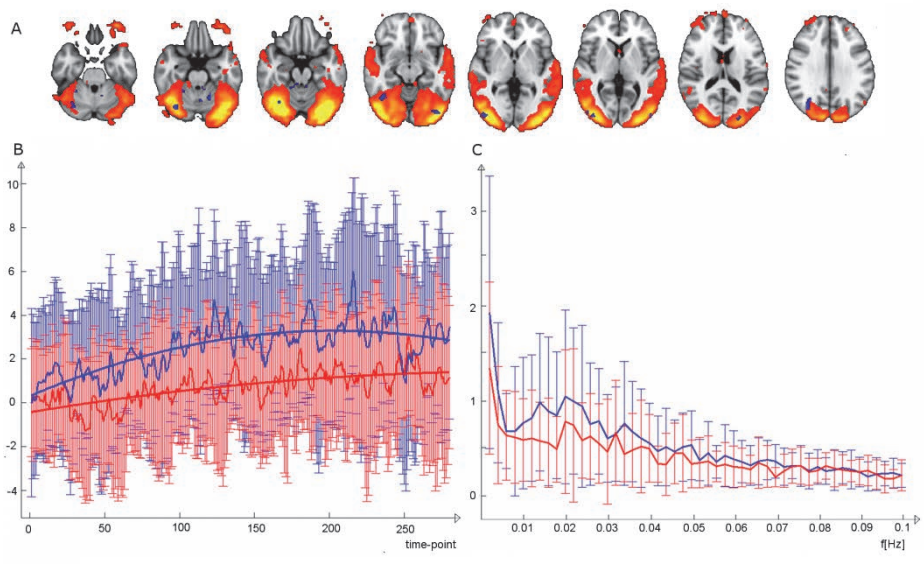

Fig. 5. (A) The lateral visual RSN (red-yellow colors) demonstrated greater functional connectivity (blue voxels) in the light stimulus group compared to controls. However, the finding did not survive after more stringent multiple comparison correction threshold at p<0.01; (B) Group mean time-courses and standard deviations for the lateral visual RSN of the light group (blue) and controls (red), time-course units are demeaned values of spatial regression fit; (C) Corresponding frequency representation with group means and standard deviations. (Study IV, published with permission from Scientific Research Publishing.)

6 Discussion

6.1 Separation of spurious signal sources with ICA (I-IV)

Motion related artefact ICs were broadly present in group ICA studies II-IV which in part speaks for their separation from RSNs. Naturally the ICA de-noising approach would be optimally performed with ICA on the individual datasets, but the correction performance on the group level analysis seems adequate. Also, in comparison to univariate methods like seed correlation analysis, the ICA multivariate approach is able to simultaneously model the global mean signal as a superposition of all ICs. While for univariate analyses global signal regression is advocated for its effects on reducing spurious FC due to motion artefacts, this is not recommended or relevant processing for ICA (Beckmann 2012).

Study III focused on motion issues and showed that the average motion estimates on the group analysis were not significantly linearly associated with any of the performed tests on RSNs comparing ASD and control groups. However, this is discrepant with a study that showed the DMN among other RSNs to be significantly affected by motion effects in ICA dual-regression (Satterthwaite *et al.* 2012). Incongruence is most probably related to their large sample size of nearly 500 subjects which makes the statistical testing far more sensitive for detecting significant results from smaller effects. In practice, beta parameter estimate maps should be compared between studies and not only t-scores. In addition, fairly stringent elimination of motion related time-points did not appreciably alter the detected DMN hypoconnectivity results in ASD. This supports the inference that ICA combined with dual-regression is in a proper extent capable of modelling the spurious signal sources. In the dual-regression phase the partial regression estimates with a full set of ICs assign the major portion of the motion effects onto dedicated motion components. On the other hand, there are pre-processing choices that can contribute to noise separability such as low-pass filtering that can make the decomposition task easier for ICA by reducing high-frequency noise including some motion related signal changes. Finally, ICA dimensionality was not found to alter the way how motion scrubbing affected DMN connectivity comparison between ASD and controls.

Concern over spurious FC measures induced by even 0.1 mm subtle motion between successive volumes has reached a level of inevitable physiological

motion in a living subject. Accurate external measurements have shown the heart pulse induced head displacement to be over 0.1 mm and that respiratory cycle related true head motion to be 0.2–0.3 mm (Maclaren *et al.* 2012). It seems likely that in single echo data acquisitions, the motion correction accuracy is limited by calculation of the motion estimates from the data itself. Accurate external measurement of head motion may be a prerequisite for prospective motion correction in current and future ultra-fast fMRI sequences.

Physiological noise correction using RETROICOR to model instantaneous and aliased effects and cardiac and respiratory LFF modelling for slower fluctuations were not found to alter the group ICA estimates in a coherent manner. A minor clean-up effect was detected in the sagittal sinus adjacent to the precuneus but otherwise the differences induced by noise correction were limited to individual subjects. On the other hand the inherent sensitivity of ICA decomposition to changes in the optimization landscape due to noise regression is a challenge for comparison between different noise removal strategies. Partitioning of certain regions between distributed RSNs is in some datasets strongly altered meaning that this region was not related to physiological noise but ended up differently assigned in the whole RSN constellation. This bias was most diminished on the highest studied model order of 40, where the results are easier to interpret: there is putative group level reduction of FC in the sagittal sinus after physiological correction but there are also noisy looking FC increases. Overall, noise regression does not unambiguously lead to better ICA performance. An additional problem is the use of a large number of noise regressors that unavoidably results also to the removal of signal of interest, which further complicates comparisons between different pre-processings.

One other way of investigating the ICA capability for noise separation would have been to conduct analysis of time-course correlation with noise regressors, as was the case in a parallel study focusing on the RVT estimate and DMN (Birn *et al.* 2008). In fact, there is another study (Beall & Lowe 2010) exploring the effects of RETROICOR for group ICA, but spatial results are difficult to interpret due to varying RSN splitting after physiological correction, that was problematic in study I too. Temporally, however, their results were more straightforward to comprehend. The default mode and visual networks were not particularly correlated to physiological signals, while the auditory network was highly correlated, and all correlations were practically nullified by passing the data to RETROICOR before ICA. They found better physiological noise separation at higher group ICA model orders (Beall and Lowe 2010) which is in concordance

with results of study I indicating a similar behaviour on individual-level ICA. Finally, it may have been more accurate to study the effects of noise correction on the DMN by measuring reduced FC under a mask defined by separate physiological noise ICs.

6.2 Effect of ICA dimensionality on RSN modularity (I-III)

Studies I-III collectively depict the course of evolving DMN connectivity on both subject-level and group ICA showing anterior and two posterior sub-networks (dorsal and ventral) already on model order 30. Additionally at high dimensionality in study III, there were the left and right lateralized networks centred on the parietal lobule that shared marked spatial coverage with canonical DMN regions. In the literature, an RSN closely related to DMN functions is the executive control network, which partially resembles our lateralized DMN RSNs. Yet, in study III their connectivity involved more clearly the PCC and precuneus regions as well. Study II explored mainly the DMN and VIS on varying ICA dimensionalities and would have been further improved by presenting a whole brain RSN modularity continuum or at least by inclusion of essential task-positive networks. However, as the effort was put on dense sampling of ICA dimensionalities a practical decision was made to reduce the complexity by limiting the number of RSNs.

Dimensionality estimation methods attempt to conclude an optimal representation level of the data decomposition, although rationality of the applied criterion can be questioned. Automatic estimation methods depend largely on data SNR, which is a sound approach and should scale according to data properties but is not equivalent to neurophysiologically meaningful criteria. Different methods produce varying model orders and the results can be affected by pre-processing choices such as spatial smoothing. As the outcome of ICA regarding the constellation of all RSNs is very sensitive for the model order parameter, and even more so on the group ICA, comparison between studies can become cumbersome due to highly varying RSN expression by varying model order.

The use of one model order, typically relatively low around 20–30, potentially discards useful information as the more complex picture of the whole brain connectivity is left aside. Furthermore, low dimensionality can be regarded as insufficient use of statistical indepence. This is since large-scale RSNs on low model orders are still mixtures of independent sources, RSN sub-networks, which

can be only obtained on high model orders. These sub-networks can be viewed as more true constituents of the large-scale RSNs.

Functional neuroanatomy as reflected in a whole RSN constellation can be expressed on many desired levels of modular organization. In our data it reaches maximal modularity around 100 ICs, depending on the properties of the group dataset. These properties are discussed in study II and included e.g. field strength and resolution, and their effect was recently confirmed in a 7 T study (Robinson *et al.* 2013). Therefore the ICASSO Iq values, presented in study II, are certainly dependent on data properties.

High model order ICA with fine-grained RSNs can be utilized to pinpoint more to the root of the investigated functional aberrations such as was shown in study III with DMN alterations in ASD. In order to obtain a ”canonical” DMN with group ICA the model order needs to be below 10, based on observations in studies II-III. For several years it was a common practise in the field to assume that ICA produces only one DMN but a more intricate nature of the DMN connectivity is now a settled fact.

A question of dimensionality is linked to varying dynamics or non-stationarity of the functional connectivity, a recent topic in fMRI. In the future, a better understanding of the functional differences within systems will build up and this will help to interpret the neurophysiological driving mechanisms of RSN splitting in high model order ICA (Beckmann 2012). The variability of the ICA result is often related to spatially distributed and overlapping RSNs and hence the robustness reflects the degree of complex inter-connections. These variably overlapping RSNs are highly challenging for attempts to present the whole brain modularity as non-overlapping entities. Repeatability analysis such as ICASSO attempt to diminish the algorithmic variability and the obtained metrics mirror the dynamic connectivity properties of the RSNs. Put in other words, the individual ICA result gives one of the possible views on the data decomposition that arise non-randomly due to data properties.

It is known that algorithmic variability of the decomposition increases with dimensionality, which implies a trade-off between high modularity vs. reproducibility and over-fitted ICs. On the other hand, result variability reflects intrinsic properties of the measured complex spatiotemporal processes that, even in the hypothetical condition of noiseless data, are difficult to present with a linear combination of IC maps. It is not fully clear what kind of ICs present over-fitting in resting state fMRI but in study III the group IC with smooth blobs in white matter arose from an individual dataset and was increasingly detected at higher

dimensionality. This suggests that a pronouncedly rounded smooth shape of an IC indicates an over-fitting result. However, over-fit ICs should not be consistently detected by ICASSO as there is no good reason why over-fits would repeatedly occur in the same location. Another observation in study III was the increasing z-score of the ICs, which is attributed to ICA dimensionality by definition of the z-scores computation. z-scoring involves division with noise residual that diminishes along increasing dimensionality, and therefore the z-scores are elevated on higher dimensionalities. Finally, the undesirable splitting of RSNs due to anatomical variability between subjects is also a possible mechanism for another kind of over-fitting (Allen *et al.* 2014), although real data examples have not yet been presented in the literature.

6.3 Other considerations on ICA methods

Study III investigated between networks full correlation analysis that was chosen instead of previously proposed maximal lagged correlation within a 10 second time window (Jafri *et al.* 2007). The preliminary analysis with lagged correlations was often found to be unable to point to clear local maxima other than the edge of the time window. This problem was more pronounced for sub-networks that presented lower connectivity. Therefore, a simple zero-lag correlation method was chosen for more straightforward inference. Further improvement in this between network analyses could have been the choice of partial correlation where indirect contributions between DMN sub-networks would be regressed out.

Research groups investigating pharmacological fMRI encounter analysis issues that parallel those of study IV with bright light stimulation via the ear canal whereby very little a priori information about the hypothesized response pattern was available. Characterization of the psychopharmacological effects has proven difficult and the challenge of developing a generally applicable methodology for repeated measurements of drug effects on the central nervous system has been acknowledged. However, recently in the research of pharmacological challenges, resting state fMRI and ICA have been found to provide a proper methodology for system-level neuroscience (Cole *et al.* 2013, Khalili-Mahani *et al.* 2012). In study IV, the analysis task started with a consideration of an appropriate method for investigating the effects that a constant stimulus would induce. Given the hypothesis of inherently photosensitive brain opsins outside retina, the analysis properties had to be specifically directed towards unknown spatiotemporal responses by analysing the full frequency band which is rarely done in fMRI.

Clearly there was a need for data-driven analysis since the hypothesis of affecting brain functions by light stimulation had not taken shape yet. ICA fulfilled the data-driven criterion but the group ICA dual-regression approach did not directly cope with the amount of signal drifts. PCA pre-processing captured dominantly signal drift variance from regions with high susceptibility artefacts and hence yielded ICs presenting mainly areas near air-sinus cavities. The problem was solved by high-pass filtering the data before an ICA estimation phase and issuing the non-filtered data back during dual-regression. On the other hand more optimally the drifts would have been dealt with by linear de-trending, which would have yielded ICA decomposition with a dataset resembling as closely as possible the dataset used in dual-regression. Further in the dual-regression process it was important to perform signal processing properly to condition the data for the hypothesis of signal changes during the course of measurement rather than to weight the baseline amplitude of the RSNs. This was accomplished by variance normalisation of the time-course in the 2nd regression of the dual-regression, in addition to demeaning the data and design in both regressions. Finally, the between subjects study design, that was used in study IV, has its limitations in statistical power. If the study setup could be formulated such that repeated measures of the same subjects would be compared, the statistical analysis would be more sensitive as the within-subject variability is smaller than between-subject variability. This relates also to major difficulties in spatial normalization procedures to map individual structures into common space.

6.4 Considerations on resting-state measurements

It is peculiar to note in retrospect how strong the disbelief has been against the functional relevance of resting state fMRI until around the year 2005. Regardless, the choice of measurement condition in resting state fMRI is between eyes open or eyes closed, which clearly has effects on awareness and vigilance. Varying vigilance has implications for resting state studies since drowsiness has been difficult to control for in the experiments, which causes unintended variability and bias into the data. Light sleep has been shown to be associated with increased BOLD fluctuations in visual and sensorimotor cortices (Horovitz *et al.* 2008). In studies I-III, resting state condition was eyes open with visual cross fixation that requires top-down attention control as a low level task. The repeatability of the RSN has been found to be slightly more reliable with eyes open with cross fixation, compared to eyes open only or eyes closed (Patriat *et al.* 2013). In

practice the visual fixation can be annoying for some participants but the advantage is that participants are less likely to fall asleep. In studies of dynamic FC, certain connectivity states are thought to reflect alterations in arousal and vigilance states (Allen *et al.* 2014). Indeed, automatic data-driven sleep staging with resting state fMRI has been demonstrated using simultaneous EEG as a gold reference (Taggliazucchi *et al.* 2012).

Physiological measurements parallel to resting state fMRI are often necessary to model physiological noise, especially in univariate analysis methods. Our experience in study I indicates that physiological monitoring itself is prone to errors, which warrants the use of data-driven methods for data correction. Errors occur in cardiac measurements due to low blood circulation in the fingers and respiratory measurements suffer from signal saturation and occasional auto-calibration of the system, which alters the signal level. In fact, the physiological signals corresponding to measures from the photoplethysmograph and respiration belt can be reconstructed from the fMRI data itself using temporal ICA for each image slice separately (Beall and Lowe 2007).

Recently the effect of mental activity preceding the actual resting state scan has been acknowledged as a possible source of bias between studies. For instance, a working memory task induced transient carry over effects into the following resting state, taking around 10–15 minutes for the BOLD dynamics to return to pre-task level (Barnes *et al.* 2009). In all studies I-IV, the MRI session was performed in a manner that minimizes variability related to preceding activity since the resting scans were always the first fMRI scans. Furthermore the MRI session was started with a 3 min anatomical scan that provided the participant some time to adapt to loud and inconvenient MRI environment.

6.5 Future directions

Functional imaging techniques evolve with a fast pace and can now provide sub-second sampling rates of the whole brain with a voxel size smaller than 3 mm. The resting state research field is still growing in popularity and is becoming better established. At the same time the data processing practices like de-noising are now more standardized and automatic where ICA has a prominent role. The improved accuracy will naturally enable more fine-grained research, using e.g. high dimensionality ICA, with increased statistical power due to more data samples. However, with increasing spatial accuracy the error due to variations in functional neuroanatomy and hence suboptimal spatial normalization will be

relatively enhanced. Faster imaging involves the increasing number of parallel coils and that implies increased sensitivity to motion artefacts, but the benefits of more samples per time unit clearly outweigh the problems.

In study III, hypoconnectivity was shown between DMN sub-networks, indicating that the alterations related to ASD are in the network interplay rather than in local connectivity differences. This result further suggests that it would be highly relevant to study not only DMN but also the orchestration of the DMN (task-negative network) vs. TPN and other related control networks in both resting state and within relevant task settings. Taking the orchestration point of view further, it is imperative to also study dynamics i.e. non-stationarity in more detail to get a better picture of what can be obtained with the average FC.

Study IV dealt with the very controversial issue of the inherent photosensivity of the brain outside the retina. The idea is based on brain opsins like OPN3 (Nissilä *et al.* 2012), which may act as photoreceptors in the human brain. Potent photoreceptor properties have been demonstrated for example by transforming mammalian cell culture photosensitive by transfecting cell with an OPN3 homologue (Koyanagi *et al.* 2013). It is a matter of future studies to confirm the light induced effect of brain opsins for transcranial light stimulation but there are interesting parallels to our findings on visuoassociative and sensorimotor networks in behavioral studies. A recent psychomotor speed study on the effect of the bright light treatment period showed acceleration of motor action time for a visual cue but not for an auditory cue for the light stimulation group (Tulppo *et al.* 2014). On the other hand, one ICA study correlated RSN temporal features with reaction times in a stop signal task that is a measure of one's ability to inhibit a prepotent response. The results revealed that shorter reaction times are associated with higher fluctuation amplitude of the visual, motor and attention RSNs (Tian *et al.* 2013).

7 Conclusions

1. Spatial analysis of the default mode network is resilient to physiological noise on the level of single subject ICA on a 1.5 T magnetic field. At high dimensionality, the comparison between ICA decompositions is least biased by changes in the algorithm optimization landscape due to noise regression. Changes after physiological noise correction were minor, adding further proof of the neurophysiological origin of resting state activity.
2. Low dimensionality ICA results are markedly sensitive for small changes in dimensionality. The default mode branches into anterior, dorsal and ventral sub-networks at a typical ICA model order of 30, although earlier it has been studied as a relatively unitary entity. Generally at higher model orders, ICA results are more variable between runs, but the variability also reflects the complex and dynamically varying inter-dependencies in fMRI data.
3. Stringent censoring of the motion related data time-points had only a minor effect on the ICA dual-regression results with group level estimates of motion level. Autism spectrum disorder was associated with significant hypoconnectivity between anterior and posterior default mode sub-networks, and particular disconnection was detected with high ICA dimensionality between anterior and ventral sub-networks.
4. Composed spatiotemporally explorative analysis with ICA enabled the identification of slow functional connectivity changes during transcranial bright light stimulation. Increased functional connectivity was detected in the lateral visual and sensorimotor resting state networks, potentially inferred as secondary effects of phototransduction.

References

Aalkjaer C, Boedtkjer D & Matchkov V (2011) Vasomotion - what is currently thought? Acta Physiol (Oxf) 202(3): 253–269.

Abou Elseoud A, Littow H, Remes J, Starck T, Nikkinen J, Nissila J, Timonen M, Tervonen O & Kiviniemi V (2011) Group-ICA Model Order Highlights Patterns of Functional Brain Connectivity. Front Syst Neurosci 5: 37.

Abou Elseoud A, Nissila J, Liettu A, Remes J, Jokelainen J, Takala T, Aunio A, Starck T, Nikkinen J, Koponen H, Zang YF, Tervonen O, Timonen M & Kiviniemi V (2014) Altered resting-state activity in seasonal affective disorder. Hum Brain Mapp 35(1): 161–172.

Adelstein JS, Shehzad Z, Mennes M, Deyoung CG, Zuo XN, Kelly C, Margulies DS, Bloomfield A, Gray JR, Castellanos FX & Milham MP (2011) Personality is reflected in the brain's intrinsic functional architecture. PLoS One 6(11): e27633.

Allen EA, Damaraju E, Plis SM, Erhardt EB, Eichele T & Calhoun VD (2014) Tracking whole-brain connectivity dynamics in the resting state. Cereb Cortex 24(3): 663–676.

Allen EA, Erhardt EB, Damaraju E, Gruner W, Segall JM, Silva RF, Havlicek M, Rachakonda S, Fries J, Kalyanam R, Michael AM, Caprihan A, Turner JA, Eichele T, Adelsheim S, Bryan AD, Bustillo J, Clark VP, Feldstein Ewing SW, Filbey F, Ford CC, Hutchison K, Jung RE, Kiehl KA, Kodituwakku P, Komesu YM, Mayer AR, Pearlson GD, Phillips JP, Sadek JR, Stevens M, Teuscher U, Thoma RJ & Calhoun VD (2011) A baseline for the multivariate comparison of resting-state networks. Front Syst Neurosci 5: 2.

Allen EA, Erhardt EB, Wei Y, Eichele T & Calhoun VD (2012) Capturing inter-subject variability with group independent component analysis of fMRI data: a simulation study. Neuroimage 59(4): 4141–4159.

Andrews-Hanna JR, Snyder AZ, Vincent JL, Lustig C, Head D, Raichle ME & Buckner RL (2007) Disruption of large-scale brain systems in advanced aging. Neuron 56(5): 924–935.

Arbabshirani MR, Kiehl KA, Pearlson GD & Calhoun VD (2013) Classification of schizophrenia patients based on resting-state functional network connectivity. Front Neurosci 7: 133.

Attwell D, Buchan AM, Charpak S, Lauritzen M, Macvicar BA & Newman EA (2010) Glial and neuronal control of brain blood flow. Nature 468(7321): 232–243.

Balsters JH, O'Connell RG, Galli A, Nolan H, Greco E, Kilcullen SM, Bokde AL, Lai R, Upton N & Robertson IH (2013) Changes in resting connectivity with age: a simultaneous electroencephalogram and functional magnetic resonance imaging investigation. Neurobiol Aging 34(9): 2194–2207.

Bandettini PA, Wong EC, Jesmanowicz A, Hinks RS & Hyde JS (1994) Spin-echo and gradient-echo EPI of human brain activation using BOLD contrast: a comparative study at 1.5 T. NMR Biomed 7(1–2): 12–20.

Baria AT, Mansour A, Huang L, Baliki MN, Cecchi GA, Mesulam MM & Apkarian AV (2013) Linking human brain local activity fluctuations to structural and functional network architectures. Neuroimage 73: 144–155.

Barnes A, Bullmore ET & Suckling J (2009) Endogenous human brain dynamics recover slowly following cognitive effort. PLoS One 4(8): e6626.

Bassett DS, Meyer-Lindenberg A, Achard S, Duke T & Bullmore E (2006) Adaptive reconfiguration of fractal small-world human brain functional networks. Proc Natl Acad Sci USA 103(51): 19518–19523.

Beall EB (2010) Adaptive cyclic physiologic noise modeling and correction in functional MRI. J Neurosci Methods 187(2): 216–228.

Beall EB & Lowe MJ (2007) Isolating physiologic noise sources with independently determined spatial measures. Neuroimage 37(4): 1286–1300.

Beall EB & Lowe MJ (2010) The non-separability of physiologic noise in functional connectivity MRI with spatial ICA at 3T. J Neurosci Methods 191(2): 263–276.

Becker R, Reinacher M, Freyer F, Villringer A & Ritter P (2011) How ongoing neuronal oscillations account for evoked fMRI variability. J Neurosci 31(30): 11016–11027.

Beckmann CF, DeLuca M, Devlin JT & Smith SM (2005) Investigations into resting-state connectivity using independent component analysis. Philos Trans R Soc Lond B Biol Sci 360(1457): 1001–1013.

Beckmann CF & Smith SM (2004) Probabilistic independent component analysis for functional magnetic resonance imaging. IEEE Trans Med Imaging 23(2): 137–152.

Behzadi Y, Restom K, Liau J & Liu TT (2007) A component based noise correction method (CompCor) for BOLD and perfusion based fMRI. Neuroimage 37(1): 90–101.

Bell AJ & Sejnowski TJ (1995) An information-maximization approach to blind separation and blind deconvolution. Neural Comput 7(6): 1129–1159.

Berne RM & Levy MN (1964) Heart. Annu Rev Physiol 26: 153–186.

Bhaganagarapu K, Jackson GD & Abbott DF (2013) An automated method for identifying artifact in independent component analysis of resting-state FMRI. Front Hum Neurosci 7: 343.

Bianciardi M, Fukunaga M, van Gelderen P, Horovitz SG, de Zwart JA, Shmueli K & Duyn JH (2009) Sources of functional magnetic resonance imaging signal fluctuations in the human brain at rest: a 7 T study. Magn Reson Imaging 27(8): 1019–1029.

Binder JR (2012) Task-induced deactivation and the "resting" state. Neuroimage 62(2): 1086–1091.

Binnewijzend MA, Schoonheim MM, Sanz-Arigita E, Wink AM, van der Flier WM, Tolboom N, Adriaanse SM, Damoiseaux JS, Scheltens P, van Berckel BN & Barkhof F (2012) Resting-state fMRI changes in Alzheimer's disease and mild cognitive impairment. Neurobiol Aging 33(9): 2018–2028.

Birn RM, Diamond JB, Smith MA & Bandettini PA (2006) Separating respiratory-variation-related fluctuations from neuronal-activity-related fluctuations in fMRI. Neuroimage 31(4): 1536–1548.

Birn RM, Murphy K & Bandettini PA (2008) The effect of respiration variations on independent component analysis results of resting state functional connectivity. Hum Brain Mapp 29(7): 740–750.

Birn RM, Smith MA, Jones TB & Bandettini PA (2008) The respiration response function: the temporal dynamics of fMRI signal fluctuations related to changes in respiration. Neuroimage 40(2): 644–654.

Biswal B, Yetkin FZ, Haughton VM & Hyde JS (1995) Functional connectivity in the motor cortex of resting human brain using echo-planar MRI. Magn Reson Med 34(4): 537–541.

Blaimer M, Breuer F, Mueller M, Heidemann RM, Griswold MA & Jakob PM (2004) SMASH, SENSE, PILS, GRAPPA: how to choose the optimal method. Top Magn Reson Imaging 15(4): 223–236.

Boly M, Balteau E, Schnakers C, Degueldre C, Moonen G, Luxen A, Phillips C, Peigneux P, Maquet P & Laureys S (2008) Baseline brain activity fluctuations predict somatosensory perception in humans. Proc Natl Acad Sci USA 104(29): 12187–12192.

Boonstra TW, He BJ & Daffertshofer A (2013) Scale-free dynamics and critical phenomena in cortical activity. Front Physiol 4: 79.

Boubela RN, Kalcher K, Huf W, Kronnerwetter C, Filzmoser P & Moser E (2013) Beyond Noise: Using Temporal ICA to Extract Meaningful Information from High-Frequency fMRI Signal Fluctuations during Rest. Front Hum Neurosci 7: 168.

Breshears JD, Roland JL, Sharma M, Gaona CM, Freudenburg ZV, Tempelhoff R, Avidan MS & Leuthardt EC (2010) Stable and dynamic cortical electrophysiology of induction and emergence with propofol anesthesia. Proc Natl Acad Sci USA 107(49): 21170–21175.

Bright MG & Murphy K (2013) Removing motion and physiological artifacts from intrinsic BOLD fluctuations using short echo data. Neuroimage 64: 526–537.

Brookes MJ, Woolrich M, Luckhoo H, Price D, Hale JR, Stephenson MC, Barnes GR, Smith SM & Morris PG (2011) Investigating the electrophysiological basis of resting state networks using magnetoencephalography. Proc Natl Acad Sci USA 108(40): 16783–16788.

Brooks JC, Beckmann CF, Miller KL, Wise RG, Porro CA, Tracey I & Jenkinson M (2008) Physiological noise modelling for spinal functional magnetic resonance imaging studies. Neuroimage 39(2): 680–692.

Bruhn H, Fransson P & Frahm J (2001) Modulation of cerebral blood oxygenation by indomethacin: MRI at rest and functional brain activation. J Magn Reson Imaging 13(3): 325–334.

Buxton RB (2012) Dynamic models of BOLD contrast. Neuroimage 62(2): 953–961.

Calhoun VD & Adali T (2012) Multisubject independent component analysis of fMRI: a decade of intrinsic networks, default mode, and neurodiagnostic discovery. IEEE Rev Biomed Eng 5: 60–73.

Calhoun VD, Adali T, Pearlson GD & Pekar JJ (2001) A method for making group inferences from functional MRI data using independent component analysis. Hum Brain Mapp 14(3): 140–151.

Calhoun VD, Adali T & Pekar JJ (2004) A method for comparing group fMRI data using independent component analysis: application to visual, motor and visuomotor tasks. Magn Reson Imaging 22(9): 1181–1191.

Calhoun VD, Potluru VK, Phlypo R, Silva RF, Pearlmutter BA, Caprihan A, Plis SM & Adali T (2013) Independent component analysis for brain FMRI does indeed select for maximal independence. PLoS One 8(8): e73309.

Cardoso MM, Sirotin YB, Lima B, Glushenkova E & Das A (2012) The neuroimaging signal is a linear sum of neurally distinct stimulus- and task-related components. Nat Neurosci 15(9): 1298–1306.

Carhart-Harris RL, Leech R, Erritzoe D, Williams TM, Stone JM, Evans J, Sharp DJ, Feilding A, Wise RG & Nutt DJ (2013) Functional connectivity measures after psilocybin inform a novel hypothesis of early psychosis. Schizophr Bull 39(6): 1343–1351.

Castellanos FX, Di Martino A, Craddock RC, Mehta AD & Milham MP (2013) Clinical applications of the functional connectome. Neuroimage 80: 527–540.

Cauli B & Hamel E (2010) Revisiting the role of neurons in neurovascular coupling. Front Neuroenergetics 2: 9.

Chang C, Cunningham JP & Glover GH (2009) Influence of heart rate on the BOLD signal: the cardiac response function. Neuroimage 44(3): 857–869.

Chang C & Glover GH (2009a) Effects of model-based physiological noise correction on default mode network anti-correlations and correlations. Neuroimage 47(4): 1448–1459.

Chang C & Glover GH (2009b) Relationship between respiration, end-tidal CO_2, and BOLD signals in resting-state fMRI. Neuroimage 47(4): 1381–1393.

Chang C & Glover GH (2010) Time-frequency dynamics of resting-state brain connectivity measured with fMRI. Neuroimage 50(1): 81–98.

Chang C, Liu Z, Chen MC, Liu X & Duyn JH (2013) EEG correlates of time-varying BOLD functional connectivity. Neuroimage 72: 227–236.

Chang C, Metzger CD, Glover GH, Duyn JH, Heinze HJ & Walter M (2013) Association between heart rate variability and fluctuations in resting-state functional connectivity. Neuroimage 68: 93–104.

Chen AC, Oathes DJ, Chang C, Bradley T, Zhou ZW, Williams LM, Glover GH, Deisseroth K & Etkin A (2013) Causal interactions between fronto-parietal central executive and default-mode networks in humans. Proc Natl Acad Sci USA 110(49): 19944–19949.

Chialvo DR (2010) Emergent complex neural dynamics. Nature Physics 6(10): 744–750.

Ciuciu P, Varoquaux G, Abry P, Sadaghiani S & Kleinschmidt A (2012) Scale-Free and Multifractal Time Dynamics of fMRI Signals during Rest and Task. Front Physiol 3: 186.

Cohen MA & Taylor JA (2002) Short-term cardiovascular oscillations in man: measuring and modelling the physiologies. J Physiol 542(Pt 3): 669–683.

Cole DM, Beckmann CF, Oei NY, Both S, van Gerven JM & Rombouts SA (2013) Differential and distributed effects of dopamine neuromodulations on resting-state network connectivity. Neuroimage 78: 59–67.

Collignon O, Dormal G, Albouy G, Vandewalle G, Voss P, Phillips C & Lepore F (2013) Impact of blindness onset on the functional organization and the connectivity of the occipital cortex. Brain 136(Pt 9): 2769–2783.

Correa N, Adali T & Calhoun VD (2007) Performance of blind source separation algorithms for fMRI analysis using a group ICA method. Magn Reson Imaging 25(5): 684–694.

Dagli MS, Ingeholm JE & Haxby JV (1999) Localization of cardiac-induced signal change in fMRI. Neuroimage 9(4): 407–415.

Damoiseaux JS, Beckmann CF, Arigita EJ, Barkhof F, Scheltens P, Stam CJ, Smith SM & Rombouts SA (2008) Reduced resting-state brain activity in the "default network" in normal aging. Cereb Cortex 18(8): 1856–1864.

Daubechies I, Roussos E, Takerkart S, Benharrosh M, Golden C, D'Ardenne K, Richter W, Cohen JD & Haxby J (2009) Independent component analysis for brain fMRI does not select for independence. Proc Natl Acad Sci USA 106(26): 10415–10422.

De Luca M, Beckmann CF, De Stefano N, Matthews PM & Smith SM (2006) fMRI resting state networks define distinct modes of long-distance interactions in the human brain. Neuroimage 29(4): 1359–1367.

De Martino F, Gentile F, Esposito F, Balsi M, Di Salle F, Goebel R & Formisano E (2007) Classification of fMRI independent components using IC-fingerprints and support vector machine classifiers. Neuroimage 34(1): 177–194.

de Munck JC, Goncalves SI, Faes TJ, Kuijer JP, Pouwels PJ, Heethaar RM & Lopes da Silva FH (2008) A study of the brain's resting state based on alpha band power, heart rate and fMRI. Neuroimage 42(1): 112–121.

de Pasquale F, Della Penna S, Snyder AZ, Marzetti L, Pizzella V, Romani GL & Corbetta M (2012) A cortical core for dynamic integration of functional networks in the resting human brain. Neuron 74(4): 753–764.

Deco G, Jirsa VK & McIntosh AR (2013) Resting brains never rest: computational insights into potential cognitive architectures. Trends Neurosci 36(5): 268–274.

Desjardins AE, Kiehl KA & Liddle PF (2001) Removal of confounding effects of global signal in functional MRI analyses. Neuroimage 13(4): 751–758.

Doria V, Beckmann CF, Arichi T, Merchant N, Groppo M, Turkheimer FE, Counsell SJ, Murgasova M, Aljabar P, Nunes RG, Larkman DJ, Rees G & Edwards AD (2010) Emergence of resting state networks in the preterm human brain. Proc Natl Acad Sci USA 107(46): 20015–20020.

Dosenbach NU, Nardos B, Cohen AL, Fair DA, Power JD, Church JA, Nelson SM, Wig GS, Vogel AC, Lessov-Schlaggar CN, Barnes KA, Dubis JW, Feczko E, Coalson RS, Pruett JR,Jr, Barch DM, Petersen SE & Schlaggar BL (2010) Prediction of individual brain maturity using fMRI. Science 329(5997): 1358–1361.

Doucet G, Naveau M, Petit L, Zago L, Crivello F, Jobard G, Delcroix N, Mellet E, Tzourio-Mazoyer N, Mazoyer B & Joliot M (2012) Patterns of hemodynamic low-frequency oscillations in the brain are modulated by the nature of free thought during rest. Neuroimage 59(4): 3194–3200.

Durand E, van de Moortele PF, Pachot-Clouard M & Le Bihan D (2001) Artifact due to B(0) fluctuations in fMRI: correction using the k-space central line. Magn Reson Med 46(1): 198–201.

Eguiluz VM, Chialvo DR, Cecchi GA, Baliki M & Apkarian AV (2005) Scale-free brain functional networks. Phys Rev Lett 94(1): 018102.

Ekstrom A (2010) How and when the fMRI BOLD signal relates to underlying neural activity: the danger in dissociation. Brain Res Rev 62(2): 233–244.

El-Sharkawy AM, Schar M, Bottomley PA & Atalar E (2006) Monitoring and correcting spatio-temporal variations of the MR scanner's static magnetic field. MAGMA 19(5): 223–236.

Engel SA, Glover GH & Wandell BA (1997) Retinotopic organization in human visual cortex and the spatial precision of functional MRI. Cereb Cortex 7(2): 181–192.

Erhardt EB, Rachakonda S, Bedrick EJ, Allen EA, Adali T & Calhoun VD (2011) Comparison of multi-subject ICA methods for analysis of fMRI data. Hum Brain Mapp 32(12): 2075–2095.

Eryilmaz H, Van De Ville D, Schwartz S & Vuilleumier P (2011) Impact of transient emotions on functional connectivity during subsequent resting state: a wavelet correlation approach. Neuroimage 54(3): 2481–2491.

Esposito F, Pignataro G, Di Renzo G, Spinali A, Paccone A, Tedeschi G & Annunziato L (2010) Alcohol increases spontaneous BOLD signal fluctuations in the visual network. Neuroimage 53(2): 534–543.

Esposito F, Scarabino T, Hyvarinen A, Himberg J, Formisano E, Comani S, Tedeschi G, Goebel R, Seifritz E & Di Salle F (2005) Independent component analysis of fMRI group studies by self-organizing clustering. Neuroimage 25(1): 193–205.

Everitt BS & Bullmore ET (1999) Mixture model mapping of the brain activation in functional magnetic resonance images. Hum Brain Mapp 7(1): 1–14.

Fair DA, Cohen AL, Dosenbach NU, Church JA, Miezin FM, Barch DM, Raichle ME, Petersen SE & Schlaggar BL (2008) The maturing architecture of the brain's default network. Proc Natl Acad Sci USA 105(10): 4028–4032.

Fair DA, Dosenbach NU, Church JA, Cohen AL, Brahmbhatt S, Miezin FM, Barch DM, Raichle ME, Petersen SE & Schlaggar BL (2007) Development of distinct control networks through segregation and integration. Proc Natl Acad Sci USA 104(33): 13507–13512.

Fan J, Xu P, Van Dam NT, Eilam-Stock T, Gu X, Luo YJ & Hof PR (2012) Spontaneous brain activity relates to autonomic arousal. J Neurosci 32(33): 11176–11186.

Foerster BU, Tomasi D & Caparelli EC (2005) Magnetic field shift due to mechanical vibration in functional magnetic resonance imaging. Magn Reson Med 54(5): 1261–1267.

Fornito A & Bullmore ET (2010) What can spontaneous fluctuations of the blood oxygenation-level-dependent signal tell us about psychiatric disorders? Curr Opin Psychiatry 23(3): 239–249.

Fox MD, Snyder AZ, Vincent JL, Corbetta M, Van Essen DC & Raichle ME (2005) The human brain is intrinsically organized into dynamic, anticorrelated functional networks. Proc Natl Acad Sci USA 102(27): 9673–9678.

Fox MD, Snyder AZ, Vincent JL & Raichle ME (2007) Intrinsic fluctuations within cortical systems account for intertrial variability in human behavior. Neuron 56(1): 171–184.

Fox MD, Snyder AZ, Zacks JM & Raichle ME (2006) Coherent spontaneous activity accounts for trial-to-trial variability in human evoked brain responses. Nat Neurosci 9(1): 23–25.

Frahm J, Merboldt KD, Hanicke W, Kleinschmidt A & Boecker H (1994) Brain or vein--oxygenation or flow? On signal physiology in functional MRI of human brain activation. NMR Biomed 7(1–2): 45–53.

Franco AR, Mannell MV, Calhoun VD & Mayer AR (2013) Impact of analysis methods on the reproducibility and reliability of resting-state networks. Brain Connect 3(4): 363–374.

Fransson P (2005) Spontaneous low-frequency BOLD signal fluctuations: an fMRI investigation of the resting-state default mode of brain function hypothesis. Hum Brain Mapp 26(1): 15–29.

Fransson P (2006) How default is the default mode of brain function? Further evidence from intrinsic BOLD signal fluctuations. Neuropsychologia 44(14): 2836–2845.

Fransson P, Aden U, Blennow M & Lagercrantz H (2011) The functional architecture of the infant brain as revealed by resting-state fMRI. Cereb Cortex 21(1): 145–154.

Freire L & Mangin JF (2001) Motion correction algorithms may create spurious brain activations in the absence of subject motion. Neuroimage 14(3): 709–722.

Fries P (2005) A mechanism for cognitive dynamics: neuronal communication through neuronal coherence. Trends Cogn Sci 9(10): 474–480.

Friston KJ (1994) Functional and effective connectivity in neuroimaging: A synthesis. Hum Brain Mapp 2(1–2): 56–78.

Friston K (2010) The free-energy principle: a unified brain theory? Nat Rev Neurosci 11(2): 127–138.

Friston KJ (2009) Modalities, modes, and models in functional neuroimaging. Science 326(5951): 399–403.

Friston KJ, Holmes AP, Poline JB, Grasby PJ, Williams SC, Frackowiak RS & Turner R (1995) Analysis of fMRI time-series revisited. Neuroimage 2(1): 45–53.

Friston KJ, Williams S, Howard R, Frackowiak RS & Turner R (1996) Movement-related effects in fMRI time-series. Magn Reson Med 35(3): 346–355.

Friston KJ (2012) What does functional MRI measure? Two complementary perspectives. Trends Cogn Sci (Regul Ed) 16(10): 491–492.

Gati JS, Menon RS, Ugurbil K & Rutt BK (1997) Experimental determination of the BOLD field strength dependence in vessels and tissue. Magn Reson Med 38(2): 296–302.

Ghuman AS, van den Honert RN & Martin A (2013) Interregional neural synchrony has similar dynamics during spontaneous and stimulus-driven states. Sci Rep 3: 1481.

Glover GH, Lemieux SK, Drangova M & Pauly JM (1996) Decomposition of inflow and blood oxygen level-dependent (BOLD) effects with dual-echo spiral gradient-recalled echo (GRE) fMRI. Magn Reson Med 35(3): 299–308.

Glover GH, Li TQ & Ress D (2000) Image-based method for retrospective correction of physiological motion effects in fMRI: RETROICOR. Magn Reson Med 44(1): 162–167.

Gonzalez-Castillo J, Duthie KN, Saad ZS, Chu C, Bandettini PA & Luh WM (2013) Effects of image contrast on functional MRI image registration. Neuroimage 67: 163–174.

Gonzalez-Castillo J, Roopchansingh V, Bandettini PA & Bodurka J (2011) Physiological noise effects on the flip angle selection in BOLD fMRI. Neuroimage 54(4): 2764–2778.

Greicius MD, Krasnow B, Reiss AL & Menon V (2003) Functional connectivity in the resting brain: a network analysis of the default mode hypothesis. Proc Natl Acad Sci USA 100(1): 253–258.

Greicius MD & Menon V (2004) Default-mode activity during a passive sensory task: uncoupled from deactivation but impacting activation. J Cogn Neurosci 16(9): 1484–1492.

Greicius MD, Supekar K, Menon V & Dougherty RF (2009) Resting-state functional connectivity reflects structural connectivity in the default mode network. Cereb Cortex 19(1): 72–78.

Greve DN, Mueller BA, Liu T, Turner JA, Voyvodic J, Yetter E, Diaz M, McCarthy G, Wallace S, Roach BJ, Ford JM, Mathalon DH, Calhoun VD, Wible CG, Brown GG, Potkin SG & Glover G (2011) A novel method for quantifying scanner instability in fMRI. Magn Reson Med 65(4): 1053–1061.

Griffanti L, Salimi-Khorshidi G, Beckmann CF, Auerbach EJ, Douaud G, Sexton CE, Zsoldos E, Ebmeier KP, Filippini N, Mackay CE, Moeller S, Xu J, Yacoub E, Baselli G, Ugurbil K, Miller KL & Smith SM (2014) ICA-based artefact removal and accelerated fMRI acquisition for improved resting state network imaging. Neuroimage .

Gusnard DA, Raichle ME & Raichle ME (2001) Searching for a baseline: functional imaging and the resting human brain. Nat Rev Neurosci 2(10): 685–694.

Helmholtz H (1867) Handbuch der Physiologischen Optik. Leipzig. Leopold Voss.

Hagmann P, Cammoun L, Gigandet X, Meuli R, Honey CJ, Wedeen VJ & Sporns O (2008) Mapping the structural core of human cerebral cortex. PLoS Biol 6(7): e159.

Hall CN, Klein-Flugge MC, Howarth C & Attwell D (2012) Oxidative phosphorylation, not glycolysis, powers presynaptic and postsynaptic mechanisms underlying brain information processing. J Neurosci 32(26): 8940–8951.

Hampton AN, Bossaerts P & O'Doherty JP (2006) The role of the ventromedial prefrontal cortex in abstract state-based inference during decision making in humans. J Neurosci 26(32): 8360–8367.

Hartvig NV & Jensen JL (2000) Spatial mixture modeling of fMRI data. Hum Brain Mapp 11(4): 233–248.

Harvey AK, Pattinson KT, Brooks JC, Mayhew SD, Jenkinson M & Wise RG (2008) Brainstem functional magnetic resonance imaging: disentangling signal from physiological noise. J Magn Reson Imaging 28(6): 1337–1344.

He BJ, Snyder AZ, Zempel JM, Smyth MD & Raichle ME (2008) Electrophysiological correlates of the brain's intrinsic large-scale functional architecture. Proc Natl Acad Sci USA 105(41): 16039–16044.

He BJ, Zempel JM, Snyder AZ & Raichle ME (2010) The temporal structures and functional significance of scale-free brain activity. Neuron 66(3): 353–369.

He Y, Wang J, Wang L, Chen ZJ, Yan C, Yang H, Tang H, Zhu C, Gong Q, Zang Y & Evans AC (2009) Uncovering intrinsic modular organization of spontaneous brain activity in humans. PLoS One 4(4): e5226.

Heavey CL & Hurlburt RT (2008) The phenomena of inner experience. Conscious Cogn 17(3): 798–810.

Heeger DJ, Huk AC, Geisler WS & Albrecht DG (2000) Spikes versus BOLD: what does neuroimaging tell us about neuronal activity? Nat Neurosci 3(7): 631–633.

Hennig J, Ernst T, Speck O, Deuschl G & Feifel E (1994) Detection of brain activation using oxygenation sensitive functional spectroscopy. Magn Reson Med 31(1): 85–90.

Hermundstad AM, Bassett DS, Brown KS, Aminoff EM, Clewett D, Freeman S, Frithsen A, Johnson A, Tipper CM, Miller MB, Grafton ST & Carlson JM (2013) Structural foundations of resting-state and task-based functional connectivity in the human brain. Proc Natl Acad Sci USA 110(15): 6169–6174.

Himberg J, Hyvarinen A & Esposito F (2004) Validating the independent components of neuroimaging time series via clustering and visualization. Neuroimage 22(3): 1214–1222.

Hipp JF, Hawellek DJ, Corbetta M, Siegel M & Engel AK (2012) Large-scale cortical correlation structure of spontaneous oscillatory activity. Nat Neurosci 15(6): 884–890.

Honey CJ, Sporns O, Cammoun L, Gigandet X, Thiran JP, Meuli R & Hagmann P (2009) Predicting human resting-state functional connectivity from structural connectivity. Proc Natl Acad Sci USA 106(6): 2035–2040.

Horovitz SG, Braun AR, Carr WS, Picchioni D, Balkin TJ, Fukunaga M & Duyn JH (2009) Decoupling of the brain's default mode network during deep sleep. Proc Natl Acad Sci USA 106(27): 11376–11381.

Horovitz SG, Fukunaga M, de Zwart JA, van Gelderen P, Fulton SC, Balkin TJ & Duyn JH (2008) Low frequency BOLD fluctuations during resting wakefulness and light sleep: a simultaneous EEG-fMRI study. Hum Brain Mapp 29(6): 671–682.

Hyde JS, Biswal BB & Jesmanowicz A (2001) High-resolution fMRI using multislice partial k-space GR-EPI with cubic voxels. Magn Reson Med 46(1): 114–125.

Hyder F, Patel AB, Gjedde A, Rothman DL, Behar KL & Shulman RG (2006) Neuronal-glial glucose oxidation and glutamatergic-GABAergic function. J Cereb Blood Flow Metab 26(7): 865–877.

Hyder F & Rothman DL (2010) Neuronal correlate of BOLD signal fluctuations at rest: err on the side of the baseline. Proc Natl Acad Sci USA 107(24): 10773–10774.

Hyvarinen A, Karhunen J & Oja E (2001) Independent Component Analysis. Hoboken, John Wiley & Sons, Inc.

Hyvarinen A (1999) Fast and robust fixed-point algorithms for independent component analysis. IEEE Trans Neural Netw 10(3): 626–634.

Hyvarinen A & Oja E (2000) Independent component analysis: algorithms and applications. Neural Netw 13(4–5): 411–430.

Iacovella V & Hasson U (2011) The relationship between BOLD signal and autonomic nervous system functions: implications for processing of "physiological noise". Magn Reson Imaging 29(10): 1338–1345.

Ing A & Schwarzbauer C (2012) A dual echo approach to motion correction for functional connectivity studies. Neuroimage 63(3): 1487–1497.

Jafri MJ, Pearlson GD, Stevens M & Calhoun VD (2008) A method for functional network connectivity among spatially independent resting-state components in schizophrenia. Neuroimage 39(4): 1666–1681.

Jenkinson M & Smith S (2001) A global optimisation method for robust affine registration of brain images. Med Image Anal 5(2): 143–156.

Jezzard P & Balaban RS (1995) Correction for geometric distortion in echo planar images from B0 field variations. Magn Reson Med 34(1): 65–73.

Jezzard P & Clare S (1999) Sources of distortion in functional MRI data. Hum Brain Mapp 8(2–3): 80–85.

Jo HJ, Saad ZS, Simmons WK, Milbury LA & Cox RW (2010) Mapping sources of correlation in resting state FMRI, with artifact detection and removal. Neuroimage 52(2): 571–582.

Joel SE, Caffo BS, van Zijl PC & Pekar JJ (2011) On the relationship between seed-based and ICA-based measures of functional connectivity. Magn Reson Med 66(3): 644–657.

Johnston JM, Vaishnavi SN, Smyth MD, Zhang D, He BJ, Zempel JM, Shimony JS, Snyder AZ & Raichle ME (2008) Loss of resting interhemispheric functional connectivity after complete section of the corpus callosum. J Neurosci 28(25): 6453–6458.

Julien C (2006) The enigma of Mayer waves: Facts and models. Cardiovasc Res 70(1): 12–21.

Kahn I, Andrews-Hanna JR, Vincent JL, Snyder AZ & Buckner RL (2008) Distinct cortical anatomy linked to subregions of the medial temporal lobe revealed by intrinsic functional connectivity. J Neurophysiol 100(1): 129–139.

Kannurpatti SS, Rypma B & Biswal BB (2012) Prediction of Task-Related BOLD fMRI with Amplitude Signatures of Resting-State fMRI. Front Syst Neurosci 6: 7.

Kapogiannis D, Reiter DA, Willette AA & Mattson MP (2013) Posteromedial cortex glutamate and GABA predict intrinsic functional connectivity of the default mode network. Neuroimage 64: 112–119.

Karvanen J & Theis FJ (2004) Spatial ICA of fMRI data in time windows. Proc. MaxEnt 2004, Garching, Germany, 735: 312–319.

Katura T, Tanaka N, Obata A, Sato H & Maki A (2006) Quantitative evaluation of interrelations between spontaneous low-frequency oscillations in cerebral hemodynamics and systemic cardiovascular dynamics. Neuroimage 31(4): 1592–1600.

Kelly RE,Jr, Alexopoulos GS, Wang Z, Gunning FM, Murphy CF, Morimoto SS, Kanellopoulos D, Jia Z, Lim KO & Hoptman MJ (2010) Visual inspection of independent components: defining a procedure for artifact removal from fMRI data. J Neurosci Methods 189(2): 233–245.

Khalili-Mahani N, Chang C, van Osch MJ, Veer IM, van Buchem MA, Dahan A, Beckmann CF, van Gerven JM & Rombouts SA (2013) The impact of "physiological correction" on functional connectivity analysis of pharmacological resting state fMRI. Neuroimage 65: 499–510.

Kim B, Boes JL, Bland PH, Chenevert TL & Meyer CR (1999) Motion correction in fMRI via registration of individual slices into an anatomical volume. Magn Reson Med 41(5): 964–972.

Kim SG & Ogawa S (2012) Biophysical and physiological origins of blood oxygenation level-dependent fMRI signals. J Cereb Blood Flow Metab 32(7): 1188–1206.

Kiviniemi V, Kantola JH, Jauhiainen J, Hyvarinen A & Tervonen O (2003) Independent component analysis of nondeterministic fMRI signal sources. Neuroimage 19(2 Pt 1): 253–260.

Kiviniemi V, Starck T, Remes J, Long X, Nikkinen J, Haapea M, Veijola J, Moilanen I, Isohanni M, Zang YF & Tervonen O (2009) Functional segmentation of the brain cortex using high model order group PICA. Hum Brain Mapp 30(12): 3865–3886.

Kiviniemi V, Vire T, Remes J, Elseoud AA, Starck T, Tervonen O & Nikkinen J (2011) A sliding time-window ICA reveals spatial variability of the default mode network in time. Brain Connect 1(4): 339–347.

Kiviniemi VJ, Haanpaa H, Kantola JH, Jauhiainen J, Vainionpaa V, Alahuhta S & Tervonen O (2005) Midazolam sedation increases fluctuation and synchrony of the resting brain BOLD signal. Magn Reson Imaging 23(4): 531–537.

Kokkonen SM, Nikkinen J, Remes J, Kantola J, Starck T, Haapea M, Tuominen J, Tervonen O & Kiviniemi V (2009) Preoperative localization of the sensorimotor area using independent component analysis of resting-state fMRI. Magn Reson Imaging 27(6): 733–740.

Kowianski P, Lietzau G, Steliga A, Waskow M & Morys J (2013) The astrocytic contribution to neurovascular coupling – Still more questions than answers? Neurosci Res 75(3): 171–183.

Koyanagi M, Takada E, Nagata T, Tsukamoto H & Terakita A (2013) Homologs of vertebrate Opn3 potentially serve as a light sensor in nonphotoreceptive tissue. Proc Natl Acad Sci USA 110(13): 4998–5003.

Kundu P, Inati SJ, Evans JW, Luh WM & Bandettini PA (2012) Differentiating BOLD and non-BOLD signals in fMRI time series using multi-echo EPI. Neuroimage 60(3): 1759–1770.

Lakatos P, Shah AS, Knuth KH, Ulbert I, Karmos G & Schroeder CE (2005) An oscillatory hierarchy controlling neuronal excitability and stimulus processing in the auditory cortex. J Neurophysiol 94(3): 1904–1911.

Lauritzen M (2005) Reading vascular changes in brain imaging: is dendritic calcium the key? Nat Rev Neurosci 6(1): 77–85.

Lauritzen M & Gold L (2003) Brain function and neurophysiological correlates of signals used in functional neuroimaging. J Neurosci 23(10): 3972–3980.

Lee HL, Zahneisen B, Hugger T, LeVan P & Hennig J (2013) Tracking dynamic resting-state networks at higher frequencies using MR-encephalography. Neuroimage 65: 216–222.

Lee TW, Girolami M & Sejnowski TJ (1999) Independent component analysis using an extended infomax algorithm for mixed subgaussian and supergaussian sources. Neural Comput 11(2): 417–441.

Leopold DA & Maier A (2012) Ongoing physiological processes in the cerebral cortex. Neuroimage 62(4): 2190–2200.

Li YO, Adali T & Calhoun VD (2007) Estimating the number of independent components for functional magnetic resonance imaging data. Hum Brain Mapp 28(11): 1251–1266.

Liang Z, King J & Zhang N (2011) Uncovering intrinsic connectional architecture of functional networks in awake rat brain. J Neurosci 31(10): 3776–3783.

Liang Z, King J & Zhang N (2012) Intrinsic organization of the anesthetized brain. J Neurosci 32(30): 10183–10191.

Lin AL, Fox PT, Hardies J, Duong TQ & Gao JH (2010) Nonlinear coupling between cerebral blood flow, oxygen consumption, and ATP production in human visual cortex. Proc Natl Acad Sci USA 107(18): 8446–8451.

Littow H, Elseoud AA, Haapea M, Isohanni M, Moilanen I, Mankinen K, Nikkinen J, Rahko J, Rantala H, Remes J, Starck T, Tervonen O, Veijola J, Beckmann C & Kiviniemi VJ (2010) Age-Related Differences in Functional Nodes of the Brain Cortex - A High Model Order Group ICA Study. Front Syst Neurosci 4: 10.3389/fnsys.2010.00032. eCollection 2010.

Liu X & Duyn JH (2013) Time-varying functional network information extracted from brief instances of spontaneous brain activity. Proc Natl Acad Sci USA 110(11): 4392–4397.

Logothetis NK (2003) The underpinnings of the BOLD functional magnetic resonance imaging signal. J Neurosci 23(10): 3963–3971.

Logothetis NK (2008) What we can do and what we cannot do with fMRI. Nature 453(7197): 869–878.

Logothetis NK, Pauls J, Augath M, Trinath T & Oeltermann A (2001) Neurophysiological investigation of the basis of the fMRI signal. Nature 412(6843): 150–157.

Lord LD, Expert P, Huckins JF & Turkheimer FE (2013) Cerebral energy metabolism and the brain's functional network architecture: an integrative review. J Cereb Blood Flow Metab 33(9): 1347–1354.

Lou HC, Luber B, Crupain M, Keenan JP, Nowak M, Kjaer TW, Sackeim HA & Lisanby SH (2004) Parietal cortex and representation of the mental Self. Proc Natl Acad Sci USA 101(17): 6827–6832.

Lowe MJ, Mock BJ & Sorenson JA (1998) Functional connectivity in single and multislice echoplanar imaging using resting-state fluctuations. Neuroimage 7(2): 119–132.

Lund TE, Madsen KH, Sidaros K, Luo WL & Nichols TE (2006) Non-white noise in fMRI: does modelling have an impact? Neuroimage 29(1): 54–66.

Ma S, Correa NM, Li XL, Eichele T, Calhoun VD & Adali T (2011) Automatic identification of functional clusters in FMRI data using spatial dependence. IEEE Trans Biomed Eng 58(12): 3406–3417.

Macey PM, Macey KE, Kumar R & Harper RM (2004) A method for removal of global effects from fMRI time series. Neuroimage 22(1): 360–366.

Mackey AP, Miller Singley AT & Bunge SA (2013) Intensive reasoning training alters patterns of brain connectivity at rest. J Neurosci 33(11): 4796–4803.

Maclaren J, Armstrong BS, Barrows RT, Danishad KA, Ernst T, Foster CL, Gumus K, Herbst M, Kadashevich IY, Kusik TP, Li Q, Lovell-Smith C, Prieto T, Schulze P, Speck O, Stucht D & Zaitsev M (2012) Measurement and correction of microscopic head motion during magnetic resonance imaging of the brain. PLoS One 7(11): e48088.

Marrelec G, Bellec P & Benali H (2006) Exploring large-scale brain networks in functional MRI. J Physiol Paris 100(4): 171–181.

Marrelec G & Fransson P (2011) Assessing the influence of different ROI selection strategies on functional connectivity analyses of fMRI data acquired during steady-state conditions. PLoS One 6(4): e14788.

Marrelec G, Krainik A, Duffau H, Pelegrini-Issac M, Lehericy S, Doyon J & Benali H (2006) Partial correlation for functional brain interactivity investigation in functional MRI. Neuroimage 32(1): 228–237.

Marx M, Pauly KB & Chang C (2013) A novel approach for global noise reduction in resting-state fMRI: APPLECOR. Neuroimage 64: 19–31.

Mason MF, Norton MI, Van Horn JD, Wegner DM, Grafton ST & Macrae CN (2007) Wandering minds: the default network and stimulus-independent thought. Science 315(5810): 393–395.

Mayhew JE, Askew S, Zheng Y, Porrill J, Westby GW, Redgrave P, Rector DM & Harper RM (1996) Cerebral vasomotion: a 0.1-Hz oscillation in reflected light imaging of neural activity. Neuroimage 4(3 Pt 1): 183–193.

McKeown MJ, Makeig S, Brown GG, Jung TP, Kindermann SS, Bell AJ & Sejnowski TJ (1998) Analysis of fMRI data by blind separation into independent spatial components. Hum Brain Mapp 6(3): 160–188.

Menon RS (2012) The great brain versus vein debate Neuroimage 62(2): 970–974.

Meunier D, Lambiotte R, Fornito A, Ersche KD & Bullmore ET (2009) Hierarchical modularity in human brain functional networks. Front Neuroinform 3: 37.

Miao X, Gu H, Yan L, Lu H, Wang DJ, Zhou XJ, Zhuo Y & Yang Y (2014) Detecting resting-state brain activity by spontaneous cerebral blood volume fluctuations using whole brain vascular space occupancy imaging. Neuroimage 84: 575–584.

Modarreszadeh M & Bruce EN (1994) Ventilatory variability induced by spontaneous variations of $PaCO_2$ in humans. J Appl Physiol (1985) 76(6): 2765–2775.

Monto S, Palva S, Voipio J & Palva JM (2008) Very slow EEG fluctuations predict the dynamics of stimulus detection and oscillation amplitudes in humans J Neurosci 28(33): 8268–8272.

Moraschi M, DiNuzzo M & Giove F (2012) On the origin of sustained negative BOLD response. J Neurophysiol 108(9): 2339–2342.

Mowinckel AM, Espeseth T & Westlye LT (2012) Network-specific effects of age and in-scanner subject motion: a resting-state fMRI study of 238 healthy adults. Neuroimage 63(3): 1364–1373.

Muresan L, Renken R, Roerdink JB & Duifhuis H (2005) Automated correction of spin-history related motion artefacts in fMRI: simulated and phantom data. IEEE Trans Biomed Eng 52(8): 1450–1460.

Murphy K, Birn RM & Bandettini PA (2013) Resting-state fMRI confounds and cleanup. Neuroimage 80: 349–359.

Murphy K, Birn RM, Handwerker DA, Jones TB & Bandettini PA (2009) The impact of global signal regression on resting state correlations: are anti-correlated networks introduced? Neuroimage 44(3): 893–905.

Muthukumaraswamy SD, Edden RA, Jones DK, Swettenham JB & Singh KD (2009) Resting GABA concentration predicts peak gamma frequency and fMRI amplitude in response to visual stimulation in humans. Proc Natl Acad Sci USA 106(20): 8356–8361.

Niessing J, Ebisch B, Schmidt KE, Niessing M, Singer W & Galuske RA (2005) Hemodynamic signals correlate tightly with synchronized gamma oscillations. Science 309(5736): 948–951.

Nikouline VV, Linkenkaer-Hansen K, Huttunen J & Ilmoniemi RJ (2001) Interhemispheric phase synchrony and amplitude correlation of spontaneous beta oscillations in human subjects: a magnetoencephalographic study. Neuroreport 12(11): 2487–2491.

Nir Y, Mukamel R, Dinstein I, Privman E, Harel M, Fisch L, Gelbard-Sagiv H, Kipervasser S, Andelman F, Neufeld MY, Kramer U, Arieli A, Fried I & Malach R (2008) Interhemispheric correlations of slow spontaneous neuronal fluctuations revealed in human sensory cortex. Nat Neurosci 11(9): 1100–1108.

Nissila J, Manttari S, Sarkioja T, Tuominen H, Takala T, Timonen M & Saarela S (2012) Encephalopsin (OPN3) protein abundance in the adult mouse brain. J Comp Physiol A Neuroethol Sens Neural Behav Physiol 198(11): 833–839.

Noll DC & Schneider W (1994) Theory, simulation, and compensation of physiological motion artifacts in functional MRI. Image Processing, 1994. Proceedings. ICIP-94., IEEE International Conference. 3: 40–44 vol.3.

Northoff G, Qin P & Nakao T (2010) Rest-stimulus interaction in the brain: a review. Trends Neurosci 33(6): 277–284.

Ogawa S, Lee TM, Kay AR & Tank DW (1990) Brain magnetic resonance imaging with contrast dependent on blood oxygenation. Proc Natl Acad Sci USA 87(24): 9868–9872.

Ogawa S, Menon RS, Tank DW, Kim SG, Merkle H, Ellermann JM & Ugurbil K (1993) Functional brain mapping by blood oxygenation level-dependent contrast magnetic resonance imaging. A comparison of signal characteristics with a biophysical model. Biophys J 64(3): 803–812.

Palva JM, Zhigalov A, Hirvonen J, Korhonen O, Linkenkaer-Hansen K & Palva S (2013) Neuronal long-range temporal correlations and avalanche dynamics are correlated with behavioral scaling laws. Proc Natl Acad Sci USA 110(9): 3585–3590.

Patriat R, Molloy EK, Meier TB, Kirk GR, Nair VA, Meyerand ME, Prabhakaran V & Birn RM (2013) The effect of resting condition on resting-state fMRI reliability and consistency: a comparison between resting with eyes open, closed, and fixated. Neuroimage 78: 463–473.

Peltier SJ & Noll DC (2002) T(2)(*) dependence of low frequency functional connectivity. Neuroimage 16(4): 985–992.

Pendse GV, Borsook D & Becerra L (2011) A simple and objective method for reproducible resting state network (RSN) detection in fMRI. PLoS One 6(12): e27594.

Perlbarg V, Bellec P, Anton JL, Pelegrini-Issac M, Doyon J & Benali H (2007) CORSICA: correction of structured noise in fMRI by automatic identification of ICA components. Magn Reson Imaging 25(1): 35–46.

Posse S, Wiese S, Gembris D, Mathiak K, Kessler C, Grosse-Ruyken ML, Elghahwagi B, Richards T, Dager SR & Kiselev VG (1999) Enhancement of BOLD-contrast sensitivity by single-shot multi-echo functional MR imaging. Magn Reson Med 42(1): 687–97.

Power JD, Barnes KA, Snyder AZ, Schlaggar BL & Petersen SE (2012) Spurious but systematic correlations in functional connectivity MRI networks arise from subject motion. Neuroimage 59(3): 2142–2154.

Rack-Gomer AL & Liu TT (2012) Caffeine increases the temporal variability of resting-state BOLD connectivity in the motor cortex. Neuroimage 59(3): 2994–3002.

Raichle ME (2011) The restless brain. Brain Connect 1(1): 3–12.

Raj A, Zhang H, Prince MR, Wang Y & Zabih R (2006) Automatic algorithm for correcting motion artifacts in time-resolved two-dimensional magnetic resoance angiography using convex projections. Magnetic Resonance in Medicine 55(3): 649–658.

Renvall V, Nangini C & Hari R (2014) All that glitters is not BOLD: inconsistencies in functional MRI. Sci Rep 4:3920.

Robinson SD, Schopf V, Cardoso P, Geissler A, Fischmeister FP, Wurnig M, Trattnig S & Beisteiner R (2013) Applying independent component analysis to clinical FMRI at 7 t. Front Hum Neurosci 7: 496.

Roelfsema PR, Engel AK, Konig P & Singer W (1997) Visuomotor integration is associated with zero time-lag synchronization among cortical areas. Nature 385(6612): 157–161.

Roy M, Piche M, Chen JI, Peretz I & Rainville P (2009) Cerebral and spinal modulation of pain by emotions. Proc Natl Acad Sci USA 106(49): 20900–20905.

Saad ZS, Gotts SJ, Murphy K, Chen G, Jo HJ, Martin A & Cox RW (2012) Trouble at rest: how correlation patterns and group differences become distorted after global signal regression. Brain Connect 2(1): 25–32.

Sadaghiani S, Hesselmann G, Friston KJ & Kleinschmidt A (2010) The relation of ongoing brain activity, evoked neural responses, and cognition. Front Syst Neurosci 4: 20.

Sadaghiani S, Hesselmann G & Kleinschmidt A (2009) Distributed and antagonistic contributions of ongoing activity fluctuations to auditory stimulus detection. J Neurosci 29(42): 13410–13417.

Sagi Y, Tavor I, Hofstetter S, Tzur-Moryosef S, Blumenfeld-Katzir T & Assaf Y (2012) Learning in the fast lane: new insights into neuroplasticity. Neuron 73(6): 1195–1203.

Sakoglu U, Pearlson GD, Kiehl KA, Wang YM, Michael AM & Calhoun VD (2010) A method for evaluating dynamic functional network connectivity and task-modulation: application to schizophrenia. MAGMA 23(5–6): 351–366.

Salimi-Khorshidi G, Douaud G, Beckmann CF, Glasser MF, Griffanti L & Smith SM (2014) Automatic denoising of functional MRI data: combining independent component analysis and hierarchical fusion of classifiers. Neuroimage 90: 449–468.

Samann PG, Tully C, Spoormaker VI, Wetter TC, Holsboer F, Wehrle R & Czisch M (2010) Increased sleep pressure reduces resting state functional connectivity. MAGMA 23(5–6): 375–389.

Samann PG, Wehrle R, Hoehn D, Spoormaker VI, Peters H, Tully C, Holsboer F & Czisch M (2011) Development of the brain's default mode network from wakefulness to slow wave sleep. Cereb Cortex 21(9): 2082–2093.

Sarkka S, Solin A, Nummenmaa A, Vehtari A, Auranen T, Vanni S & Lin FH (2012) Dynamic retrospective filtering of physiological noise in BOLD fMRI: DRIFTER. Neuroimage 60(2): 1517–1527.

Satterthwaite TD, Elliott MA, Gerraty RT, Ruparel K, Loughead J, Calkins ME, Eickhoff SB, Hakonarson H, Gur RC, Gur RE & Wolf DH (2013) An improved framework for confound regression and filtering for control of motion artifact in the preprocessing of resting-state functional connectivity data. Neuroimage 64: 240–256.

Satterthwaite TD, Wolf DH, Loughead J, Ruparel K, Elliott MA, Hakonarson H, Gur RC & Gur RE (2012) Impact of in-scanner head motion on multiple measures of functional connectivity: relevance for studies of neurodevelopment in youth. Neuroimage 60(1): 623–632.

Scholvinck ML, Maier A, Ye FQ, Duyn JH & Leopold DA (2010) Neural basis of global resting-state fMRI activity. Proc Natl Acad Sci USA 107(22): 10238–10243.

Seeley WW, Menon V, Schatzberg AF, Keller J, Glover GH, Kenna H, Reiss AL & Greicius MD (2007) Dissociable intrinsic connectivity networks for salience processing and executive control. J Neurosci 27(9): 2349–2356.

Seifritz E, Esposito F, Hennel F, Mustovic H, Neuhoff JG, Bilecen D, Tedeschi G, Scheffler K & Di Salle F (2002) Spatiotemporal pattern of neural processing in the human auditory cortex. Science 297(5587): 1706–1708.

Shimada Y, Kochiyama T, Fujimoto I, Masaki S & Murasek K (2010) Effect of Fat-saturation Pulse on EPI Time Series in the Presence of B0 Drift. Magn Reson Med Sci 9(1): 9–16.

Shmuel A, Augath M, Oeltermann A & Logothetis NK (2006) Negative functional MRI response correlates with decreases in neuronal activity in monkey visual area V1. Nat Neurosci 9(4): 569–577.

Shmueli K, van Gelderen P, de Zwart JA, Horovitz SG, Fukunaga M, Jansma JM & Duyn JH (2007) Low-frequency fluctuations in the cardiac rate as a source of variance in the resting-state fMRI BOLD signal. Neuroimage 38(2): 306–320.

Stam CJ (2004) Functional connectivity patterns of human magnetoencephalographic recordings: a 'small-world' network? Neurosci Lett 355(1–2): 25–28.

Särelä J, Vigário R (2003) Overlearning in marginal distribution-based ICA: Analysis and solutions. J Mach Learn Res 4: 1447–1469.

Tagliazucchi E, von Wegner F, Morzelewski A, Borisov S, Jahnke K & Laufs H (2012) Automatic sleep staging using fMRI functional connectivity data. Neuroimage 63(1): 63–72.

Tal O, Diwakar M, Wong CW, Olafsson V, Lee R, Huang MX & Liu TT (2013) Caffeine-Induced Global Reductions in Resting-State BOLD Connectivity Reflect Widespread Decreases in MEG Connectivity. Front Hum Neurosci 7: 63.

Tanabe J, Nyberg E, Martin LF, Martin J, Cordes D, Kronberg E & Tregellas JR (2011) Nicotine effects on default mode network during resting state. Psychopharmacology (Berl) 216(2): 287–295.

Thomas CG, Harshman RA & Menon RS (2002) Noise reduction in BOLD-based fMRI using component analysis. Neuroimage 17(3): 1521–1537.

Tian L, Kong Y, Ren J, Varoquaux G, Zang Y & Smith SM (2013) Spatial vs. Temporal Features in ICA of Resting-State fMRI - A Quantitative and Qualitative Investigation in the Context of Response Inhibition. PLoS One 8(6): e66572.

Tohka J, Foerde K, Aron AR, Tom SM, Toga AW & Poldrack RA (2008) Automatic independent component labeling for artifact removal in fMRI. Neuroimage 39(3): 1227–1245.

Tong Y, Hocke LM, Nickerson LD, Licata SC, Lindsey KP & Frederick B (2013) Evaluating the effects of systemic low frequency oscillations measured in the periphery on the independent component analysis results of resting state networks. Neuroimage 76: 202–215.

Triantafyllou C, Hoge RD, Krueger G, Wiggins CJ, Potthast A, Wiggins GC & Wald LL (2005) Comparison of physiological noise at 1.5 T, 3 T and 7 T and optimization of fMRI acquisition parameters. Neuroimage 26(1): 243–250.

Tulppo MP, Jurvelin H, Roivainen E, Nissilä J, Hautala AJ, Kiviniemi AM, Kiviniemi VJ & Takala T (2014) Effects of Bright Light Treatment on Psychomotor Speed in Athletes. Frontiers in physiology 5.

Tyszka JM, Kennedy DP, Adolphs R & Paul LK (2011) Intact bilateral resting-state networks in the absence of the corpus callosum. J Neurosci 31(42): 15154–15162.

Uddin LQ, Mooshagian E, Zaidel E, Scheres A, Margulies DS, Kelly AM, Shehzad Z, Adelstein JS, Castellanos FX, Biswal BB & Milham MP (2008) Residual functional connectivity in the split-brain revealed with resting-state functional MRI. Neuroreport 19(7): 703–709.

Van Dijk KR, Sabuncu MR & Buckner RL (2012) The influence of head motion on intrinsic functional connectivity MRI. Neuroimage 59(1): 431–438.

Vanhatalo S, Palva JM, Holmes MD, Miller JW, Voipio J & Kaila K (2004) Infraslow oscillations modulate excitability and interictal epileptic activity in the human cortex during sleep. Proc Natl Acad Sci USA 101(14): 5053–5057.

Veer IM, Beckmann CF, van Tol MJ, Ferrarini L, Milles J, Veltman DJ, Aleman A, van Buchem MA, van der Wee NJ & Rombouts SA (2010) Whole brain resting-state analysis reveals decreased functional connectivity in major depression. Front Syst Neurosci 4: 10.3389/fnsys.2010.00041. eCollection 2010.

Vincent JL, Patel GH, Fox MD, Snyder AZ, Baker JT, Van Essen DC, Zempel JM, Snyder LH, Corbetta M & Raichle ME (2007) Intrinsic functional architecture in the anaesthetized monkey brain. Nature 447(7140): 83–86.

von Stein A & Sarnthein J (2000) Different frequencies for different scales of cortical integration: from local gamma to long range alpha/theta synchronization. Int J Psychophysiol 38(3): 301–313.

Wald LL (2012) The future of acquisition speed, coverage, sensitivity, and resolution. Neuroimage 62(2): 1221–1229.

Wang J, Wang Z, Aguirre GK & Detre JA (2005) To smooth or not to smooth? ROC analysis of perfusion fMRI data. Magn Reson Imaging 23(1): 75–81.

Wang L, Saalmann YB, Pinsk MA, Arcaro MJ & Kastner S (2012) Electrophysiological low-frequency coherence and cross-frequency coupling contribute to BOLD connectivity. Neuron 76(5): 1010–1020.

Weissenbacher A, Kasess C, Gerstl F, Lanzenberger R, Moser E & Windischberger C (2009) Correlations and anticorrelations in resting-state functional connectivity MRI: a quantitative comparison of preprocessing strategies. Neuroimage 47(4): 1408–1416.

Whitman JC, Ward LM & Woodward TS (2013) Patterns of Cortical Oscillations Organize Neural Activity into Whole-Brain Functional Networks Evident in the fMRI BOLD Signal. Front Hum Neurosci 7: 80.

Wise RG, Ide K, Poulin MJ & Tracey I (2004) Resting fluctuations in arterial carbon dioxide induce significant low frequency variations in BOLD signal. Neuroimage 21(4): 1652–1664.

Wong CW, Olafsson V, Tal O & Liu TT (2013) The amplitude of the resting-state fMRI global signal is related to EEG vigilance measures. Neuroimage 83: 983–990.

Worsley KJ & Friston KJ (1995) Analysis of fMRI time-series revisited—again. Neuroimage 2(3): 173–181.

Wu G & Li SJ (2005) Theoretical noise model for oxygenation-sensitive magnetic resonance imaging. Magn Reson Med 53(5): 1046–1054.

Xu J, Potenza MN & Calhoun VD (2013) Spatial ICA reveals functional activity hidden from traditional fMRI GLM-based analyses. Front Neurosci 7: 154.

Yan CG, Craddock RC, Zuo XN, Zang YF & Milham MP (2013) Standardizing the intrinsic brain: towards robust measurement of inter-individual variation in 1000 functional connectomes. Neuroimage 80: 246–262.

Yan L, Zhuo Y, Ye Y, Xie SX, An J, Aguirre GK & Wang J (2009) Physiological origin of low-frequency drift in blood oxygen level dependent (BOLD) functional magnetic resonance imaging (fMRI). Magn Reson Med 61(4): 819–827.

Yeo BT, Krienen FM, Chee MW & Buckner RL (2013) Estimates of segregation and overlap of functional connectivity networks in the human cerebral cortex. Neuroimage 88C: 212–227.

Ylipaavalniemi J & Vigário R (2008) Analyzing consistency of independent components: an fMRI illustration. Neuroimage 39(1): 169–180.

Zhang D & Raichle ME (2010) Disease and the brain's dark energy. Nat Rev Neurol 6(1): 15–28.

Zuo XN, Kelly C, Adelstein JS, Klein DF, Castellanos FX & Milham MP (2010) Reliable intrinsic connectivity networks: test-retest evaluation using ICA and dual regression approach. Neuroimage 49(3): 2163–2177.

Original publications

I Starck T, Remes J, Nikkinen J, Tervonen O & Kiviniemi V (2010) Correction of low-frequency physiological noise from the resting state BOLD fMRI-Effect on ICA default mode analysis at 1.5T. J Neurosci Methods 186(2): 179–185.

II Abou Elseoud A, Starck T, Remes J, Veijola J, Nikkinen J, Tervonen O & Kiviniemi V (2010) The effect of model order selection in group PICA. Hum Brain Mapp 31(8): 1207–1216.

III Starck T, Nikkinen J, Rahko J, Remes J, Hurtig T, Haapsamo H, Jussila K, Kuusikko-Gauffin S, Mattila M-L, Jansson-Verkasalo E, Ebeling H, Moilanen I, Tervonen O & Kiviniemi V (2013) Resting state fMRI reveals a default mode dissociation between retrosplenial and medial prefrontal subnetworks in ASD despite motion scrubbing. Front Hum Neurosci 7: 802.

IV Starck T, Nissilä J, Aunio A, Abou-Elseoud A, Remes J, Nikkinen J, Timonen M, Takala T, Tervonen O & Kiviniemi V (2012) Stimulating brain tissue with bright light alters functional connectivity in brain at the resting state. World J of Neurosci 2(2): 81–90.

Original publications are not included in the electronic version of the dissertation.

1238. Turunen, Sanna (2014) Protein-bound citrulline and homocitrulline in rheumatoid arthritis : confounding features arising from structural homology

1239. Kuorilehto, Ritva (2014) Moniasiantuntijuus sosiaali- ja terveydenhuollon perhetyössä : monitahoarviointi Q-metodologialla

1240. Sova, Henri (2014) Oxidative stress in breast and gynaecological carcinogenesis

1241. Tiirinki, Hanna (2014) Näkyvien ja piilotettujen merkitysten rajapinnoilla : terveyskeskukseen liittyvät kulttuurimallit asiakkaan näkökulmasta

1242. Syrjänen, Riikka (2014) TIM family molecules in hematopoiesis

1243. Kauppila, Joonas (2014) Toll-like receptor 9 in alimentary tract cancers

1244. Honkavuori-Toivola, Maria (2014) The prognostic role of matrix metalloproteinase-2 and -9 and their tissue inhibitor-1 and -2 in endometrial carcinoma

1245. Pienimäki, Tuula (2014) Factors, complications and health-related quality of life associated with diabetes mellitus developed after midlife in men

1246. Kallio, Miki (2014) Muuttuuko lääketieteen opiskelijoiden käsitys terveydestä peruskoulutuksen aikana : kuusivuotinen seurantatutkimus

1247. Haanpää, Maria (2014) Hereditary predisposition to breast cancer – with a focus on *AATF*, *MRG15*, *PALB2*, and three Fanconi anaemia genes

1248. Alanne, Sami (2014) Musiikkipsykoterapia : teoria ja käytäntö

1249. Nagy, Irina I. (2014) Wnt-11 signaling roles during heart and kidney development

1250. Prunskaite-Hyyryläinen, Renata (2014) Role of Wnt4 signaling in mammalian sex determination, ovariogenesis and female sex duct differentiation

1251. Huusko, Johanna (2014) Genetic background of spontaneous preterm birth and lung diseases in preterm infants : studies of potential susceptibility genes and polymorphisms

1252. Jämsä, Ulla (2014) Kuntoutuksen muutosagentit : tutkimus työelämälähtöisestä oppimisesta ylemmässä ammattikorkeakoulutuksessa

1253. Kaikkonen, Leena (2014) p38 mitogen-activated protein kinase and transcription factor GATA-4 in the regulation of cardiomyocyte function

1254. Finnilä, Mikko A. J. (2014) Bone toxicity of persistent organic pollutants

Book orders:
Granum: Virtual book store
http://granum.uta.fi/granum/

UNIVERSITY OF OULU P.O. Box 8000 FI-90014 UNIVERSITY OF OULU FINLAND

ACTA UNIVERSITATIS OULUENSIS

ISBN 978-952-62-0517-5 (Paperback)
ISBN 978-952-62-0518-2 (PDF)
ISSN 0355-3221 (Print)
ISSN 1796-2234 (Online)

UNIVERSITY of OULU
OULUN YLIOPISTO